IISN0379-301X

UNIVERSITE LIBRE DE BRUXELLES - VRIJE UNIVERSITEIT BRUSSEL

INTER-UNIVERSITY INSTITUTE FOR HIGH ENERGIES.

LOW Q^2, HIGH ν NEUTRINO PHYSICS

(CVC, PCAC, HADRON DOMINANCE)

B. Z. Kopeliovich.
Joint Institute for Nuclear Research - Dubna
Head Post Office, P.O. Box 79
101000 Moscow Russia

P. Marage.
Experimental Particle Physics Department
Université Libre de Bruxelles - CP 230
B-1050 Brussels Belgium

Universities of Brussels (ULB-VUB)
Pleinlaan 2
1050 Brussels

IIHE-92.02

LOW Q^2, HIGH ν NEUTRINO PHYSICS

(CVC, PCAC, HADRON DOMINANCE)

B. Z. Kopeliovich.
Joint Institute for Nuclear Research - Dubna
Head Post Office, P.O. Box 79
101000 Moscow Russia

P. Marage.
Experimental Particle Physics Department
Université Libre de Bruxelles - CP 230
B-1050 Brussels Belgium

TABLE OF CONTENTS.

ABSTRACT.

A critical review is given of the main theoretical bases and of the experimental results of neutrino physics at low four-momentum transfer ($Q^2 \leq 1$ GeV^2) and high energy transfer ($\nu \geq$ a few GeV).

The theoretical predictions for the vector current are first presented, using the CVC hypothesis and the hadron dominance model of Piketty and Stodolsky. The predictions for the axial current at very small Q^2-values are discussed on the basis of the PCAC hypothesis (Adler's theorem), and extended for $Q^2 \leq 1$ GeV^2 in the lines of hadron dominance; the structure of the longitudinal component of the axial current is particularly discussed.

Experimental data on neutrino and antineutrino interactions on nucleons are reviewed, in particular the total cross sections, which provide good tests of the PCAC hypothesis and of the model of Piketty and Stodolsky; also reviewed are the data on diffractive production of π, ρ and a_1 mesons.

The observation of shadowing, from the comparison of the total cross sections of neutrinos and antineutrinos on neon and deuterium nuclei, is discussed in detail with emphasis on the predictions of the PCAC hypothesis, in the framework of the Glauber-Gribov model.

Finally a review is given of the results on coherent neutrino and antineutrino interactions on atomic nuclei :

- π meson production, by charged and neutral currents in several experiments, providing a detailed test of the PCAC hypothesis ;
- ρ meson production, providing a test of the CVC hypothesis in weak interactions ;
- a_1 meson or non-resonant $\rho\pi$ system production, allowing the study of the weak axial current structure.

I. INTRODUCTION.

The weak interactions of high energy leptons with hadrons can be studied with the help of the two invariants Q^2, (minus) the square of the four-momentum transfer, and ν, the energy transfer from the leptons to the hadrons in the target rest frame.

In the last 30 years, most regions of the (Q^2, ν) plane have been studied in detail (see Fig.1). Region I, with very small (negative) Q^2- and ν- values, is the region of weak decays. The diagonal line II represents (quasi-) elastic neutrino scattering, while region III is the resonance region, starting with the line $W = M + m_\pi$ (W is the hadronic mass, M is the proton mass, m_π is the pion mass). For high values of Q^2 and ν, region IV is the domain of deep inelastic scattering. In the present work, we shall concentrate on region V, with low Q^2- and high ν- values ($Q^2 \leq 1$ GeV^2, $\nu \geq 2$ GeV).

In the very low (positive) Q^2- region ($Q^2 \leq$ a few m_π^2), neutrino reactions allow to study two basic properties of the weak current : the conservation of the vector current (the "CVC hypothesis"), and the partial conservation of the axial current (the "PCAC hypothesis"). The former was introduced to explain the equality (in the framework of Cabibbo's theory) of the vector muon and nuclear β decay constants, the latter to explain the small (~ 20%) renormalization of the nuclear axial decay constant by the strong interactions.

The particular importance of the PCAC hypothesis lies in the following. If the fermion masses are due to a spontaneous breaking of the (global) chiral symmetry, this breaking must be accompanied by the appearance of massless Goldstone bosons, identified with (massless) pions. Although real pions are not exactly massless, their mass is "small" on the hadron mass scale. The PCAC hypothesis relates this "small" mass to a "small" non-conservation of the axial current :

$$\partial_\mu A_\mu = f_\pi m_\pi^2 \phi_\pi \quad , \tag{1}$$

where A_μ is the axial current, f_π the pion decay constant ($f_\pi \approx 0.93\ m_\pi$) and ϕ_π the pion field. Tests of the PCAC hypothesis were obtained in muon capture and in decay processes (Goldberger - Treiman relation). However, it is important to test this hypothesis also in processes with different underlying dynamics. In neutrino reactions, such tests are given by Adler's theorem [Adler 1964], which relates neutrino- and pion- production of the same final hadronic states. The results discussed here provide several tests of Adler's theorem.

In an intermediate Q^2- region ($m_\pi^2 \leq Q^2 \leq$ 1-2 GeV^2), the hadron dominance approach of Piketty and Stodolsky [Piketty 1970] can be used to compute the neutrino cross section. The weak current can indeed be seen as a superposition of (virtual) hadron resonances, with appropriate quantum numbers. According to the uncertainty principle, these can fluctuate into real states, changing the energy of the system for times corresponding to a "coherence length" l_c:

$$l_c = \Delta t_c \approx \frac{2\nu}{Q^2 + m^2} \quad , \qquad (2)$$

where m is the mass of the (real) hadron (throughout this paper, we use $h/2\pi = c = 1$). If $\Delta t_c \geq \Delta t_i$, the typical interaction time of the process, the weak current thus behaves as a (real) hadron current.

The basic theoretical ideas presented in this paper were expressed more than 20 years ago, - although several new results will be incorporated here. Experimental data have been accumulated only in the last 6-8 years, providing a rich and consistent picture of the low Q^2, high ν neutrino physics. These results were obtained mainly by the various Collaborations using large bubble chambers at CERN and FNAL, exposed to the high energy neutrino and antineutrino beams, and filled with hydrogen, deuterium and neon.

In section II of this paper, the theoretical framework is introduced ; predictions for the vector and the axial current are deduced (Adler's theorem, Piketty - Stodolsky model) ; special attention is paid to the problem of the longitudinal axial current, in relation with PCAC.

In section III, experimental data are reviewed concerning low Q^2, high ν (anti)neutrino interactions on nucleons, especially the total cross sections.

In section IV, the observation of shadowing in (anti)neutrino-nucleus interactions is discussed, in the framework of the Glauber-Gribov theory and of PCAC.

In section V, the data on coherent (anti)neutrino interactions on nuclei are reviewed and discussed ; in particular, coherent pion production provides another detailed test of the PCAC hypothesis.

In section VI, conclusions are drawn.

II. THEORETICAL INTRODUCTION.

1. Kinematics.

Let us consider the interaction of a neutrino ν_l with a target T, giving in the final state the lepton l and the hadron state F :

$$\nu_l + T \rightarrow l + F \tag{3}$$

(the modifications for an incident antineutrino are trivial). The 4-momentum vectors are defined in Fig.2.

With the invariants $Q^2 = - q^2$ and ν (= E_ν - E_l in the target rest frame), one defines the Bjorken variables :

$$x = \frac{Q^2}{2M\nu} \tag{4}$$

$$y = \frac{qp}{kp} = \frac{\nu}{E_\nu} \quad ; \tag{5}$$

the hadronic invariant mass W is given by

$$W^2 = 2M\nu - Q^2 + M^2 = Q^2 (\frac{1}{x} - 1) + M^2 \quad . \tag{6}$$

The amplitude for reaction (3) is :

$$M = \frac{G}{\sqrt{2}} l^\mu (V_\mu + A_\mu) \quad , \tag{7}$$

where G is the Fermi coupling constant of weak interactions :

$$G = 1.166\ 10^{-5}\ GeV^{-2} \quad , \tag{8}$$

and l_μ is the lepton current :

$$l_\mu = \bar{l}(k') \gamma_\mu (1 + \gamma_5) \nu(k) \ ; \tag{9}$$

the hadron current has been separated into a vector part V_μ and an axial part A_μ.

After squaring the amplitude (7), and taking the average over the initial spin states and the sum over the final states, one has

$$|\bar{M}|^2 = \frac{G^2}{2} L^{\mu\nu} (V_{\mu\nu} + A_{\mu\nu} + W_{\mu\nu}) \quad , \qquad (10)$$

where the tensors $V_{\mu\nu}$, $A_{\mu\nu}$ and $W_{\mu\nu}$ correspond, respectively, to the contributions of the vector current, of the axial current, and of their interference. The lepton tensor $L_{\mu\nu}$ is :

$$\begin{aligned} L_{\mu\nu} &= k_\mu k'_\nu + k_\nu k'_\mu - (kk') g_{\mu\nu} + i \varepsilon_{\mu\nu\rho\sigma} k_\rho k_\sigma \\ &= 2 k_\mu k_\nu - k_\mu q_\nu - q_\mu k_\nu + (kq) g_{\mu\nu} + i \varepsilon_{\mu\nu\rho\sigma} k_\rho q_\sigma \quad . \qquad (11) \end{aligned}$$

For $Q^2 = 0$, $L_{\mu\nu}$ can be written as :

$$L_{\mu\nu}(Q^2 = 0) = 2 \frac{E(E - \nu)}{\nu^2} q_\mu q_\nu \quad . \qquad (12)$$

2. Vector current.

2.1. Conservation of the vector current.

The first term in (10) comes from the pure vector current contribution.

The possibility of the weak vector current conservation :

$$q_\mu V^\mu = 0 \qquad (13)$$

was first emphasized by Gershtein and Zeldovich [Gershtein 1955]. At a time where the β-decay was attributed to the scalar and tensor currents, they noticed that the weak coupling constant would not be renormalized if β-decay was dominated by a conserved vector current. This effect is similar to the non-renormalization of the electromagnetic coupling constant by the strong interactions, due to the conservation of the electric charge. Later, within the V-A weak interaction theory, Feynman and Gell-Mann [Feynman 1958] showed that the CVC hypothesis naturally explains the equality of the nuclear β- and muon decay coupling constants. Actually, the CVC hypothesis finds its justification in the unified electroweak theory, where the charged weak current and the electromagnetic current belong to the same

isotopic triplet. Let us note, however, that CVC being the consequence of the isotopic invariance, both are violated because of the electromagnetic interactions, responsible for the u and d quark mass difference. The right hand side of (13) is thus in fact proportional to the small parameter $(m_u - m_d)$.

An immediate consequence of the conservation of the vector current is the vanishing of the vector current contribution to the weak cross section for $Q^2 = 0$. This follows from the form (12) of the $L_{\mu\nu}$ tensor for $Q^2 = 0$ and from relation (13) :

$$Q^2 \to 0 : L_{\mu\nu} V^{\mu\nu} \propto q_\mu \; V^\mu V^{*\nu} \; q_\nu = 0 \quad . \tag{14}$$

2.2. Formal cross section.

The pure vector contribution to the cross section can be formally deduced as follows. The polarization state of the vector current can be characterized using the longitudinal and transverse polarization vectors e_μ^L and e_μ^T, which are determined by the conditions

$$q_\mu \, e_\mu^{L,T} = 0 \quad ; \tag{15}$$

$$(e_\mu^T)^2 = -1 \quad , \quad (e_\mu^L)^2 = 1 \text{ (for } Q^2 > 0) \; . \tag{16}$$

One thus has :

$$e_\mu^L = \frac{1}{\sqrt{Q^2}} (\sqrt{\nu^2 + Q^2} \, , 0 \, , 0 \, , \nu) \tag{17}$$

$$e_\mu^T = (0 \, , \sqrt{\tfrac{1}{2}(1 + \varepsilon)} \, , \sqrt{\tfrac{1}{2}(1 - \varepsilon)} \, , 0) \; ; \tag{18}$$

the parameter ε is related to the angle θ between the polarization plane and the x-axis :

$$\varepsilon = 2 \cos\theta - 1 \tag{19}$$

One defines the cross sections for the production of the final state F by the polarized current :

$$\sigma_V^L(Q^2) = \frac{1}{\sqrt{\nu^2 + Q^2}}\, e_\mu^L\, e_\nu^{L*}\, V^{\mu\nu} \qquad (20)$$

$$\sigma_V^T(Q^2) = \frac{1}{\sqrt{\nu^2 + Q^2}}\, e_\mu^T\, e_\nu^{T*}\, V^{\mu\nu} \quad . \qquad (21)$$

The factor $\phi = 1/\sqrt{\nu^2 + Q^2} = 1/|\vec{q}|$ is a flux factor. The polarized cross sections are defined up to the flux factor, which can be chosen according to a different convention, e.g. $\phi = \nu(1 - x)$ [Hand 1963].

Using the polarization vectors, the lepton tensor has the form

$$L_{\mu\nu} = (\alpha\, e_\mu^L + \beta\, e_\mu^T)\,(\alpha\, e_\nu^L + \beta\, e_\nu^T)^* \quad ; \qquad (22)$$

the constants α and β, and the parameter ε are found by comparison with (11) :

$$\alpha^2 = \frac{1}{2}\,\frac{Q^2}{\nu^2 + Q^2}\,[4E(E - \nu) - Q^2] \qquad (23)$$

$$\beta^2 = \frac{1}{2}\,\frac{Q^2}{\nu^2 + Q^2}\,[4E(E - \nu) + Q^2 + 2\nu^2] \qquad (24)$$

$$\varepsilon = \frac{4E(E - \nu) - Q^2}{4E(E - \nu) + Q^2 + 2\nu^2} \quad . \qquad (25)$$

Putting the definitions (20) - (22) in (10), one gets for the vector current contribution to the neutrino cross section :

$$\frac{d^2\sigma_V(\nu T \to lF)}{dQ^2\, d\nu} = \frac{G^2}{4\pi^2}\,\frac{|\vec{q}|}{E^2}\,\frac{Q^2}{1 - \varepsilon}\,[\sigma_V^T(Q^2) + \varepsilon\,\sigma_V^L(Q^2)] \quad . \qquad (26)$$

This cross section vanishes for $Q^2 \to 0$. Note however that the factor Q^2 in (27) is not a consequence of CVC, but of the structure of the lepton current.The role of CVC is to guarantee the absence of a pole in σ_V^T and σ_V^L for $Q^2 \to 0$, and to connect these cross sections to the corresponding ones for the electromagnetic current.

2.3. Hadron dominance.

To compute the unknown cross sections in (26), Piketty and Stodolsky [Piketty 1970] proposed a straightforward extension of the vector meson dominance (VMD) model of the electromagnetic interactions (see e.g. [Stodolsky 1964], [Bauer 1978], [Donnachie 1978a]).

In the simple VMD model, the weak (or electromagnetic) current is considered as a superposition of the lightest hadrons with relevant quantum numbers. In the present case :

$$\sigma_V^{T,L}(Q^2) = \sum_{\nu} f_\nu^2 \left(\frac{1}{Q^2 + m_\nu^2}\right)^2 \sigma_\nu^{T,L}(Q^2) \quad , \tag{27}$$

where ν is the $\rho^{+(-)}$ meson for the charged current interactions, and the ρ^0, ω and ϕ mesons for the neutral current (electromagnetic) interactions; m_ν is the mass of the meson ν, $\sigma_\nu^{T,L}$ are the polarized cross sections, and f_ν is the coupling constant to the weak current. For charged currents, the latter can be obtained from $e^+ e^-$ annihilation into hadrons :

$$f_\nu^{(\pm)} = \sqrt{2}\, f_\nu^{(em)} \quad . \tag{28}$$

For charged ρ mesons, one has :

$$f_{\rho^\pm}^2 = 2\, m_\rho^4 / \gamma_\rho^2 \quad , \tag{29}$$

with

$$\gamma_\rho^2 / 4\pi = 2.4 \quad . \tag{30}$$

The cross section (26) thus takes the form :

$$\frac{d^2\sigma_V\,(\nu T \to lF)}{dQ^2\, d\nu} = \frac{G^2}{4\pi^2} \frac{f_\rho^2}{E^2} \frac{|\vec{q}|}{} \frac{Q^2}{(Q^2 + m_\rho^2)^2} \frac{1}{1 - \varepsilon} \cdot$$

$$[\, \sigma_{\rho \to F}^T(Q^2) + \varepsilon\, \sigma_{\rho \to F}^L(Q^2)\,] \quad . \tag{31}$$

Two remarks are in order here.

Firstly, as was mentioned in the Introduction, the hadron constituents of the current can only show up if the hadronic fluctuation exists for a "sufficient" time. This is expressed as the "high energy condition" : at high energy, the hadron fluctuation can cover long distances, such that

$$\Delta t_c \geq \Delta t_i \quad , \tag{32}$$

where

$$\Delta t_c = lc \approx \frac{2\nu}{Q^2 + m^2} = \frac{1}{xM} \left(1 + \frac{m^2}{Q^2} \right)^{-1} \tag{33}$$

is the "coherence time" of the fluctuation, and Δt_i is a typical interaction time. (In deducing (33), the hypothesis was made that $\nu >> (Q^2 + m^2)^{1/2}$) .

Secondly, the basic hypothesis of the VMD model is the following : the coupling constants f_v and the cross sections $\sigma_v^{T,L}(Q^2)$ are not affected (or only weakly) by the Q^2 extrapolation from $Q^2 = - m_v^2$ to $Q^2 \geq 0$, i.e. the coupling constants and the cross sections for real hadrons can be used in computing (31). This hypothesis is the key for any predictive power of the model. The successes of the VMD model of the electromagnetic interactions (see e.g. [Bauer 1978]) are by themselves a justification a posteriori of this hypothesis.

2.4. Generalized hadron dominance ; dispersion relations.

The simple VMD model, however, is not completely satisfactory. On one hand, the ρ - ω - ϕ dominance accounts for only ~ 80% of the photon cross section; this has led to the suggestion of an additional "point - like component" [Gunion 1972]. On the other hand, it looks arbitrary to restrict the sum in (27) to the lightest mesons, neglecting non-resonant hadronic fluctuations and high mass resonances, e.g. ρ (1450) and ρ (1700) [PDG 1990]. It was thus proposed to extend the sum (27) to heavier states, in the framework of "generalized vector dominance" (GVD) models (see e.g. [Donnachie 1978b]).

The predictive power of GVD models, however, is limited because little experimental data exist on the coupling constants (including their sign) and the cross sections of the heavy states. In fact, these models meet a major difficulty when trying to account for the scaling

($\propto$ 1 / Q^2) behaviour of the photon cross section, since they tend to predict a 1 / Q^4 dependence (cf. [Sakuraï 1972]). Suggestions were thus made that the coupling constants and the cross sections could be mass dependent ([Bramón 1972], [Schildkneckt 1973]), or that off-diagonal transitions should be taken into account, possibly with alternating signs, leading to compensation effects ([Fraas 1975a], [Devenish 1976]) (this would account for the effective mass dependence of the cross sections in diagonal GVD models). The necessity of taking into account inelastic corrections was indeed suggested as an extension of Glauber's model for interactions on nuclei ([Pumplin 1968], [Gribov 1969a]); experimentally this was confirmed by the study of the interactions on several nuclei of neutrons ([Murthy 1975], [Biel 1976]) and of K_L^0 mesons [Gsponer 1979].

The meson dominance models use the Feynman diagram approach in formulating eq. (26) - (27), leading to the problem of the Q^2-extrapolation of coupling constants and cross sections. An alternative to this approach, which avoids in principle this problem, is based on dispersion relations. In this case, the amplitudes are computed in the complex Q^2-plane, using the residues of the poles, corresponding to on - mass - shell mesons : $\sigma_\nu^{T,L}(Q^2 = m_\nu^2)$. From this point of view, the poles contributing to relation (27) are not the poles in the Q^2-plane. Instead, the Q^2-dependence of $\sigma_\nu^{T,L}$ accounts for the effective inclusion of other singularities.

The general dispersion relation for the amplitude $V_\mu(Q^2)$ of the vector current interaction giving the final state F is the following :

$$V_\mu(Q^2) = \Sigma \int \frac{dM^2}{Q^2 + M^2} \; \Gamma(M^2) \; \nu_\mu(M^2) \qquad , \qquad (34)$$

where the vertices $\Gamma(M^2)$ can be obtained from $e^+ e^-$ annihilation experiments, and the amplitudes $\nu_\mu(M^2)$ are the amplitudes of production of the state F, by the interaction of a multi-particle state of mass M with the target. The summations in (34) are performed over the numbers of particles in the state of mass M, and over their momenta. Note that there is no real justification for the use of unsubtracted dispersion relations like (34).

The dispersion relation approach is formally valid but, even in their most general form, these relations are of little use for Q^2-values ≥ 1 GeV^2 : they require indeed abundant experimental information on the interaction amplitudes of a large number of hadronic systems, which are generally not available. Attempts made to use simplified dispersion relations led to difficulties. In particular, the use of double dispersion relations for computing the photon cross section [Gribov 1969b] neglecting off-diagonal transition amplitudes led to a severe violation of the scaling behaviour, known as the " Bjorken puzzle " [Bjorken

1973]. As expected, one meets difficulties similar to these encountered by the most sophisticated GVD models.

2.5. Longitudinal cross section.

Let us come back, as a reasonable approximation for our purpose, to eq. (31). A specific difficulty concerns the Q^2-dependence of the longitudinal cross section. The latter is indeed necessarily modified by the Q^2-extrapolation, since it vanishes for $Q^2 = 0$:

$$\sigma^L(Q^2) \xrightarrow[Q^2 \to 0]{} 0 \ . \tag{35}$$

For small Q^2-values ($Q^2 \leq 1$ GeV^2), a prediction is made for the cross section ratio :

$$R\,(Q^2) = \sigma^L(Q^2) / \sigma^T(Q^2) = \xi^2\, Q^2 / m_\rho^2 \quad , \tag{36}$$

based on dispersion relations (see [Sakuraï 1969], [Fraas 1969]),

$$\xi^2 = \sigma^L(\rho) / \sigma^T(\rho) \tag{37}$$

being the ratio of the cross sections for real mesons. The parametrization (36) implies a vanishing longitudinal cross section for $Q^2 \to 0$. It cannot, however, be extended up to high values of Q^2. For Q^2 far from 0, one knows indeed from QCD analyses that the longitudinal cross section has to vanish again. For Q^2 larger than a few GeV^2, deep inelastic scattering data indicate that $R \approx 0$, and the Callan-Gross relation is reasonably well verified (see [Mishra 1989]). A slight violation of the latter, due to gluon bremsstrahlung and decreasing as $1/\ln Q^2$, is predicted by QCD and is not contradicted by the data for $Q^2 \geq 1$ GeV^2. However, higher twist effects in $1/Q^2$ and $1/Q^4$ must also be taken into account, due to mass and binding energy effects in the target. These could even dominate the QCD calculated effects ([Whitlow 1990], [Mishra 1990]).

In the low Q^2-domain ($Q^2 \leq 1$ GeV^2) of interest here, the higher twist effects are certainly important, but the experimental situation is unclear. The data come mainly from electro- and muoproduction of ρ mesons.

For $Q^2 \leq 1$ GeV^2, relation (36) is verified by [Ballam 1974] and [Joos 1976], with $0.3 < \xi^2 < 0.5$. Two groups ([Del Papa 1979] and [Cassel 1981]) find values of R

increasing up to $R \geq 1$ for $Q^2 \approx 1$ GeV^2, then decreasing with $R \approx 0.5$ - 0.6 for $Q^2 \approx 1.5$ - 2.5 GeV^2. At high W- values, but for $Q^2 \leq 2$ GeV^2, [Shambroom 1982] find $R \approx 0$ and notice, when comparing several results in the same Q^2-domain, that R seems to decrease as W increases. All these results are obtained from the analysis of the angular dependence of the cross section, assuming s-channel helicity conservation (SCHC hypothesis - see [Schilling 1973]). For all these experiments, the Q^2-dependence of the ρ-production cross section is found to agree with the R-value deduced from the helicity analysis. On the other hand, for higher Q^2-values (up to $Q^2 \geq 10$ GeV^2), the EMC Collaboration [Aubert 1985] has parametrized the ρ-production angular dependence with $\xi^2 = 0.4$, assuming the SCHC hypothesis. However the Q^2-dependence of the production cross section is well described by a law in $(Q^2 + m_\rho^2)^{-2}$, thus suggesting $R \approx 0$: this contradiction suggests that the SCHC hypothesis is not valid in this domain, at variance with lower Q^2-values ([Joos 1976], [Shambroom 1982]).The same conclusion is reached when solving the equation

$$\sigma_\gamma(Q^2) = \sigma^T(Q^2) + \varepsilon \, \sigma^L (Q^2) \qquad (38)$$

for the two values of ε corresponding respectively to the experimental conditions of [Shambroom 1982] and [Aubert 1985].

In this unclear situation, two hypotheses were considered by experimental groups for the Q^2-values of interest in this paper :

(i) R is small and (approximately) constant :

$$R \approx 0 - 0.2 \; ; \qquad (39)$$

this hypothesis looks plausible for high W-values;

(ii) R depends on Q^2 : for $Q^2 \leq 1$ GeV^2 ,

$$R = \xi^2 \, Q^2 / m_\rho^2 \;\; , \text{with} \;\; \xi^2 = 0.4 - 0.6 \;\; , \qquad (40)$$

giving $R \leq 1$ for $Q^2 \approx 1$ GeV^2. For $Q^2 > 1$ GeV^2, R remains ≤ 1, and probably decreases, with $R \approx 0$ for $Q^2 \geq$ a few GeV^2 .

3. Axial current.

3.1. The PCAC hypothesis.

The contribution of the axial current to the neutrino cross section, i.e. the second term in eq. (10), can be formally represented in the same form as eq. (26) for the vector current, with the change of the indices V into A. Although the non-conservation of the axial current does not allow the simplifications made in the vector case, nevertheless the PCAC hypothesis provides useful informations on the structure of the axial cross section.

The problem of the renormalization induced by the strong interactions is more complicated in the axial than in the vector case. In β-decay, the derivative of the vector term vanishes (up to isospin violating terms), but the axial-vector term is obviously not conserved, its derivative being proportional to twice the nucleon mass :

$$q_\mu \; g_A(Q^2) \; \bar{p} \, \gamma_5 \, \gamma_\mu \, n \; = \; (m_p + m_n) \; g_A(Q^2) \; \bar{p} \, \gamma_5 \, n \; . \qquad (41)$$

However, the very fact that the nucleon mass is large whereas the quark masses are very small, suggests the existence of a mechanism of spontaneous breaking of the chiral symmetry : the latter provides the nucleon a mass, even at the limit of massless quarks. As a result of this symmetry breaking, a triplet of (pseudo) Goldstone mesons appears, identified with the pions. The existence of (almost) massless pions gives the possibility to preserve the conservation of the axial current : they generate a pseudoscalar contribution, which cancels the contribution arising from the non-conserved axial-vector part in (41) :

$$(m_p + m_n) \; g_A(Q^2) - Q^2 \, g_P(Q^2) \; = \; 0 \qquad , \qquad (42)$$

with

$$g_P(Q^2) \; = \; f_\pi \; \frac{\sqrt{2} \, g_{\pi NN}}{m_\pi^2 + Q^2} \; (m_\pi = 0) \quad , \qquad (43)$$

where f_π is the pion decay constant and $g_{\pi NN}$ is the πNN coupling constant. Relations (42) and (43) are combined to give the Goldberger- Treiman relation [Goldberger 1958] :

$$(m_p + m_n) \; g_A(0) \; = \; \sqrt{2} \; f_\pi \; g_{\pi NN} \quad . \qquad (44)$$

In the chiral limit of massless quarks and pions and of a conserved axial current, the axial coupling constant should not be renormalized, i.e. $g_A(0) = 1$. However the experimentally measured value is about 20% higher, this correction being thus connected to the non-zero pion mass. The smallness of this correction supports the hypothesis of the partial conservation of the axial current (PCAC). Let us remark that this partial non-conservation is related to the non-vanishing of the quark masses, in a way similar to the correlation between the small violation of CVC and the u and d quark mass difference (we neglected in this discussion, the small violation of the axial current conservation originating in Adler's anomaly, even in the chiral limit of massless quarks).

The derivative of the axial current is thus proportional to the small parameter, the pion mass squared. In a field theory approach, the PCAC hypothesis reads :

$$\partial_\mu A^\mu = f_\pi \, m_\pi^2 \, \phi_\pi \quad , \tag{45}$$

where ϕ_π is the pion field.

The PCAC hypothesis is thus related with a major phenomenon in QCD : the spontaneous breaking of the chiral symmetry, which determines the hadron masses. The renormalization of the axial quark current by the strong interactions being specific to every reaction, it is important to test this fundamental hypothesis in the largest number of different processes. Hence the importance of the PCAC tests in high energy neutrino reactions, complementary to the low-energy processes like β-decay and muon capture and to the results on Δ production in low-energy neutrino interactions.

3.2. Adler's theorem.

For $Q^2 = 0$, Adler has deduced from the PCAC relation (45) a prediction for the (inelastic) neutrino cross section ([Adler 1964], [Piketty 1970]).

For $Q^2 = 0$, the lepton tensor $L_{\mu\nu}$ has the form (12). In computing the neutrino cross section, the contraction of $L_{\mu\nu}$ with the vector tensor in (10) thus gives a null result, because of CVC, and all the cross section comes from the contraction with the axial tensor. Using PCAC, one finds the following relation, involving the axial tensor of (10) :

$$q_\mu A^{\mu\nu} q_\nu = f_\pi^2 \frac{1}{\sqrt{\nu^2 + Q^2}} \sigma(\pi T \to F) \quad , \tag{46}$$

$\sqrt{\nu^2 + Q^2}$ being the flux factor. With the help of (46) and neglecting the lepton mass terms (see below), one thus finds Adler's relation for the neutrino cross section, for $Q^2 \to 0$:

$$\frac{d^2\sigma(\nu T \to lF)}{dQ^2\, d\nu}\Big|_{Q^2=0} = \frac{G^2}{2\pi^2} f_\pi^2 \frac{E - \nu}{E\,\nu} \sigma(\pi T \to F) \quad , \tag{47}$$

the pion cross section on the right-hand-side being taken at the pion energy $E_\pi = \nu$.

Adler's relation gives, for $Q^2 = 0$, a direct connection between the weak neutrino-nucleon cross section and the strong pion-nucleon interaction. Neutrino scattering thus exhibits, in this particular kinematical domain, features characteristic of hadron interactions. However, this behaviour is <u>not</u> a consequence of the pion dominance of the axial current. To show this, we follow the arguments given by J.S. Bell [Bell 1971].

Let us indeed single out the pion pole contribution $T(\pi \to F)$ to the axial current, the rest of which is noted $M_\mu(J \to F)$:

$$A_\mu(J \to F) = f_\pi \frac{q_\mu}{m_\pi^2 + Q^2} T(\pi \to F) + M_\mu(J \to F) . \tag{48}$$

The lepton current l_μ is conserved (up to a small lepton mass term) :

$$q_\mu\, l^\mu \approx 0, \tag{49}$$

and the contribution of the pion pole vanishes after contraction with the lepton tensor. All the cross section thus comes from the M_μ term, which is due to heavier hadronic fluctuations and does <u>not</u> contain a pion contribution. The PCAC hypothesis thus provides a relation between the higher mass contributions to the axial current and the pion cross section; this reminds the connection given by the Goldberger-Treiman relation (44) between the pseudoscalar and the axial coupling constants.

Let us quote Bell [Bell 1971] :

We insist on this because it is sometimes said that the phenomena with which we will be concerned must a priori be restricted to a very small q^2 region 'because they are dominated by the pion pole'. This is incorrect.

To be complete, let us give the form of Adler's relation when the lepton mass terms are taken into account in (49), now exhibiting the pion pole contribution :

$$\frac{d^2\sigma\ (\nu T \to lF)}{dQ^2\, d\nu}\Big|_{Q^2 \le m_\pi^2} = \frac{G^2}{2\pi^2} f_\pi^2 \frac{1}{\nu}\ .$$

$$\left[\ \frac{E-\nu}{E} - \frac{\nu}{E}\frac{m_l^2}{m_\pi^2 - Q^2} + \frac{\nu^2}{4E^2}\frac{m_l^2\,(m_l^2+Q^2)}{(m_\pi^2+Q^2)^2}\ \right]\ \sigma(\pi T \to F)\,. \qquad (50)$$

3.3. Hadron dominance and the Piketty-Stodolsky paradox.

Let us now discuss the axial cross section for $Q^2 \neq 0$, using the hadron dominance in a way similar to (32).

In the simple hadron dominance model, the axial current contains two contributions : one due to the pion and the other due to the a_1 meson, the chiral partner of the ρ meson and the lightest $J^{PC} = 1^{++}$ meson. Neglecting again the lepton mass and thus the pion contribution, this gives for the axial cross section :

$$\frac{d^2\sigma^A\ (\nu T \to lF)}{dQ^2\, d\nu} = \frac{G^2}{4\pi^2} f_a^2 \frac{|\bar{q}|}{E^2} \frac{Q^2}{(Q^2+m_a^2)^2} \frac{1}{1-\varepsilon}\ \cdot$$

$$\left[\ \sigma^T_{a_1 \to F}(Q^2) + \varepsilon\, \sigma^L_{a_1 \to F}(Q^2)\ \right]\ , \qquad (51)$$

where m_a and f_a are the a_1 mass and coupling constant.

Let us remind that, in the vector case, the conservation of the vector current imposed the vanishing of the cross section for $Q^2 = 0$, and thus the absence of a pole in the polarized cross sections. The axial current, on the other hand, is not conserved, and the latter assertion is not true. Let us indeed identify, for $Q^2 = 0$, relations (51) and (47), noting that only the longitudinal part of the current can behave as a spinless pion; one has for $Q^2 \to 0$:

$$\frac{1}{m_a^4} f_a^2\, Q^2\, \sigma^L(a_1 \to F) = f_\pi^2\, \sigma(\pi \to F) \qquad , \qquad (52)$$

and σ^L must be singular for $Q^2 = 0$. This behaviour is obviously in contradiction with the basic assumption of the hadron dominance model, requiring no Q^2-dependance of the cross sections.

In this model, the axial current is dominated by the a_1 meson, and one can also be tempted to extrapolate Adler's relation (47), with the a_1 propagator :

$$\frac{d^2\sigma_L^A\,(\,\nu T \rightarrow 1F\,)}{dQ^2\,d\nu} = \frac{G^2}{4\pi^2}\,f_\pi^2\,\frac{|\bar{q}|}{E^2}\,\Big(\frac{m_a^2}{Q^2+m_a^2}\Big)^2\,\frac{\varepsilon}{1-\varepsilon}\,\sigma\,(\pi \rightarrow F). \qquad (53)$$

Identifying relations (53) and (51), one finds again relation (52), this time for $Q^2 \neq 0$.

Piketty and Stodolsky have shown that, in practice, relation (52) is grossly violated [Piketty 1970]. Let us indeed take $Q^2 = m_a^2$, and use Weinberg's sum rules :

$$f_a^2 = f_\rho^2 \qquad ; \qquad m_a^2 = 2\,m_\rho^2 \quad . \qquad (54)$$

Then (52) gives :

$$\frac{m_\rho^2}{\gamma_\rho^2}\,\sigma_L\,(a_1 \rightarrow F \,|\, Q^2 = m_a^2\,) = f_\pi^2\;\sigma\,(\pi \rightarrow F \,|\, Q^2 = m_a^2\,)\,. \qquad (55)$$

Using (29)-(30), one has thus approximately

$$\sigma_L\,(a_1 \rightarrow F \,|\, Q^2 = m_a^2\,) \approx \sigma\,(\pi \rightarrow F \,|\, Q^2 = m_a^2\,)\,. \qquad (56)$$

Let us take $F = \{\pi\}$. The time reversal cross sections are identical :

$$\sigma_L\,(a_1 \rightarrow \pi \,|\, Q^2 = m_a^2\,) \approx \sigma\,(\pi \rightarrow a_1 \,|\, Q^2 = m_a^2)\,, \qquad (57)$$

and one should thus expect, according to (56) :

$$\sigma\,(\pi \rightarrow a_1 \,|\, Q^2 = m_a^2\,) \approx \sigma\,(\pi \rightarrow \pi \,|\, Q^2 = m_a^2)\,, \qquad (58)$$

The Q^2-extrapolation is supposed to have a small effect, and

$$\sigma\,(\pi \rightarrow \pi \,|\, Q^2 = m_a^2\,) \approx \sigma\,(\pi \rightarrow \pi \,|\, Q^2 = -\,m_\pi^2\,) \qquad (59)$$

$$\sigma\,(\pi \rightarrow a_1 \,|\, Q^2 = m_a^2\,) \approx \sigma\,(\pi \rightarrow a_1 \,|\, Q^2 = -\,m_\pi^2\,) \quad , \qquad (60)$$

but one has experimentally

$$\sigma\,(\pi \to \pi \mid Q^2 = -\,m_\pi^2) \approx 3\ \text{mb} \tag{61}$$

$$\sigma\,(\pi \to a_1 \mid Q^2 = -\,m_\pi^2) \approx 0.1\ \text{mb} \quad , \tag{62}$$

in contradiction with (58).

In the present approach, the Q^2-extrapolation thus apparently implies important changes in the longitudinal cross section of virtual hadrons. To understand better this feature, we now turn to the dispersion relation approach.

3.4. Dispersion relations for the longitudinal cross section: multi-pole dominance.

One can try to throw some light on the source of the Piketty-Stodolsky paradox using the dispersion relation approach. As was mentioned already, in this approach the amplitudes are computed using an analytic continuation in the complex Q^2-plane of the on-mass-shell amplitudes at the poles and cuts on the real axis. The extrapolation in Q^2 of the previous section is a way of taking "effectively" into account all these contributions.

Considering the π and a_1 contributions to the axial amplitude $A_\mu(Q^2)$, one has :

$$A_\mu(Q^2) = \frac{f_\pi}{m_\pi^2 + Q^2}\, q_\mu^\pi\, T(\pi \to F) + \frac{f_a}{m_a^2 + Q^2}\, M_\mu\,(a_1 \to F) \quad , \tag{63}$$

where the on-mass-shell 4-vector q_μ^π has the components

$$q_\mu^\pi : (\nu, 0, 0, (\nu^2 - m_\pi^2)^{1/2}) \quad , \tag{64}$$

and the amplitudes $M_\mu\,(a_1 \to F)$ are connected to the scattering amplitude $M\,(a_1 \to F)$ for real a_1-mesons :

$$e^\mu\, M_\mu\,(a_1 \to F) = M\,(a_1 \to F) \quad , \tag{65}$$

the 4-vector e^μ being the polarization vector of the a_1-meson, normalized to unity :

$$e_\mu e^\mu = -1 ; \quad q_\mu e^\mu = 0 . \tag{66}$$

The amplitudes M_0 and M_3 are connected with the scattering amplitude for longitudinally polarized a_1-mesons

$$e_L^\mu \, M_\mu (a_1 \to F) = M_L (a_1 \to F) ; \tag{67}$$

using the polarization vector in the form

$$e_L^\mu : \frac{1}{m_a} ((\nu^2 - m_a^2)^{1/2}, 0, 0 ,\nu) , \tag{68}$$

one gets, neglecting small terms of the order $O (m_a^4 / \nu^4)$:

$$(1 - \frac{m_a^2}{2\nu^2}) \, M_0 (a_1 \to F) - M_3 (a_1 \to F) \approx \frac{m_a}{\nu} \, M_L (a_1 \to F) . \tag{69}$$

Putting now (63) into the PCAC condition

$$q^\mu A_\mu = \frac{m_\pi^2}{m_\pi^2 + Q^2} \, f_\pi \, T(\pi \to F) , \tag{70}$$

and neglecting small terms of the order $O (Q^2 / \nu^2)$ and $O (m_\pi^2 / \nu^2)$, one finds :

$$M_0 (a_1 \to F) - (1 + \frac{Q^2}{2\nu^2}) \, M_3 (a_1 \to F) \approx \frac{m_a^2 + Q^2}{f_a} \, \frac{f_\pi}{2\nu} \, T(\pi \to F) . \tag{71}$$

It is important to note the role of the pion pole in obtaining this result, with the on-mass-shell form (64) for q_μ^π.

The determinant of the system of linear equations (69) and (71) vanishes (up to $O (m_a^4 / \nu^4)$) for $Q^2 = m_a^2$, and a solution exists at this point when the right-hand-sides are equal, i.e.

$$\frac{f_a}{m_a} \, M_L (a_1 \to F) = f_\pi \, T (\pi \to F). \tag{72}$$

This relation leads to the one deduced by Piketty and Stodolsky (58) :

$$\sigma_L (a_1 \to F) \approx \sigma (\pi \to F). \tag{73}$$

The latter is thus not the result of the extrapolation of the Q^2-dependent cross section, the present approach being free of such assumptions. It is really the result of the hypothesis of the dominance of a single axial meson pole, combined with the PCAC relation.

Let us now consider the case of several poles. Relation (71) becomes :

$$\sum_i \frac{f_i}{m_i^2 + Q^2} \left[M_0^i (i \to F) - \left(1 + \frac{Q^2}{2\nu^2} \right) M_3^i (i \to F) \right] \approx \frac{f_\pi}{2\nu} T (\pi \to F) \ , \tag{74}$$

where the index i refers to the $i^{\underline{th}}$ pole. For each of these poles, the condition (71) holds. The system of equations (69) and (74) has for solution

$$M_0^i (i \to F) = - \frac{\nu}{m_i} \left(1 - \frac{m_i^2}{2\nu^2} \right) M_L^i (i \to F) \tag{75}$$

$$M_3^i (i \to F) = - \frac{\nu}{m_i} M_L^i (i \to F) \ , \tag{76}$$

with the relation

$$\sum_i \frac{f_i}{m_i} M_L^i (i \to F) \approx f_\pi \ T(\pi \to F) \ , \tag{77}$$

which generalizes (72). The Q^2-independence of this expression confirms the self-consistency of the present considerations.

This time, relation (77) does not suffer of the difficulties of the single pole approximation. It does not contradict the experimental data for $F = \{\pi\}$, since the cross section for pion diffractive dissociation, integrated over the masses, is of the order of the cross section for elastic scattering. On the other hand, for $F = \{a_1\}$, the (large) contribution of the diagonal amplitude $M_L (a_1 \to a_1)$ in the left-hand-side of (77) can be mostly cancelled by the presence of a number of negative non-diagonal amplitudes $M_L^{i \neq a_1}(i \to a_1)$; a similar assumption is also proposed to solve Bjorken's puzzle mentioned above.

Let us now compute the cross section for the neutrino production of the hadronic state F. Using (74) - (76) and the following forms of the longitudinal components of $L_{\mu\nu}$:

$$L_{00} = 2 E (E - \nu) - Q^2 / 2$$

$$L_{33} = \frac{\nu^2}{\nu^2 + Q^2} L_{00}$$

$$L_{30} = L_{03} = \frac{\nu}{(\nu^2 + Q^2)^{1/2}} L_{00} \ , \qquad (78)$$

one obtains for the longitudinal part of the cross section :

$$L_{\mu\nu} A_L^{\mu} A_L^{\nu} \approx L_{00} \left[A_0 - (1 + \frac{Q^2}{2\nu^2}) A_3 \right]^2$$

$$= \frac{L_{00}}{\nu^2} \left[f_\pi T(\pi \rightarrow F) - Q^2 \sum_i \frac{f_i}{m_i} \frac{1}{m_i^2 + Q^2} M_L^i (i \rightarrow F) \right]^2 \qquad (79)$$

and

$$\frac{d^2\sigma_L (\nu T \rightarrow lF)}{dQ^2 \, d\nu} = \frac{G^2}{4\pi^2} \frac{\nu}{E^2} \frac{\varepsilon}{1 - \varepsilon} \left[f_\pi \left[\sigma(\pi \rightarrow F) \right]^{1/2} \right.$$

$$\left. - Q^2 \sum_i \frac{f_i}{m_i} \frac{1}{m_i^2 + Q^2} \left[\sigma_L (i \rightarrow F) \right]^{1/2} \right]^2 . \qquad (80)$$

One has thus derived a Q^2-dependent expression for the longitudinal neutrino cross section, which coincides with Adler's relation for $Q^2 = 0$. In spite of the lack of experimental information on the values of f_i and $\sigma_L (i \rightarrow F)$, some conclusions can be drawn :

(i) A formal solution was found for the problem of joining the $Q^2 = 0$ cross section fixed by Adler's relation (47), and the high Q^2 ($Q^2 >> m_\pi^2$) behaviour of the longitudinal cross section (51). This is achieved by considering simultaneously the two parts of eq. (80).

(ii) It is seen explicitly in (80) that the Q^2-behaviour of the amplitude is not governed by the pion mass, but by the heavier hadron contributions.

(iii) For low Q^2-values, the Q^2-dependence of the amplitude can be parametrized as

$$\frac{d\sigma_L}{dQ^2} \propto \frac{m^2}{m^2 + Q^2} \ , \qquad (81)$$

where m is some effective mass, which can be obtained from expression (79) using (77) :

$$\frac{1}{m^2} = < \frac{1}{m_i^2} > \ , \qquad (82)$$

where

$$< \frac{1}{m_i^2} > = \frac{\sum_i f_i \, M_L(i \to F)/m_i^3}{\sum_i f_i \, M_L(i \to F)/m_i} \quad . \tag{83}$$

For $F = \{\pi\}$, m^2 is in the vicinity of the center of gravity of the mass distribution for pion diffractive dissociation, i.e around $m \approx 1.1$ GeV.

In the low Q^2-region, the longitudinal cross section can thus be parametrized (keeping the lepton mass terms) as :

$$\frac{d^2\sigma_L \, (\nu T \to 1F)}{dQ^2 \, d\nu} = \frac{G^2}{4\pi^2} f_\pi^2 \frac{|\vec{q}|}{E \, (E - \nu)} \frac{\varepsilon}{1 - \varepsilon} \quad .$$

$$\left[\frac{E - \nu}{E} \left(\frac{m^2}{Q^2 + m^2} \right)^2 - \frac{\nu}{E} \frac{m^2}{Q^2 + m^2} \frac{m_\mu^2}{Q^2 + m_\pi^2} + \frac{\nu^2}{4E^2} \frac{m_\mu^2 \, (Q^2 + m_\mu^2)}{(Q^2 + m_\pi^2)^2} \right]$$

$$. \sigma \, (\pi \to F) \quad . \tag{84}$$

(iv) If the mass spectrum is limited by some maximum value m_M, then the longitudinal cross section has the following behaviour for $Q^2 >> m_M^2$:

$$L_{\mu\nu} A_L^\mu A_L^\nu \underset{Q2 >> m_M^2}{\approx} \frac{L_{00}}{\nu^2} \frac{1}{Q^4} \left[\sum_i f_i \, m_i \, M_L(i \to F) \right]^2 . \tag{85}$$

(v) The transverse cross section being given in (51), the ratio $R(Q^2) = \sigma_L(Q^2) / \sigma_T(Q^2)$ thus increases for low Q^2-values, and decreases as

$$R(Q^2) \sim 1/Q^2 \tag{86}$$

for Q^2-values much higher than the relevant hadron masses.

4. Vector - axial-vector interference.

Piketty and Stodolsky have established an upper limit for the contribution of the ρ - a_1 interference term in (10) :

$$\frac{d^2\sigma^{VA}\,(\,\nu T \rightarrow 1F\,)}{dQ^2\,d\nu} \leq \frac{G^2}{\pi^2}\;\frac{2E - \nu}{2E^2}\;\frac{f\rho\, fa}{(Q^2 + m_\rho^2)\,(Q^2 + m_a^2)}\;\cdot$$

$$Q^2\,[\,\sigma_T(\rho \rightarrow F).\,\sigma_T(a_1 \rightarrow F)\,]^{1/2}\,. \quad (87)$$

(Note that a kinematical factor is corrected with respect to [Piketty 1970]). This interference term is usually small, and relevant only in cases where the same final state F can be produced by a ρ or an a_1 meson. It is worth nothing that in the case of neutrino production of a single pion ($F = \{\pi\}$), the vector and the axial vector contributions do not interfere. Indeed, the former amplitude is dominated by pion exchange, and is thus (mostly) real, whereas the latter is diffractive, i.e. imaginary. As a result, π^+ production by neutrinos and π^- production by antineutrinos should coincide.

III. NEUTRINO INTERACTIONS ON NUCLEONS.

We begin the review of experimental data by the (scarce) results obtained in low Q^2, high ν neutrino and antineutrino interactions on nucleons.

1. Total cross section and PCAC.

The total cross section was compared to the predictions from Adler's theorem and Piketty-Stodolsky's model by two experiments.

i. At the CERN PS.

In the PS neutrino beam, at CERN, a total of 393 charged current neutrino interactions with $p_\mu > 1$ GeV were collected in 1967 in the HLBC bubble chamber filled with propane. A first analysis [Bonetti 1969] showed an agreement with the PCAC prediction, for $Q^2 \leq 0.1$ GeV^2 (22 events). The data with $Q^2 \leq 0.3$ GeV^2 were subsequently compared with the Piketty-Stodolsky model, including the transverse axial current and the vector current contributions, showing again a good agreement (Fig. 3) [Masnou 1972].

ii. At the CERN SPS.

The second experiment is due to the WA21 Collaboration (Birmingham, CERN, Imperial College London, MPI Munich, Oxford, University College London), which collected from 1977 to 1983 about 20 000 neutrino and 11 500 antineutrino charged current interactions with $p_\mu > 5$ GeV, in the SPS wide band beam at CERN [Jones 1987]. The detector was the bubble chamber BEBC (with a fiducial volume of 19 m^3), filled with hydrogen and equipped with an external muon identifier (EMI).

Fig. 4 shows the Q^2-distribution of the total number of events with $\nu > 2$ GeV : 795 (109) neutrino events and 442 (38) antineutrino events have $Q^2 < 0.6$ (0.1) GeV^2. The ν- and E- distributions for the events with $Q^2 < 0.1$ GeV^2 and $\nu > 2$ GeV are shown in Figs. 5-6. The distributions are corrected for the scanning and measurement inefficiencies, for the muon momentum cut, for the EMI background and losses, and for the contributions of strangeness-and charm- changing reactions.

The data are compared with the predictions of the Piketty-Stodolsky model (eq. (31)-(51)). For the longitudinal axial cross section, a form slightly different from rel. (84) was used, but this has only a minor effect. (A discussion of the details of the cross section used can be found in [Marage 1991b]). The smearing effects due to measurement errors and neutral particle losses have been included.

The agreement between the predictions and the data is excellent for $Q^2 < 0.1$ GeV^2, where the longitudinal part of the axial current dominates (curve 1. on Fig. 4); little uncertainty affects the model in this region. This measurement thus provides a good test of Adler's theorem and of the CVC and PCAC hypotheses.

For $0.1 < Q^2 < 0.6$ GeV^2, the agreement between the data and the Piketty-Stodolsky model is quite good for the neutrino data, but less satisfactory for the antineutrino data. However, several uncertainties affect the details of the model (e.g. virtual pion cross section and longitudinal cross section) and the treatment of the data (e.g. low multiplicity events). The general picture is thus in reasonable agreement with the hadron dominance model.

2. Single pion production.

Abundant data have been collected for single pion production by charged and neutral current interactions of neutrinos and antineutrinos on protons and neutrons, in bubble chamber experiments, at low and high energy, at CERN, FNAL and Serpukhov (see [Allasia 1990], [Grabosch 1989], [Jones 1989], [Rein 1987], and references therein). Most studied were the charged current interactions on protons :

$$\nu + p \rightarrow \mu^- + p + \pi^- \qquad (88)$$

$$\bar{\nu} + p \rightarrow \mu^+ + p + \pi^+ \quad . \qquad (89)$$

Interactions on neutrons were also studied, in particular by the WA25 Collaboration (Amsterdam, Bologna, Padova, Pisa, Saclay, Torino), which collected from 1979 to 1983 about 22 000 neutrino and 15 000 antineutrino charged current interactions ($p_\mu > 5$ GeV) on deuterium in BEBC, at the CERN SPS.

Fig. 7 shows the hadronic invariant mass distributions for reactions (88) and (89), obtained by the WA21 Collaboration [Allen 1986]. Reaction (88) is dominated by the production of the Δ^{++} (1232) resonance, whereas reaction (89) is due, for $W < 2$ GeV, to several resonance production (see also the WA25 data on deuterium in [Allasia 1983] and [Allasia 1990]).

The discussion of resonance production, for low ν-values, is outside the scope of the present review. Let us mention, however, that a good test of the PCAC hypothesis is provided by Δ resonance production, for $\nu < 0.7$ GeV. In particular, a good agreement with the PCAC-based predictions for the Q^2-distribution is observed by the WA21 Collaboration, for neutrino and antineutrino interactions, as shown by the solid lines on Fig. 8, the dashed lines corresponding to a model with a conserved axial current [Jones 1989]. For the entire domain with $W < 2$ GeV, the resonance production model of Rein and Sehgal, including the PCAC hypothesis [Rein 1981a], gives a good description of the data (see the analysis by [Rein 1987] of the WA21 antineutrino data of [Allen 1986]; see also the deuterium data of [Allasia 1990]).

Beyond the resonance region ($W > 2$ GeV), data are available from the WA21 Collaboration, corresponding to 2/3 of their final statistics [Allen 1986] and from the WA25 Collaboration [Allasia 1990]. The WA21 data were reanalysed by D. Rein [Rein 1986], and compared with predictions for the diffractive scattering of the longitudinal component of the axial current (those predictions, however, did not contain any correction for smearing effects). Some features of the data tend to confirm this interpretation : similarity of the cross sections for neutrinos and antineutrinos; W^2-dependence of the total cross section, at least for $W^2 > 8$ GeV^2 (see Fig. 9); peaking of the $z_\pi = E_\pi/\nu$ distribution for $z_\pi \rightarrow 1$. However, the $|t|$-distribution is wider than was expected (t is the 4-momentum transfer to the recoil proton), and the Q^2-distribution is also wider, especially in the antineutrino case (for details, see [Marage 1991b]). The WA25 data for ν and $\bar{\nu}$ single pion production protons, with $W > 2$ GeV, are reported to give cross sections, $|t|$-and Q^2-distributions compatible with the results of WA21 [Allasia 1990]. The authors tend to explain the $|t|$-distribution by one pion Regge exchange. However, single pion production is indeed mainly due to the scattering of the axial current, which is of diffractive type, and for which one pion exchange is forbidden. Moreover, the slope of the t-distribution for diffractive dissociation is known to be less than 1/2 of the elastic one; in the reaction $p + p \rightarrow p + X$ for instance, $B = 4$ GeV^{-2} [Kazarinov

1976]. This is connected with the absence of the form factor at the inelastic vertex of the Pomeron exchange diagram. On the other hand, a careful analysis of the complete data sets should include a study of the effects of the smearing and of more severe cuts in W and ν, in order to decrease the influence of resonance production.

3. Diffractive production of (axial) vector mesons.

In the framework of the vector-meson dominance model, ρ meson diffractive production should provide a test of the CVC hypothesis in the case of the weak interactions. Theoretical predictions were made by Piketty and Stodolsky [Piketty 1970], Gaillard, Jackson and Nanopoulos [Gaillard 1976], Chen, Henyey and Kane [Chen 1977], Bartl, Fraas and Majerotto [Bartl 1977], and Gaillard and Piketty [Gaillard 1977] (Note that a normalization factor 1/2 is missing in [Gaillard 1976], and a factor 2 in [Chen 1977]). Few results, with rather low statistics, were obtained at high energy.

(i) The Fermilab - Berkeley - Hawaii - Michigan Collaboration studied the reaction

$$\nu + p \rightarrow \mu^- + p + \rho^+ \quad ; \quad \rho^+ \rightarrow \pi^+ + \pi^o \qquad (90)$$

in the 15' Bubble Chamber at Fermilab, filled with hydrogen, among 3 000 charged current interactions. A total of 16 events of type (90) were selected using a kinematical fit, of which 3 were attributed to background. The corresponding cross section was $(8 \pm 3).10^{-40}$ cm^2/nucleon [Bell 1978].

(ii) The WA21 Collaboration selected events corresponding to reaction (90), in the first part of their data; the measured cross section was $(6 \pm 2).10^{-40}$ cm^2/nucleon [Morrison 1978].

(iii) The E180 Collaboration (Fermilab, IHEP Serpukhov, ITEP Moscow, Michigan) studied the reaction

$$\bar{\nu} + N \rightarrow \mu^+ + N + \rho^- \quad ; \quad \rho^- \rightarrow \pi^- + \pi^o \ , \qquad (91)$$

among their 6 000 charged current antineutrino interactions on neon, in the 15' Bubble Chamber [Ammosov 1984]; 16 events were attributed to reaction (91), of which 6 were due to background, corresponding to a cross section of $(13 \pm 6).10^{-40}$ cm^2/nucleon after

correction for several losses. However, this figure does not take into account the coherent ρ production on neon nuclei, which could correspond to some 7.10^{-40} cm^2/nucleon (see section V. 3). The cross section for diffractive ρ production on nucleons is thus probably of the order of (6 to 8 ± 4).10^{-40} cm^2/nucleus.

These three results, obtained in beams with comparable energy spectra, are thus close to each other. They are lower but not incompatible with the theoretical estimates quoted in [Bell 1978] : 12.10^{-40} cm^2/nucleon for [Gaillard 1976], (from 5 to 9).10^{-40} cm^2 for the different models of [Chen 1977], and 14.10^{-40} cm^2 for [Bartl 1977] (the corrections for the missing normalization factors are included). It is clear, however, that these analyses suffer of their low statistics, and of the absence of comparison of the differential distributions with the model predictions.

The a_1 or ρπ diffractive production on protons has been studied by the WA25 Collaboration in the charged pions channels

$$\nu + p \rightarrow \mu^- + p + \pi^+ + \pi^+ + \pi^- \qquad (92)$$

$$\bar{\nu} + p \rightarrow \mu^+ + p + \pi^+ + \pi^- + \pi^- \quad . \qquad (93)$$

The effective mass of one of the $\pi^+ + \pi^-$ combinations had to satisfy the condition $0.47 < M^2_{\pi\pi} < 0.78$ (GeV/c^2)^2. Events with a pπ combination within ± 50 MeV/c^2 around the Δ mass were removed in order to discard the contribution of the process

$$\nu + p \rightarrow \mu + \Delta + \pi + \pi$$

$$\qquad\qquad \downarrow \rightarrow p + \pi \quad . \qquad (94)$$

The signal results in a combined cross section of (18 ± 4).10^{-40} cm^2, averaged over the $\nu / \bar{\nu}$ incident energy interval. The diffractive model is claimed to predict a number of events 'considerably larger' than the observed value. This claim is difficult to understand. Indeed, the diffractive model predicts a cross section of the order of (5 - 7).10^{-40} cm^2 for E ~ 30 GeV, for $f_a = f_\rho$ as suggested by Weinberg's sum rule (see [Bartl 1977], Fig.4).

The slope of the | t |-distribution of the events with $M_{3\pi} < 1.6$ GeV/c^2 is B = -3.4 GeV^{-2} (no error is quoted). The authors claim that this is another indication that the ρπ systems are not diffractively produced. As was mentioned already, the slope of the t-distribution for diffractive dissociation is about 1 / 2 of that for elastic scattering. On the other hand, the relevant quantity to plot is $t' = |t| - t_{min}$ (see section V), in order to discard the purely kinematical increase of | t | due to the creation of a heavy state by the virtual intermediate boson. Secondly, it is useful, in order to extract the diffractive signal, to fit the

t'-distribution as the sum of two exponentials, corresponding respectively to the contributions of the diffractive process and of the background. Finally, one should also consider the possible broadening of the distribution due to instrumental smearing effects.

In the present stage, the analysis of the WA25 data has thus not provided enough details for a complete discussion of the production mechanisms.

Let us also mention that [Bell 1978] and [Morrison 1978] quote upper limits for a_1 production, but in view of the low statistics, these limits are of little significance.

4. Conclusions.

The main result of this chapter concerns the study of the total cross section of neutrinos and antineutrinos on protons, with $Q^2 < 0.1$ GeV^2 : this provides a good test of Adler's theorem and of the CVC and PCAC hypotheses, with little model uncertainty. For $0.1 < Q^2 < 0.6$ GeV^2, the data show also reasonable agreement with the hadron dominance model of Piketty and Stodolsky.

Another good test of the PCAC hypothesis,- although beyond the scope of this review-, is provided by the study of Δ (1232) resonance production, by neutrino and antineutrino charged current interactions. For $W > 2$ GeV, single pion production in charged current interactions exhibits features attributed to the diffractive scattering of the longitudinal component of the axial current, but the analysis is not really convincing. One must hope for a new analysis of the complete data sample by the WA21 Collaboration.

Finally, a few results were obtained on diffractive ρ and $\rho\pi$ (possibly a_1) production.These results suffer from limited statistics or from the absence of a detailed discussion of the differential distributions. A careful analysis of the complete data, especially on hydrogen, could still provide useful information in this field.

IV. TOTAL CROSS SECTION ON NUCLEI : SHADOWING AND PCAC.

1. Introduction.

Already in 1964, inspired by Adler's theorem, Bell predicted that, for small Q^2-values, the total neutrino-nucleus cross section should be attenuated, and reveal the existence of "shadowing", like in the case of hadron-nucleus interactions [Bell 1964].

Not less than 25 years were required to obtain an experimental confirmation of this basic prediction. Meanwhile, it had been applied to photon interactions, in the framework of vector-meson dominance models [Stodolsky 1967], leading to an abundant theoretical and experimental literature (see [Grammer 1978], [Bauer 1978] and ref. therein; see also below).

The propagation of hadrons in nuclear matter is characterized by a mean free path l_h, typically of the order of 2.4 fm for a hadron-nucleon cross section σ_{hN} of 25 mb and a nucleon density n of 1 nucleon / 6 fm^3 :

$$l_h = 1 / \sigma_{hN} \cdot n \, . \tag{95}$$

The nuclear radius being of the order of

$$R \approx r_0 A^{1/3} \quad , \quad r_0 \approx 1.2 \text{ fm} \, , \tag{96}$$

where A is the atomic mass number, an incident hadron wave is thus strongly absorbed on the outer face of the nucleus, and is much attenuated when it reaches the nucleus core, even for light nuclei. This effect, known as "shadowing", implies that the interaction cross section on a nucleus σ_{hA} is smaller than the sum of the cross sections on the constituent nucleons :

$$\sigma_{hA} = A_{eff} \cdot \sigma_{hN} \quad ; \quad A^{2/3} < A_{eff} < A \quad ; \tag{97}$$

the limit $A_{eff} = A^{2/3}$ would only be attained if the ratio $R/l_h \rightarrow \infty$, i.e. if the surface absorption was complete.

Photons and neutrinos, on the other hand, have small cross sections and can propagate with very small attenuation through large amounts of matter : the mean free path in the nuclear matter of a 1 GeV neutrino is of the order of a cm! However, their interactions can also be shadowed due to the fluctuation of the incident state into a hadronic state, which interacts strongly with the nuclear matter. This is thus a purely quantum-mechanical effect.

Before discussing the neutrino experimental results, let us briefly survey the results obtained for electromagnetic interactions.

2. Shadowing in electromagnetic interactions.

2.1. The Glauber-Gribov model.

The Glauber-Gribov model ([Glauber 1955], [Gribov 1969a]) provides the basis for the interpretation of interactions on nuclei of hadrons, photons and neutrinos. We briefly introduce it here.

Glauber 's model aims at describing the nuclear cross section in terms of two-body interactions with the constituent nucleons. The fundamental hypothesis is that the scattering on the nucleus can be described as a succession of independent scatterings on nucleons, with free movement between two collisions. It thus implies that the nucleus phase shift is the sum of the constituent nucleon phase shifts, or else that the nuclear profile function is the product of the nucleon profile functions. Gribov underlined the necessity of adding inelastic corrections to Glauber's approximation, to take into account the propagation through the nucleus of the whole hadronic wave packet, since the hadron has no time to form its wave function between two interactions.

Let us consider the elastic (Compton) scattering on a nucleus, which is related to the total cross section through the optical theorem. At first order, the nuclear cross section is just the sum of the nucleon cross sections, and there is no shadowing. However, one also has to consider the effect of the following two-step process : the photon interacts on a first nucleon to produce a vector meson which then interacts on a second nucleon in such a way as to yield a photon. The latter being reintroduced into the incident beam, the total cross section is thus decreased (at the condition that the phases are essentially unchanged). In the framework of the vector meson dominance model, one finds that a part of this two-step contribution exactly cancels the first order contribution; the elastic photon-nucleus cross section is then proportional to the hadron-nucleus cross section, and shadowing shows up. The destructive interference between one-step and two-step contributions, however, only takes place if the phase difference exp ($i\Delta_L z$) between them is negligible, Δ_L being the longitudinal momentum transfer to the nucleon :

$$\Delta_L = k - k_{VL} = 1/l_c \approx \frac{Q^2 + m_v^2}{2\nu} = x M (1 + \frac{m_v^2}{Q^2}) \qquad (98)$$

At low energy, this phase difference cannot be neglected, and shadowing is incomplete.

Let us thus summarize the conditions of the appearance of shadowing :

1. The nucleus dimensions must be large compared to the average mean free path l_h of the hadron in nuclear matter :

$$R >> l_h. \qquad (99)$$

For mesons with $\sigma_{hN} \sim 25$ mb, this condition is partially fulfilled even for light nuclei.

2. The coherence condition needed for the cancellation of the one-step contribution is

$$l_c >> l_h \ , \qquad (100)$$

with l_c given by (98). This is really the high energy condition (32)-(33), which expresses the requirement that the fluctuation must have a sufficient life time for the photon to interact through its hadronic components. For real photons fluctuating into ρ mesons, this condition reads

$$\nu > 3.6 \text{ GeV} \quad . \qquad (101)$$

2.2. Beyond the simple VMD model.

Generalized vector dominance models were used to predict the Q^2-evolution of shadowing, for small x-values (see condition (100) and l_c definition (98)). The off-diagonal model of Fraas, Read and Schidknecht [Fraas 1975a] was applied to scattering on nuclei by Ditsas, Read and Shaw ([Ditsas 1975], [Ditsas 1976]). For these authors, the presence of inelastic corrections tends to decrease the shadowing effects, because of the alternating signs of the coupling constants of the heavy states, introduced in order to explain the compensation effects responsible for the scaling behaviour of the cross section (see section II. 2.4.). In the diagonal model of [Schildknecht 1973], the effective decrease of the heavy state cross section has the same consequence.

In the framework of the parton model, Nikolaev and Zakharov explain the shadowing by parton coalescence ([Kancheli 1973], [Nikolaev 1975], [Zakharov 1975]). In the "infinite momentum frame" (Breit frame), the target nucleus appears as rapidly moving. Because of the relativistic contraction of longitudinal distances, the nucleus depth becomes comparable to the parton delocalization for small x-values ($x < x_0 \approx 0.05 - 0.10$), due to the uncertainty principle. The partons from several nucleons thus superimpose and recombine, and the number of small x partons on which the interaction takes place is proportional to $R^2 = A^{2/3}$; so is also the cross section. In this model, the conservation of the total momentum of the partons which recombined induces an increase of the number of partons with $x > x_0$, and thus the presence of antishadowing.

In the last years, several authors discussed the theory of shadowing in the framework of pertubative QCD, for $Q^2 >$ a few GeV^2. All these analyses recognize the role of parton coalescence at small x, but disagree concerning the Q^2-evolution of shadowing and the existence of antishadowing (see [Nikolaev 1990], [Brodsky 1990], [Frankfurt 1989], [Kwiecinski 1988], [Qiu 1987]).

2.3. Experimental data.

Shadowing has been abundantly studied in real photon interactions on several nuclei, in total cross section as well as in Compton cross section measurements (see the reviews [Grammer 1978] and [Bauer 1978]). Fig. 10 shows the progressive show up of shadowing in total cross section measurements, as required by the high-energy condition (100)-(101). A high energy experiment, with photon momenta between 45 and 82 GeV [Cadwell 1979] reports a continuous increase of shadowing with ν (see Fig. 11) : this feature is attributed by the authors to the effect of inelastic corrections, similarly to the case of hadron scattering (see section. II. 2.4.).

For virtual photons, the condition (99) and the form (98) for l_c suggest that shadowing should show up even at high Q^2-values, for small x-values. In spite of several measurements, the situation however remained somewhat confused (see references in [Grammer 1978], [Bauer 1978] and [Franz 1981]; see also measurements in [Stein 1975], [Franz 1981], [Miller 1981], [Goodman 1981]). The discovery of the EMC effect in 1983 [Aubert 1983] added to the confusion, but triggered a new series of measurements ([Bodek 1983a,b], [Arnold 1984], [Bari 1985], [Benvenuti 1987]). With a new high statistics

experiment on several nuclei, the EMC Collaboration has definitely established the existence of shadowing for small x- and small Q^2-values (see Fig. 12 [Ameodo 1988]) as well as for small x- and high Q^2-values (see Fig. 13 [Ashman 1988]).

It should be noticed that, in principle, the EMC results do not contradict the GVD models, which take into account the existence of heavy states; this is shown in [Bilchack 1988] and [Bilchack 1989] for Schildknecht's diagonal model, and in [Shaw 1989] for the non-diagonal model of Ditsas, Read and Shaw. However, these models cannot be tested in detail, since the data are not precise enough to study the Q^2-evolution of shadowing for a given x-value. For the same reason, the present data also cannot distinguish between the several QCD-based models, which do not provide very different predictions in the measured Q^2-range.

3. Shadowing in neutrino interactions.

3.1. Low energy experiments.

At the end of the '60's, two experiments studied neutrino-nucleus cross sections, in view of testing Bell's prediction of shadowing. They used the CERN neutrino beam, obtained from interactions of the 21 GeV protons from the PS, with a maximum of the neutrino flux around 1.5 GeV.

The first experiment [Bauer 1969] used C, Al, Fe and Pb plates, in alternance with spark chambers, followed by a concrete absorber, magnetized iron plates and spark chambers, for muon identification and momentum measurement. The data consisted of 3 350 charged current interactions ($p_\mu > 1$ GeV, $< Q^2 > \approx 0.3$ GeV^2). The ratios of the cross sections on the various nuclei, shown in Fig. 14, do not exhibit the $A^{2/3}$ dependence (unrealistically) expected by the authors, but are compatible with 1. For the 183 interactions on C and Pb with $Q^2 < 0.1$ GeV^2, the ratio $R(C / Pb) = 0.92 \pm 0.15$.

The other experiment [Holder 1970] used Al spark chambers, surrounded by a Pb wall. The cross section ratio is compatible with 1 for all the considered domain ($0 \leq \theta_{\mu\nu} \leq 25°$).

Anticipating on the discussion below, one can ascribe these negative results to the difficulty to select the very small Q^2-values ($Q^2 < 0.1$ GeV^2), where the longitudinal component of the axial current dominates. Indeed, only the latter is shadowed for the low ν-values available in these experiments, whereas the vector current and the transverse axial current contributions, which dominate for higher Q^2-values, are only weakly shadowed. This was noted already in 1970 by Bell and Llewellyn-Smith [Bell 1970].

3.2. The BEBC experiment.

Positive results were finally obtained in 1989 [Allport 1989], by combining the data of two experiments performed in the wide band neutrino and antineutrino beams, produced by the interaction of the 400 GeV protons of the CERN SPS; the detector was the bubble chamber BEBC equipped with an external muon identifier :
- the WA59 experiment (Bari, Birmingham, Brussels, CERN, Cracow, Demokritos-Athens, Ecole Polytechnique-Palaiseau, Imperial College London, MPI-Munich, Oxford, Rutherford, Saclay, Stockholm, University College London) collected in 1980 about 9500 neutrino and 16000 antineutrino charged current interactions ($p_\mu > 5$ GeV), in a 75 mole % neon-hydrogen mixture;
- the WA25 experiment, on deuterium.

For the shadowing analysis, about 20000 neon and 16000 deuterium interactions were used, which had been taken in very similar beam extraction and energy spectrum conditions. Great care was taken to avoid systematic effects related to the different experimental conditions, e.g. for neutral particle detection (photon materialisation, neutron and K°_L interactions), secondary interactions in the liquid of charged particles, and measurement quality. In particular, the incident neutrino energy was estimated using only the charged particles, and the event sample was restricted to the well-controlled $15 < E_\nu < 160$ GeV region (see [Cooper 1984], [Guy 1987]).

Fig. 15 shows the Q^2-dependence of the neon to deuterium ratio of the cross sections per nucleon, for $x < 0.2$, for neutrinos and antineutrinos separately, and for the two samples combined. The normalization assumes the equality of the total cross sections per nucleon, integrated over the two complete samples. The full curve represents the predictions for shadowing of Bell's optical model, which describes the effect of nuclear matter on the amplitude of the virtual hadron wave accompanying the incident lepton ([Bell 1964], [Bell

1971]). For the combined samples with $Q^2 < 1$ GeV^2, the χ^2-value corresponding to no shadowing ($A_{eff}/A = 1$) is 21.3/4 degrees of freedom, whereas it is 4.2 for the model prediction. This difference in χ^2 of 17.1 corresponds to a 4.1 σ effect.

Fig. 16 presents the ratio of the cross sections on Ne and D in function of x for several Q^2-intervals. In view of the statistical imprecision, little information on the x- and Q^2-dependence of the shadowing can be obtained from this figure, but the data are certainly compatible with the model predictions (solid curves).

Fig. 17 shows the cross section ratio for $x < 0.2$ and $Q^2 < 0.2$ GeV^2, in function of ν and W. One notices that shadowing shows up already for the smallest ν- and W-values.

A special attention was paid to check the possible influence of phenomena, like coherent meson production, which might affect the cross section ratio for small x- and Q^2-values; imposing appropriate cuts, it was shown that the effect was not modified in any systematic or significant way. It was also shown that it is not dependent on the chosen energy correction method, nor is it modified by effects related to the Fermi motion, to the nuclear reinteractions or to the measurement errors.

It is thus a firm conclusion of this analysis that the cross section per nucleon on neon nuclei is lower than on deuterium, for small x- and Q^2-values. This establishes the existence of shadowing in neutrino interactions.

3.3. Interpretation of the BEBC results - a PCAC test.

The most striking feature of the BEBC data is the show up of shadowing already for the smallest ν-values (Fig.17), in contrast with the electromagnetic case where shadowing only completely develops for ν-values of a few GeV (cf. Fig.10).

One knows, of course, from Adler's theorem that the neutrino has to behave like a pion as $Q^2 \rightarrow 0$, without energy condition. The observation of shadowing at low energy is thus a consequence of PCAC.

However, one also knows that the pion component of the axial current (for $Q^2 \rightarrow 0$, one has to consider only the axial current) has a negligible contribution to the cross section (proportional to the outgoing lepton mass squared). Shadowing is thus due to the non-pionic

contribution to the axial current, and one might have expected the high energy condition (100) to apply, with an axial mass of the order of 1 GeV in (98).

The solution of this paradox can be found in the framework of the Glauber-Gribov model, by considering the inelastic corrections [Kopeliovich 1989]. Let us indeed consider simultaneously, for $Q^2 = 0$, the one-step contribution of Fig. 18a to the elastic scattering, and the first inelastic correction in the two-step process of Fig. 18b, where pion production takes place in the intermediate stage; the elastic scattering is related to the total cross section through the optical theorem. Formally, one is in a case similar to that of photon interactions discussed in section 2.1. Applying Adler's relation between neutrino and pion cross sections, one finds that the volume term [$\propto A\, \sigma_{tot}(\nu N)$] from the one-step process is exactly cancelled by a part of the two-step process, leaving only a contribution proportional to the pion-nucleus cross section; as in the photon case, this is true if a coherence condition holds. One thus finds with no surprise that, given this condition, the validity of Adler's theorem for interactions on nucleons implies its validity for interactions on nuclei. However, the coherence condition (100) now applies to the longitudinal momentum transfer to the pion, and the pion mass appears instead of the vector meson mass in (98). The coherence condition is thus already satisfied for very small ν-values.

For $Q^2 \neq 0$, the contributions to the cross section of the vector current and of the transverse component of the axial current increase rapidly (both vanish for $Q^2 = 0$). In the hadron dominance model, these contributions are dominated by the ρ and a_1 mesons (or non-resonant $\rho\,\pi$ systems); in these cases, the high energy condition holds with the ρ and a_1 masses in (98). For intermediate ν-values, those contributions thus show a reduced shadowing. As for the longitudinal component of the axial current, the presence of the Q^2 term in (98) also reduces the shadowing when compared to the case with $Q^2 = 0$.

In spite of the formal similarity, let us stress again the difference between the photon and the neutrino cases. Photons require high energy to convert into hadronic states, responsible for shadowing, long before the interaction. Neutrinos emit heavier fluctuation, but shadowing takes place at much lower energies. This is because, in spite of the impossibility of spontaneous pion emission by neutrinos, pions can be diffractively produced on a bound nucleon at low energy, and propagate for a long time (if Q^2 is small). Only at higher energy appears an additional contribution to shadowing, coming from the production of heavier states, like for photon interactions; this provides only a correction to the main effect.

The WA59 Collaboration evaluated quantitatively the effects discussed here, using Bell's optical model. Using the PCAC prescription concerning the coherence condition, one finds the full curves on Fig. 15-17, which are in agreement with the data. (Note that Bell's

model predicts insufficient shadowing for the very low ν-values, compared to the Glauber-Gribov model prediction (see [Kopeliovich 1989]). However, this difference is not significant for the interpretation of the present data, in view of their statistical precision).

In conclusion, the comparison of the neutrino cross sections on neon and deuterium in BEBC provides a demonstration of the existence of shadowing in neutrino-nucleus interactions for low Q^2-values. These data confirm the role of the inelastic corrections, in the framework of the Glauber-Gribov approach : although the pion component of the axial current itself does not contribute significantly to the cross section, shadowing is explained by the diffractive production of a pion by the longitudinal axial current on a first nucleon, followed by the inverse process on a second nucleon. In addition, the quantitative agreement between the predicted and observed sizes of the effect confirms that the first inelastic correction is governed by the f_π coupling constant, and thus provides a test of Adler's theorem and of the PCAC hypothesis.

V. COHERENT INTERACTIONS ON NUCLEI.

1. Introduction.

1.1. General characteristics.

Coherent diffractive interactions of (anti)neutrinos on nuclei, which were the subject of intense studies in the last few years, provide a striking illustration of quantum mechanics in two ways. Firstly, by the fact that coherent interactions on nuclei are, in general, an example of the effects of wave-particle duality : they are the result of constructive interferences between the scattering amplitudes of the incident wave on the various nucleons in the target, which cooperate in such a way that the effect produced on each of them is enhanced by the presence of the others. Secondly, by the fact that diffractive scattering is the result of strong absorption, whereas neutrinos have a very small cross section : as in the case of shadowing, the strong interaction features in coherent scattering are the result of the uncertainty principle, which allows non-conservation of energy for times at least comparable to the interaction time, and the appearance of hadronic fluctuations.

Maximum constructive interferences, in the case of coherent interaction (see e.g. [Stodolsky 1970]), imply that the distortion of the incident wave by the nucleus must be small enough, so that all nucleons react in phase. In other words, the momentum transfer

$$\vec{k} = \vec{q} - \vec{q'} \qquad (102)$$

between the incident and scattered waves can only induce a small phase difference between two nucleons in a nucleus of radius R, whence the condition

$$|\vec{k}| R < 1 \ . \qquad (103)$$

Coherent interactions are also characterized by the fact that the nucleus recoils as a whole, without break up, since the effect of the incident wave must be approximately the same on all nucleons. If this were not the case, the numerous final states would combine in a random way, the cooperative effects between nucleons would be destroyed, and coherence would disappear. The momentum transmitted to any nucleon must thus be small enough that it remains bound in the nucleus. To fix the ideas, let us consider the case of neon nuclei ($R \approx 3$ fm) : condition (103) implies

$$|\vec{k}| < 1/R = 1/3 \text{ fm}^{-1} \approx 65 \text{ MeV}, \quad (104)$$

well below Fermi momentum ($\leq$ 230 MeV for neon). The kinetic energy acquired by the nucleon is

$$T = \frac{|\vec{k}|^2}{2M} \lesssim 2 \text{ MeV}. \quad (105)$$

The fact that the nucleus has to recoil as a whole, unaltered, has also important consequences on the mechanisms at work in coherent interactions, imposing specific selection rules and allowing to select reactions which would otherwise remain intricated in the background.

i. The transfer of charge or any additive quantum number is forbidden : this would single out a specific nucleon, and destroy cooperative effects. In particular, the third component of isospin of the exchanged state must be 0.

ii. The total isospin I of the exchanged state must be zero as well; this excludes e.g. π°, ρ° or a_1° transfer. Indeed, the operator I_3 induces amplitudes with different signs on neutrons and protons, resulting in a null effect on nuclei with total isospin I = 0. (In the case of interactions on heavy nuclei, with a neutron number slightly in excess to the proton number Z, processes with isospin exchange are suppressed by a factor (1 - 2 Z / A) in comparison with zero-isospin exchange).

iii. Similarly, the nuclei can be considered as having total spin J = 0; the effects of the spin operator σ_3 on nucleons with spins up and down then cancel (if the nucleus has spin S, spin terms in the coherent amplitude are suppressed by a factor S / A). When the scattered particle is emitted in the forward direction - which is generally the case as will be seen - coherent interactions thus conserve helicity.

iv. For forward scattering, the spin and parity of the initial and final hadron states ($s_{i,f}$ and $P_{i,f}$) must be related by the Gribov-Morrison rule

$$P_f = P_i \, (-1)^{s_i - s_f} \quad . \quad (106)$$

For non-zero scattering angles, processes violating this rule are suppressed by a factor $\sin^2\theta \leq (1 / R_A \nu)^2$ (since $k_T \approx \nu \sin\theta \leq 1 / R_A$)

1.2. Coherent cross section

To be specific, let us consider the coherent reaction of Fig.19. The 4-momentum transfer q $(\nu, \vec{q})$ takes place at the lepton vertex. A meson h with momentum q' and mass m_h is created. The 4-momentum k transmitted to the nucleus is space-like :

$$t = k^2 = -|t|; \tag{107}$$

k_L and $\vec{k_T}$ are the $\vec{k}$ components parallel and transverse to $\vec{q}$.

Neglecting the nucleus kinetic energy (cf (105)), one has for the minimum energy transfer ($k_T = 0$) :

$$t_{min} = -t(min) \approx \left(\frac{m_h^2 + Q^2}{2\nu} \right)^2 \tag{108}$$

In Glauber's model (see a.o.[Kölbig 1968], [Belkov 1987]), one has for the coherent scattering amplitude :

$$f_A(k) = f_N(0) \int d^2b \int dz \ \rho(b, z)\, e^{i\vec{k_T}\vec{b}}\, e^{ik_L z}\, e^{-1/2\,(1 - i\alpha)\,\sigma_{hN} \int_z^\infty dz'\, \rho(b,z')}, \tag{109}$$

where b is the impact parameter, z the longitudinal coordinate, σ_{hN} the total hadron-nucleon cross section,

$$\alpha = \mathrm{Re}\, f_{hN}(0) \,/\, \mathrm{Im}\, f_{hN}(0) \tag{110}$$

the ratio of the real to imaginary parts of the forward elastic amplitude, and ρ (b, z) the nuclear matter density function. The optical approximation was used in deriving (109).

The attenuation effect of the decreasing exponential in (109) is due to the reinteraction probability of the coherently produced h meson, within the nucleus. As a consequence of this absorption, the main contribution to the cross section comes from the backward nucleus region of depth l_h (l_h is the mean free path of the meson h in the nuclear matter); the coherence condition thus really applies to this backward slice.

The cross section (109), which can be calculated numerically for any value of k_L and k_T, is simplified in two limiting cases (see [Belkov 1987]).

i) $\underline{k_L = 0}$

The z-integration of eq. (109) gives :

$$\frac{d^3\sigma^A}{d\vec{k}}\Big|_{k_L=0} = \frac{d^3\sigma^N}{d\vec{k}}\Big|_{k=0} \Big| \frac{2}{\sigma_{hN}} \int d^2b \; e^{i\vec{k_T}\vec{b}} \; [\, 1 - e^{-1/2\, \sigma_{hN}\, T(b)} \,] \Big|^2 , \tag{111}$$

where

$$T(b) = \int_{-\infty}^{\infty} \rho(b,z')\; dz' \tag{112}$$

and where α was taken to be 0.

For $k_T R << 1$, eq. (111) can be approximated by an exponentially falling function :

$$\frac{d^3\sigma^A}{d\vec{k}}\Big|_{k_L=0} = \frac{d^3\sigma^A}{d\vec{k}}\Big|_{k=0} e^{-B_T k_T^2} , \tag{113}$$

where

$$B_T = \frac{1}{2} < b^2 >$$

$$= \frac{1}{\sigma_{hA}} \int d^2b\, b^2 \, [\, 1 - e^{-1/2\, \sigma_{hN}\, T(b)} \,] \; . \tag{114}$$

Table 1 (from [Belkov 1987]) gives B_T-values for pion neutrino-production, for several nuclei, using the Woods- Saxon parametrization of the nuclear density :

$$\rho(r) = \rho_0 \, [\, 1 + e^{(r - R) / a} \,] \; , \tag{115}$$

with

$$\rho_0 = \frac{3A}{4\pi R^3} \; \frac{1}{1 + \pi^2 \, a^2 / R^2} \; ; \tag{116}$$

(the Table gives the values used for R, the average nuclear radius, and for a, the nuclear surface thickness - see [De Vries 1987]).

A	R (fm)	a (fm)	$\sigma_{tot}(\pi A)$ (mb)	B_T (GeV^{-2})
20	2.80	0.571	381	89.6
27	2.84	0.569	493	94.5
40	3.39	0.612	656	125.1
64	4.20	0.569	915	153.1
110	5.33	0.535	1382	215.5
150	5.72	0.650	1813	272.2
184	6.51	0.535	2308	308.2
207	6.62	0.546	2502	323.6
238	6.80	0.605	2843	346.7

Table 1 : Woods-Saxon parameters, and pion nucleus cross section and B_T slope computed using Glauber's model, for several nuclei.

An experimental value for B_T can be deduced from the k_T^2 dependence of the coherent ρ^0 meson production by real photons ([Alvensleben 1970]; the assumption is made that $\sigma_{\rho N} = \sigma_{\pi N}$). For neon, this value is

$$B_T(Ne) = (80 \pm 3)\ GeV^{-2} \ , \tag{117}$$

in reasonable agreement with the value in Table 1.

ii) $k_T = 0$

In this case, (109) gives :

$$\left.\frac{d^3\sigma^A}{d\vec{k}}\right|_{k_T=0} = \left.\frac{d^3\sigma^N}{d\vec{k}}\right|_{k=0} \left| \int d^2b \int_{-\infty}^{\infty} dz\ \rho(b,z)\ e^{ik_L z}\ e^{-1/2\ \sigma_{hN} \int_z^{\infty} dz'\ \rho(b,z')} \right|^2 , \tag{118}$$

which, for $k_L R << 1$, is approximated as

$$\left.\frac{d^3\sigma^A}{d\vec{k}}\right|_{k_T=0} = \left.\frac{d^3\sigma^A}{d\vec{k}}\right|_{k=0} e^{-B_L k_L^2} \ , \tag{119}$$

where

$$B_L = \langle z^2 \rangle - \langle z \rangle^2 \ , \tag{120}$$

$< z^n >$ being the average of z^n over the nucleus radius, taking the absorption into account :

$$< z^n > = \frac{\sigma_{hN}}{\sigma_{hA}} \int d^2b \int_{-\infty}^{\infty} dz\, z^n\, \rho(bz)\; e^{-1/2\,(1 - i\alpha)\,\sigma_{hN} \int_z^{\infty} dz'\, \rho(b,z')} . \qquad (121)$$

The slope B_L depends on the cross section σ_{hN} of the meson in the nuclear matter on its way out of the nucleus. It really defines, for a given cross section, the depth of the nucleus slice on which the coherence condition must apply, i.e. the slice over which the phase exp ($ik_L z$) must not vary too rapidly. In agreement with this interpretation, one notices in (120) the sensitivity of B_L to the nucleus edges. Table 2 presents, for the neon case, the B_L-values computed for two different values of σ_{hN}, for the Woods-Saxon and for the harmonic oscillator nucleus parametrizations, the latter being of the form

$$\rho(r) = \rho_0 [\, 1 + \beta\, (r/R)^2 \,]\, e^{-(r\,/\,R)^2} \;, \qquad (122)$$

with, for neon [De Vries 1987] :

$$r = 1.84 \text{ fm}, \quad \beta = 1.544 \;. \qquad (123)$$

Neon	Woods-Saxon		Harmonic Oscillator	
σ_{hN} (mb)	24	50	24	50
B_L (GeV^{-2})	82	72	63	55

Table 2 : B_L slope computed for neon nuclei using Glauber's model, for two values of the hadron-nucleon cross section and for two different parametrizations of the nuclear density.

As expected, B_L decreases when σ increases : the absorption being more important, the backward nucleus slice on which the coherence condition must apply is thinner, and the momentum transfer k_L can be larger without inducing too large a change in phase. On the other hand, the B_L-value is smaller when computed with the harmonic oscillator model : the coherence condition applies to a thinner slice, the nuclear edges being sharper in this parametrization.

One can note that, in the neon case, the B_L- and B_T-values are numerically similar, for the Woods-Saxon parametrization and for σ_{hN} = 24 mb. However, the two parameters have a completely different physical origin, and the difference between them increases with A : B_T increases faster than B_L, because it is more directly related to the radius R.

In general, for k_L and $k_T \neq 0$, a correlation exists between the cross section dependences in these two variables, through eq. (109). Table 3 gives the value of the B_T parameter, defined as in (114), for several values of k_L. For practical purposes, however, the correlation between k_L and k_T can be neglected (the relevant k_L-values are such that B_T is only weakly affected).

k_L^2 (GeV^2)		0.	.02	.04	.06	.08	.10
B_T (GeV^{-2})	σ = 24 mb	89.6	92.2	101.4	124.6	217.3	295.3
	σ = 50 mb	99.6	103.0	114.8	145.4	291.4	444.3

Table 3 : B_T slope computed for neon nuclei using Glauber's model, for several values of the longitudinal momentum transfer k_L, and for two values of the hadron-nucleon cross section.

One also finds, neglecting $(|t| + 2\nu T) / (m_h^2 + Q^2)$ (T is the nucleus kinetic energy), that

$$k_L^2 \approx t_{min} \tag{124}$$

$$k_T^2 \approx |t| - t_{min} = t' \tag{125}$$

The coherent cross section can thus factorize, with

$$\frac{d\sigma^A}{dt} = \frac{d\sigma^A}{dt}\Big|_{t=0} \; e^{-B_L t_{min}} \; e^{-B_T t'} \; . \tag{126}$$

Sometimes, the numerical similarity of B_L and B_T for nuclei like neon is used to parametrize the coherent cross section with a single parameter $B \approx B_L \approx B_T$. Let us insist again on the fact that this numerical coincidence has no physical foundation.

For the discussion of experimental papers, let us also note that several authors use for the coherent cross section an expression given by Rein and Sehgal [Rein 1983] (they used $B_L = B_T$) :

$$\frac{d\sigma\,(hA \rightarrow hA)}{dt} = \frac{A^2}{16\pi}\,\sigma_{tot}^2\,(hN)\;(1+\alpha^2)\;\; e^{-B_L t_{min}}\; e^{-B_T t'}\, F_{abs} \tag{127}$$

(α is often taken as 0). The σ(hN) cross section is usually chosen for $\nu = E_h$, neglecting virtuality effects on the cross section. F_{abs} is a nuclear absorption factor, for which experimental data on coherent ρ production ([Alvensleben 1970], [Mc Clellan 1971]) suggest

$$< F_{abs} > = 0.47 \pm 0.03 \qquad (128)$$

(one does not consider a possible dependence of F_{abs} in the meson momentum). Note that, strictly speaking, (127) contradicts the quantum mechanical meaning of diffraction, for which the stronger the absorption, the larger the diffractive cross section.

2. Experimental procedures.

The coherent interactions which will be discussed here belong to two classes :
- charged current interactions in bubble chambers, with vertex observation and detailed knowledge of the reaction kinematics;
- neutral current interactions, where the vertex is not observed and the only measured quantities are the direction and usually the momentum of the produced meson.

2.1. Charged current interactions

These experiments have provided by far the most numerous and the most detailed information. Some of their characteristics are collected in Table 4. Together, they cover an energy range extending over two orders of magnitude (from 2 GeV at SKAT to 200 GeV for E632), and collected more than 60 000 charged current interactions.

For the study of coherent interactions, bubble chambers are a remarkable tool, providing a complete knowledge of the reaction : all charged and most neutral particles are detected, and can be measured with great precision. In addition, BEBC and the 15' Bubble Chamber were equipped with an external muon identifier (EMI), made of two planes of multiwire proportional chambers. Muons with momentum greater than 5 GeV/c are identified with high efficiency and background rejection. The heavy liquid in SKAT provides a good muon identification as well. The heavy liquids used in all chambers provide a good gamma detection efficiency.

	SKAT	BEBC WA59	15' E180	15' E546	15' E632
Beam	WBB	WBB	WBB	QTB	QTB
Proton energy (GeV)	80	400	400	400	800
Chamber volume (m^3)	6.5	35	33	33	33
Fiducial volume (m^3)	1.7	16	15	15	15
Liquid	CF_3 Br	H_2-Ne	H_2-Ne	H_2-Ne	H_2-Ne
neon mole %		75%	78%	64%	76%
γ radiation length (cm)	11	42	41	53	42
Nb. CC interactions ν	8 000	9 500	-	8 500	14 700
$\bar{\nu}$	650	16 000	8 000	-	2 700
mean CC energy ν	7	50	-	80	150
$\bar{\nu}$		39	40	-	110
p_μ minimum (GeV)	ν : 1 ; $\bar{\nu}$: 0.5	5	4	4	10
Studied channels :					
π^+	Grabosch 1986	Marage 1989	-	-	Aderholz 1989
π^-	ibid.	Marage 1986	Ammosov 1987a	-	ibid.
ρ^+	-	-	-	Ballagh 1988	-
ρ^-	-	Marage 1987	-	-	-
$a_1^- / (\rho\pi)^-$	Marage	Ammosov 1991a	- 1988	-	

Table 4 : Characteristics of the bubble chamber experiments having provided results on coherent production by charged current neutrino and antineutrino interactions on nuclei.

The nucleus recoiling as a whole and acquiring very low kinetic energy, is not detected in bubble chamber experiments. The total visible charge of the event is thus 0, and the number of observed charged particles is even : the muon and the meson with opposite charge, possibly decaying with the emission of an odd number of charged particles.

On the other hand, as the nucleus remains intact, one does not observe at the interaction vertex the protons due to evaporation or nuclear reinteractions often visible in

neutrino interactions on nuclei. To the contrary, the presence of such protons or nuclear fragments implies that the reaction was not coherent.

Finally, the coherent interactions are characterized by their kinematics : the 4-momentum transfer to the nucleus is small, and the cross section falls off exponentially with $|t|$. The latter can not be measured directly, since the nucleus remains undetected, but it can be estimated from the measurement of the muon and meson momenta : neglecting the nucleus recoil energy, one finds:

$$|t| \approx [\sum_i (E^i - P_L^i)]^2 + [\sum_i \vec{P}_T^{\,i}]^2 \quad . \tag{129}$$

The quantity noted $|t|$ can be computed for all coherent and incoherent interactions. In the case where identified protons or nuclear fragments are detected at the interaction vertex, however, they are not included in the $|t|$ calculation; they are also not taken into account to compute the total charge or any kinematical quantity characterizing the interaction, nor to define the event topology.

The procedure to extract the coherent interaction signal is based, for most experiments discussed below, on the $|t|$-distribution of the events with the relevant even-prong, charge 0 topology ($\mu\pi$, $\mu\rho$, etc), containing at the primary vertex no proton or nuclear fragment.

As can be seen in Fig. 20, the $|t|$-distribution of the two-prong events ($\mu^+ \pi^-$ and possible gammas), without protons or nuclear fragments, for the WA59 antineutrino experiment [Marage 1984] shows indeed an important peak for small $|t|$-values (solid histogram). The shape of the background, on the other hand, is obtained from the $|t|$-distribution of events containing protons; at small $|t|$-values, a dip is observed instead of a peak (Fig. 20, dashed histogram).

As was shown empirically [ibid.], the $|t|$-distributions of events with or without protons are very similar, for the 3- and 5-prong topologies (not counting the protons). As those odd-prong events are all incoherent, this suggests that the incoherent background distribution is well described by that of events with protons. For a given topology, the incoherent background below a given value t_0 of $|t|$ is thus obtained from the distribution of events with protons, the two distributions being normalized for $|t| > t_0$.

This empirical method used to describe the background has the advantage that it reproduces the decrease of the incoherent background for small momentum transfers, due to

Pauli blocking. In addition, the contribution of diffractive interactions on a single neutron is automatically subtracted from the signal.

2.2. Neutral current interactions.

Five experiments using different techniques have observed neutral current π^0 coherent production by neutrinos and antineutrinos.

The first observation of neutrino and antineutrino coherent interactions was reported by the Aachen-Padova Collaboration, in 1983 [Faissner 1983]. This experiment used aluminium spark chambers, exposed to the CERN PS beams. The analysis of the production of isolated π^0 mesons was initially part of the background study for the purely leptonic neutral current reaction:

$$\overset{(-)}{\nu}_\mu + e \rightarrow \overset{(-)}{\nu}_\mu + e \quad , \tag{130}$$

aimed to measure the electroweak θ_W angle. The signal is obtained from the distribution of the angle θ_γ between the π^0 and the incident neutrino directions (Fig. 21) which shows an important excess for small values.

The CHARM experiment [Bergsma 1985] measured the coherent π^0 cross section, for small $E\,\theta_\gamma^2$-values (E is the gamma energy).

Three bubble chamber experiments reported a signal for neutral current pion production in the θ_γ^2-distribution of isolated gammas. In bubble chamber experiments, the presence of an apparently isolated γ is often due to π^0 decay, especially at high energy : the second gamma can have escaped detection because it converted inside the electromagnetic shower of the first one. These experiments were performed with the Gargamelle chamber at the CERN PS [Isiksal 1984], with the SKAT chamber at Serpukhov [Grabosch 1986] and with the 15' Bubble Chamber exposed to the FNAL WBB [Baltay 1986].

The neutral current experiments are generally faced with the problem of subtracting important backgrounds, obtained using empirical methods or using models.

3. Single pion coherent production.

Coherent π meson production on nuclei has been reported in the four possible channels :

$$\nu_\mu + A \rightarrow \mu^- + \pi^+ + A \qquad (131)$$

$$\nu_\mu + A \rightarrow \nu_\mu + \pi^0 + A \qquad (132)$$

$$\bar{\nu}_\mu + A \rightarrow \mu^+ + \pi^- + A \qquad (133)$$

$$\bar{\nu}_\mu + A \rightarrow \bar{\nu}_\mu + \pi^0 + A \ . \qquad (134)$$

This production could be studied in detail and (compared to the other coherent channels) with relatively large statistics and small background, thanks to the favourable kinematics due to the small pion mass and the simple topology.

It thus allowed the study of the longitudinal axial current for very small Q^2-values, providing one of the first, and probably the most detailed test of the PCAC hypothesis at high energy, over two orders of magnitude in neutrino energy (from 2 to more than 200 GeV).

A good knowledge of these reactions is also important for practical purposes, especially as a background to Weinberg electron production. For $x < 0.1$, pion coherent production accounts for about 3 % of the total charged current antineutrino cross section at the CERN SPS energies, for neon nuclei (A = 20).

3.1. Production mechanisms and model.

Several possible production mechanisms for π meson coherent production on nuclei are illustrated in Fig. 22. The dominant contribution is by diagram a., i.e. the diffractive scattering of the longitudinal component of the axial current, dominated by a_1 mesons or by the non-resonant ($\rho\ \pi$) cut.

For $Q^2 = 0$, the only non-vanishing contribution comes from the longitudinal component of the axial current. As ρ meson exchange gives a null cross section on isoscalar

nuclei, only the diffractive contributions of diagrams a. and b. remain. Let us note that the latter, due to the pionic component of the axial current, is proportional to the final state lepton mass squared, and plays a role only for $Q^2 = 0$ or very small ($\leq$ a few m_π^2).

For $Q^2 \neq 0$, the vector current can not contribute through π or a_1 exchange, because their isospin is non-zero. The contribution of diagram c. itself is small. Indeed, for small Q^2-values, helicity conservation implies that the vector current contributes through its longitudinal component, which is damped by an additional Q^2 factor ($R = \xi^2 Q^2 / m^2$); for larger Q^2-values, the suppression comes from the violation of the spin-parity selection rule. As for the transverse axial current, its contribution is vanishing because of the non-zero isospin of the exchanged ρ meson (moreover, helicity flip is suppressed in the forward direction).

The cross sections for coherent pion production is thus directly obtained from eq (84) :

$$\frac{d^3\sigma^A(\nu A \rightarrow l\pi A)}{dQ^2\, d\nu\, dt} = \frac{G^2}{4\pi^2} f_\pi^2 \frac{|\vec{q}|}{EE'} \frac{\varepsilon}{1-\varepsilon} \cdot$$

$$\left[\frac{E'}{E}\left(\frac{m_a^2}{Q^2+m_a^2}\right)^2 - \frac{\nu}{E}\frac{m_a^2}{Q^2+m_a^2}\frac{m_\mu^2}{Q^2+m_\pi^2} + \frac{\nu^2}{4E^2}\frac{m_\mu^2(Q^2+m_\mu^2)}{(Q^2+m_\pi^2)^2}\right]$$

$$\cdot \frac{d\sigma(\pi A \rightarrow \pi A)}{dt} \cdot \qquad (135)$$

The parametrization for the elastic pion-nucleus scattering was discussed in section 1.2.

3.2. Signal extraction and total cross section.

The 14 published results, from 8 different experiments, are summarized in Table 5 : 8 results are about π^0 meson production by neutral current, and 6 about charged pion production.

Experiment	Reference	Channel	E_ν energy (GeV)	A	Nb. seen	Signal	Cross section (10^{-40}cm^2 / nucleus A)	
Aachen-Padova	Faissner 1983	$\nu\,\pi^0$	<E> = 2	27	748	287 ± 100	29 ± 10	
		$\bar{\nu}\,\pi^0$			126	73 ± 20	25 ± 7	
Gargamelle	Isiksal 1984	$\nu\,\pi^0$	<E> = 2	30	64	39 ± 25	31 ± 20	
		$\bar{\nu}\,\pi^0$			80	62 ± 33	45 ± 24	
CHARM	Bergsma 1985	$\nu\,\pi^0$	<E> = 31	20	766	233 ± 53 ± 72	96 ± 42	
		$\bar{\nu}\,\pi^0$	<E> = 24		1442	482 ± 83 ± 99	79 ± 26	
BEBC - WA59	Marage 1986	$\bar{\nu}\,\pi^-$	5 - 100	20	130	177 ± 15	175 ± 25	(0.9 ± 0.1) % CC
	Marage 1989	$\nu\,\pi^+$			42	41 ± 8	250 ± 49	
SKAT	Grabosch 1986	$\nu\,\pi^+$	3 - 20	30	71	59 ± 8	106 ± 16	
		$\bar{\nu}\,\pi^-$			19	12 ± 4	113 ± 35	
		$\nu\,\pi^0$			20	14 ± 5	52 ± 19	
15' C-B	Baltay 1986	$\nu\,\pi^0$	2 - 100	20	33	28 ± 6		(0.20 ± 0.04) % CC
15' - E180	Ammosov 1987a	$\bar{\nu}\,\pi^-$	10 - 100	20	~90	61 ± 12		(0.76 ± 0.15) % CC
15' - E632	Aderholz 1986	$\nu\,\pi^+$ ($\bar{\nu}\,\pi^-$)	40 - 250	20	25	20 ± 6	315 ± 120	(0.26 ± 0.10) % CC

Table 5 : Experimental results on single pion coherent production.

The corresponding cross sections are presented in Fig. 23, in function of the incident neutrino energy; some results were grouped by experiment or divided in function of energy. Aluminium and freon data were scaled to correspond to results on neon. Neutral current data were multiplied by a factor 2, for comparison with charged current results.

A consistent picture emerges from Fig. 23. Only 2 points of experiment E180 [Ammosov 1987] seem low, compared to the CHARM and WA59 data. However, the total signal for E180 is in agreement with WA59, for similar beam conditions (see Table 5 - we comment more on the possible source of this apparent discrepancy in the next section). All the bubble chamber experiments (WA59, SKAT, E632), except E180, use for the signal extraction the method described in section 2.1.

On Fig. 23 and Table 5, one observes a good agreement between the cross sections for coherent π^+ production by neutrinos and π^- production by antineutrinos, whereas the total cross sections differ by a factor 2. The Aachen-Padova, Gargamelle and CHARM experiments also give very similar results for π^0 coherent productions by neutrinos and antineutrinos. This is expected within the standard model.

Coherent π^0 production was used to study the structure of the axial neutral current. The latter can be described as [Hung 1981] :

$$J^A = \beta\ A^{I=1} + \delta\, A^{I=0}\ , \tag{136}$$

corresponding to the axial current with exchange of isospin I = 1 or 0. The coherent π^0 production cross section is proportional to

$$\beta^2 = (u_a - d_a)^2\, \rho^2\ , \tag{137}$$

where u_a and d_a are the coupling constants of the u and d quarks to the axial current, and ρ is the ratio of the coupling constants to the neutral and charged currents; in the standard model, $u_a = -d_a = 1/2$, $\rho = 1$ and $\beta = 1$.

The β value can be extracted from the comparison of the measured cross section with the standard model prediction (the expression given by Rein and Sehgal is generally used). The following results have been obtained :

- [Faissner 1983] : $|\beta| = 0.93 \pm 0.12$ (138)

  $\delta < 0.7$ (90 % CL) (139)

  (no observation of coherently produced η meson)

- [Bergsma 1985] : $|\beta| = 1.08 \pm 0.24$ (140)

- [Baltay 1986] : $|\beta| = 0.98 \pm 0.24$. (141)

On the other hand, β can be obtained directly, without using a model, from the comparison of the coherent production of charged and neutral pions. Combining its results with those of WA59, the CHARM Collaboration obtained (with the assumption $\rho = 1$) :

$$| \beta | = | u_a - d_a | = 1.10 \pm 0.23 \ . \tag{142}$$

The SKAT experiment succeeded in measuring, in the same beam and with the same detector, the coherent production of π^+ and π^0 mesons by neutrinos, and of π^- mesons by antineutrinos. A direct comparison was then possible, minimizing the effect of experimental biases, and they found (see Table 5) :

$$\sigma (\nu \rightarrow \pi^+) \approx \sigma (\bar{\nu} \rightarrow \pi^-) \approx 2 \sigma (\nu \rightarrow \pi^0) \ ; \tag{143}$$

using

$$\sigma_{coh} (\pi^0) / \sigma_{coh} (\pi^{\pm}) = 1/2 \, \rho^2 \, \beta^2 \ , \tag{144}$$

they found, for $\rho = 1$:

$$| \beta | = 0.99 \pm 0.20 \ . \tag{145}$$

Fig. 23 also presents the predictions of the model (135), (127), compared to the data. The solid curve corresponds to the standard parameter choice :

$$m_a = m_{a1} = 1.260 \text{ GeV} \tag{146}$$

$$B_T = 80 \text{ GeV}^{-2} \tag{147}$$

$$B_L = 80 \text{ GeV}^{-2} \tag{148}$$

$$F_{abs} = 0.47. \tag{149}$$

The general trend of the cross section is well described by the model. This confirms the PCAC hypothesis and Adler's theorem : the coherent pion production cross section by neutrino interactions is proportional to the elastic pion-nucleus cross section, the strength of the process being given by the coupling constant f_π.

3.3. Differential cross sections.

Bubble chamber experiments can measure the muon and pion momenta, and hence completely reconstruct the reaction kinematics. The WA59 and E632 experiments have compared their results with the predictions of a Monte Carlo simulation based on the model (135)-(127), including the experimental errors (measurement errors, uncertainty on the incident neutrino direction).

	Data	Model		
		$m_a = m_{a1}$	m_a = 1.15 GeV	m_a = 1.55 GeV
$< E_\nu >$ (GeV)	30.4 ± 2.0	29.6	29.3	29.8
$< \nu >$ (GeV)	4.8 ± 0.4	4.7	4.4	5.1
$< Q^2 >$ (GeV^2)	0.375 ± 0.04	0.355	0.325	0.415
$< W >$ (GeV/c^2)	2.76 ± 0.11	2.68	2.62	2.80
$< x >$	0.058 ± 0.004	0.057	0.057	0.059
$< y >$	0.184 ± 0.014	0.167	0.160	0.181
$< \lvert t \rvert >$ (GeV^2)	0.0196 ± 0.0012	0.0184	0.0184	0.0187
$< t' >$ (GeV^2)	0.0149 ± 0.0011	0.0139	0.0138	0.0140

Table 6 : Average values of several kinematical quantities for the single π^- coherent events with $x < 0.3$, $Q^2 < 4$ GeV^2 and $\lvert t \rvert < 0.05$ GeV^2, produced by antineutrino-neon charged current interactions (WA59 Collaboration); the predictions of the model based on eq. (135), (127), (147)-(149), including the effects of the experimental resolution, are given for several values of the axial mass m_a.

Fig. 24-25, taken from [Marage 1986], present the differential distributions for E, ν, Q^2, W, x, y, $\lvert t \rvert$ and t', for the coherent π^- production by antineutrinos, with $\lvert t \rvert < 0.05$ GeV^2 and $p_\mu > 5$ GeV/c. The background, which is only (10 ± 3) % of the events with $\lvert t \rvert < 0.05$ GeV^2, is estimated from the events with protons and subtracted from the distributions (hatched on the figures); the average values for the displayed variables are given in Table 6. Fig 24 also shows (dashed histograms) the distributions for all the WA59 charged current antineutrino interactions. The coherent π^- production accounts for a non negligible fraction of

the total cross section, at these energies : more than 6 % for $Q^2 < 0.4$ GeV^2, and 3 % for $x < 0.1$.

The model predictions are superimposed to the data in Figs. 24-25. It should be noted that the model predictions show some sensitivity to the details of the parametrizations, - in particular the energy dependence of the total virtual pion-nucleus cross section and of the F_{abs} factor (see [Marage 1991b]). Keeping this in mind, a good agreement is observed in [Marage 1986], [Marage 1989] and [Aderholz 1989] between the predictions of the model and the data.

The events are concentrated at small x-values, as expected for long distance interactions.

The Q^2-distribution has a maximum for $Q^2 = 0$, and extends beyond 1 GeV^2 (although it is softer than for the complete charged current sample, for which $< Q^2 > = 4.2$ GeV^2). This confirms that the non-pionic component of the axial current gives the main contribution : for $Q^2 \neq 0$, its behaviour is governed by the propagator with the m_a mass, close to the a_1 meson mass. The WA59 experiment [Marage 1986] used the Q^2-distribution to estimate the axial mass :

$$m_a = (1.35 \pm 0.18) \text{ GeV} \quad . \tag{150}$$

The use of a smaller axial mass (e.g. $m_a = 1.050$ GeV instead of $m_a = 1.260$ GeV) modifies only slightly the distributions. The total cross section is decreased by about 20 %.

The $|t|$- and t'-distributions in Fig.25 show a reasonable agreement with the model predictions after including the smearing effects. The E180 Collaboration [Ammosov 1987] has fitted the t'-distribution as the sum of two exponentials, one corresponding to the coherent signal, with a slope $B_c = (75 \pm 25)$ GeV^{-2}, the other corresponding to the background, with a slope $B_i = (4 \pm 3)$ GeV^{-2}. The coherent signal in this experiment is thus estimated to be (61 ± 12) events, the background being of the order of 30 events. In fact, the WA59 data indicate that this background is rather concentrated at small energies, and it is thus possible that an uniform background subtraction is responsible for the apparent lack of high energy events in E180, as suggested by the coherent cross section distribution in Fig. 23.

The SKAT experiment reported an asymmetry in the distribution of the angle ϕ between the lepton plane (defined by the neutrino and the muon directions) and the hadron plane (defined by the current $\vec{q}$ and the pion directions) - see [Grabosch 1986]. Such an asymmetry would indicate an interference between the vector and axial currents, which would be surprising since the vector current is not expected to contribute significantly to the

coherent pion production. In the WA59 data, such an asymmetry is also observed : it can be parametrized as :

$$A = (N - P) / (N + P) \ , \tag{151}$$

where N and P are respectively the numbers of events with $\cos \phi < 0$ and $\cos \phi > 0$. One finds

$$A = 0.29 \pm 0.09 \tag{152}$$

for the signal with $| t | < 0.05$ GeV^2 (0.22 ± 0.08 for $| t | < 0.10$ GeV^2). However, the Monte Carlo simulation shows that the asymmetry, absent from the initial distribution, reaches 0.17 after the smearing due to the measurement errors has been taken into account (see [Marage 1991b]). The effect thus appears to be instrumental in origin.

In conclusion, the data on π^+, π^- and π^0 coherent production, in charged and in neutral current interactions of neutrinos and of antineutrinos, on nuclei with atomic number 20 to 30, and for neutrino energies from 2 to 200 GeV, is well described in the framework of the Standard Model, using the PCAC hypothesis and Adler's theorem, extended for $Q^2 \neq 0$ along the lines of the hadron dominance model.

4. ρ meson coherent production.

In contrast with the abundant literature on coherent production of charged and neutral pions, the coherent production of ρ mesons was studied in two publications only, concerning charged current interactions with $p_\mu > 5$ GeV/c : experiment WA59 with BEBC [Marage 1987] and experiment E546, with the 15' Bubble Chamber [Ballagh 1988].

The reason is that, up to an energy of about 100 GeV, the cross section for coherent $\rho^\pm$ production by charged current interactions remains smaller than that for pion production; the $\rho^\pm$ meson production is also more difficult to study, because it implies π^0 reconstruction. As for neutral currents, the Salam-Weinberg model (cf. [Gaillard 1976]) predicts that the cross section ratio between reaction

$$\overset{(-)}{\nu} + A \rightarrow \overset{(-)}{\nu} + A + \rho^0 \tag{153}$$

and reaction

$$\nu + A \rightarrow \mu^{(-)} + A + \rho^{(+)} \qquad (154)$$

is

$$1/2\,(1 - 2\sin^2\theta_W)^2 \approx 0.14\ . \qquad (155)$$

4.1. Model.

The coherent ρ meson production is due to the diffractive scattering of the vector current, as shown on Fig.26. Along arguments similar to those in section 3.1. for pion production, the only axial current contribution would arise from its pionic component, with ω exchange; this contribution is totally negligible.

The cross section is given along eq. (31) (see also [Piketty 1970], [Gaillard 1976], [Chen 1977], [Bartl 1977], [Gaillard 1977]) :

$$\frac{d^3\sigma\,(\nu A \rightarrow l\rho A)}{dQ^2\,d\nu\,dt} = \frac{G^2}{2\pi^2}\,\frac{1}{\gamma_\rho^2}\left(\frac{m_\rho^2}{Q^2 + m_\rho^2}\right)^2 \frac{|\vec{q}|}{E^2}\,\frac{Q^2}{1 - \varepsilon}\,(1 + \varepsilon R) \cdot \frac{d\sigma^T\,(\rho A \rightarrow \rho A)}{dt}\ . \qquad (156)$$

A Monte Carlo simulation was performed in [Marage 1987] on basis of eq. (156) and (127) with $B_L = B_T = 80\ \text{GeV}^{-2}$, $F_{abs} = 0.47$ and $\sigma_{tot}(\rho N) = 25$ mb.

4.2. Signal and total cross section.

The WA59 experiment reported the observation of 40 events with $|t| < 0.10\ \text{GeV}^2$, of the type

$$\mu^+ \pi^- \pi^0\ ;\ \pi^0 \rightarrow \gamma\gamma\ , \qquad (157)$$

the π^0 being completely reconstructed. The background of 7 ± 4 events is estimated from the $|t|$-distribution of events with protons or nuclear fragments.

The E546 experiment observed 12 events

$$\mu^- \pi^+ \pi^0 \ ; \ \pi^0 \rightarrow \gamma\gamma \ , \tag{158}$$

with $(\gamma\gamma)$ mass between 100 and 155 MeV; the background is (1.5 ± 1) events.

To be complete, let us still mention two unpublished results, with the bubble chamber Gargamelle, at CERN, filled with CF_3Br freon : 3 candidates at low energy, in the antineutrino PS beam [Picard 1979], and 17 events (of which 7 attributed to background) in the SPS neutrino beam [Bouchakour 1980].

The $(\pi^-\pi^0)$ invariant mass for WA59 is shown in Fig. 27. It is compared to the model prediction, obtained with a relativistic Breit-Wigner distribution (solid curve). The distribution obtained with a skewing factor of 3 is shown by the dashed curve; this factor induces very small modifications of the differential distributions discussed below, and increases slightly the predicted total cross section.

Taking into account several corrections to the observed number of events, the cross section measured by WA59 is :

$$\sigma = (95 \pm 25).10^{-40} \text{ cm}^2 / \text{neon nucleus}, \tag{159}$$

i.e. (0.58 ± 0.15) % of the total charged current antineutrino cross section at the CERN SPS. For E546, the ρ coherent production amounts to (0.28 ± 0.10) % of the total charged current neutrino cross section at the FNAL Quadrupole Triplet Beam.

The cross section for WA59 is presented in Fig. 28, were it is compared to the model predictions. The curves on the figure correspond to the two extreme parametrizations for the longitudinal cross section (cf. eq. (39)-(40)) :

$$\text{(i)} \ R = 0 \tag{160}$$

$$\text{(ii)} \ R = 0.4 \, Q^2 / m_\rho^2 \ , \ R \leq 1. \tag{161}$$

Both parametrizations are compatible with the WA59 data : (26 ± 4) events are expected for (160), and (36 ± 6) are expected for (161), whereas (33 ± 7) events are observed.

4.3. Differential distributions.

The differential cross sections for the usual kinematical variables are presented in Fig. 29 (experiment WA59), and compared to the model predictions (with R = 0); the background, estimated from the events with protons, is shown hatched. The average values are presented in Table 7.

Qualitatively, the agreement is rather good. In particular, the Q^2-distribution is compatible with vanishing for $Q^2 \to 0$, as expected for the vector current. The contrast is striking with the distribution for coherent π production, which has a maximum for $Q^2 = 0$: see Fig. 30, which compares the kinematical distributions for the two reactions. Only the x-distributions are similar, which is due to the coherence condition and the long distances implied by these two coherent reactions.

	Data	Model	
		R = 0	$R = 0.4\, Q^2 / m_\rho^2$ $R \leq 1$
E_ν (GeV)	30.6 ± 3.9	37.9	39.5
p_μ (GeV/c)	19.7 ± 3.6	23.2	24.5
ν (GeV)	10.9 ± 1.9	14.6	14.9
p_{π^-} (GeV/c)	6.0 ± 1.4	7.5	7.7
p_{π° (GeV/c)	5.0 ± 1.0	7.2	7.3
Q^2 (GeV^2)	1.26 ± 0.24	1.27	1.40
W (GeV/c^2)	4.21 ± 0.34	4.82	4.88
x	0.071 ± 0.014	0.052	0.057
y	0.333 ± 0.038	0.402	0.394
ε	0.891 ± 0.025	0.827	0.837

Table 7 : Average values of several kinematical quantities for the $\pi^-\pi^\circ$ coherent events with $|t| < 0.1$ GeV^2 produced by antineutrino-neon charged current interactions (WA59 Collaboration); the predictions of the model based on eq. (156), (127), (147)-(149), including the effects of the experimental resolution, are given for the values (160) and (161) of the ratio R of the longitudinal to transverse cross sections.

Table 7, however, shows a possible lack of high energy events (or an excess of low energy events). Such a lack is also suggested by experiment E546 : only one event on a total of 12 has an energy greater than 80 GeV, whereas this should be the case for half of the (10.5 ± 1) events in the signal. However, one might fear that this effect is due to an experimental bias : in the case of high energy π^0's, the presence of an intense electromagnetic shower from one of the gammas can jeopardize the detection of the second gamma and the π^0 reconstruction; no experimental evidence is reported for such an effect, but it is difficult to quantify and cannot be excluded. The experiment E546 also reports a lack of events with higher Q^2-values ($Q^2 > 2$ GeV^2), which is not the case for WA59.

Fig. 31 presents the | t |- and t'- distributions for WA59. The agreement is good. However, with $B_L = 60$ GeV^{-2} instead of 80 GeV^{-2}, the predicted ν- and E-values are smaller, and the agreement with the energy distributions looks better, although the sensitivity is limited.

The angular distributions provide information on the ρ meson polarization (see detailed discussion in [Bartl 1977]). In the case of coherent production, helicity is conserved, and one has :

$$R = \sigma_L / \sigma_T = \frac{1}{\varepsilon} [\, r_{00}^{04} / (1 - r_{00}^{04}) \,] \,, \qquad (162)$$

where the matrix element r_{00}^{04} is estimated from the distribution for the angle θ, which is the angle between the π^- and the nucleus directions, in the ρ meson rest frame:

$$W(\cos\theta) \propto [1 - r_{00}^{04} + (3r_{00}^{04} - 1)\cos^2\theta] \,. \qquad (163)$$

A purely transverse ρ meson production would thus give a $\sin^2\theta$ distribution ($r_{00}^{04} = 0$), and a purely longitudinal production a $\cos^2\theta$ distribution ($r_{00}^{04} = 1$). The $\cos\theta$ distributions for WA59 and E546 both indicate a non-negligible production of longitudinal mesons (see Fig. 32). (The parametrization (161), for which $< R > = 0.6$ for WA59, gives an essentially flat $\cos\theta$ distribution). The Collaboration E546 also examined the distribution for the angle ψ (for the definition, see [Joos 1976]), which favours a rather low value for R.

In conclusion, the coherent ρ meson production is well described, in its general features, by the predictions of the model based on the CVC hypothesis and vector meson dominance, in spite of a possible lack of high energy events. The angular distributions suggest a non-negligible production of longitudinally polarized ρ mesons.

5. Coherent production of a_1 mesons and $(\rho\pi)$ systems.

The last channel studied in this chapter is the coherent production of three pion systems, in antineutrino charged current interactions with $p_\mu > 5$ GeV/c :

$$\bar{\nu} + A \rightarrow \mu^+ + (3\pi)^- + A, \tag{164}$$

attributed to the coherent production of $\rho\pi$ systems or of a_1 meson. The latter decays in $\rho\pi$ systems :

$$a_1^- \rightarrow \rho^- + \pi^0 \rightarrow \pi^- + \pi^0 + \pi^0 \tag{165}$$

$$a_1^- \rightarrow \rho^0 + \pi^- \rightarrow \pi^- + \pi^+ + \pi^- \quad . \tag{166}$$

5.1. Model.

The search for a_1 meson production by diffractive pion interactions was long and difficult (see [Daum 1981], [Dankowych 1981] and ref. therein), since it is darkened by the "Deck mechanism", due to the non-resonant $(\rho\pi)$ production (see [Deck 1964], [Bowler 1975]). Similarly, the axial current could be dominated by the a_1 meson and by non-resonant $(\rho\pi)$ systems along the diagrams shown in Fig. 33. (Neutrino a_1 production was discussed a.o. in [Piketty 1970], [Gaillard 1976], [Bartl 1979], [Belkov 1987]).

The production of a_1 mesons or $(\rho\pi)$ systems is attributed to the axial current scattering, since a ρ-dominated vector current contribution would imply the exchange of π mesons (a_1 and $\rho\pi$ production) or of ω or a_1 mesons ($\rho\pi$ production).

The transverse cross section is given (see eq. (51)) by :

$$\frac{d^3\sigma^T (\bar{\nu}\, A \rightarrow \mu^+ a_1^- A)}{dQ^2\, d\nu\, dt} = \frac{G^2}{4\pi^2} f_a^2 \left(\frac{1}{Q^2 + m_a^2}\right)^2 Q^2 \frac{\nu}{E^2} \frac{1}{1 - \varepsilon} \frac{d\sigma^T (a_1^- A \rightarrow a_1^- A)}{dt}, \tag{167}$$

where a_1 can also mean ($\rho\pi$) systems. The a_1 (or $\rho\pi$) coupling constant to the axial current f_a is taken according to Weinberg's sum rule (54).

In order to take into account the uncertainty on the nature of the systems dominating the axial current, the WA59 Collaboration compared the data with the model predictions for two mass choices :

$$\text{(i) } m_a = m_{a_1} = 1.260 \text{ GeV}, \tag{168}$$

for a_1 dominance of the axial current;

$$\text{(ii) } m_a = 1.050 \text{ GeV} , \tag{169}$$

as a test value for a lower effective ($\rho\pi$) mass. (In both cases, a relativistic Breit-Wigner of width $\Gamma_a = 0.330$ GeV is used)

(iii) here, one also takes the cross section as a sum of terms corresponding to the mass distribution obtained from the τ lepton decay by the ARGUS collaboration (see the spectral function Fig. 5, in [Albrecht 1986]).

The longitudinal cross section has been approximated and parametrized in [Marage 1991a] as :

$$\frac{d^3\sigma^L (\bar{\nu} A \rightarrow \mu^+ a_1^- A)}{dQ^2 \, d\nu \, dt} = \frac{G^2}{4\pi^2} \left(\frac{m_a^2}{Q^2 + m_a^2}\right)^2 \frac{|\vec{q}|}{E^2} \frac{\varepsilon}{1 - \varepsilon} \cdot$$

$$\left[f_\pi^2 \frac{d\sigma (\pi^- A \rightarrow a_1^- A)}{dt} + \frac{f_a^2}{m_a^4} R Q^2 \frac{d\sigma^T (a_1^- A \rightarrow a_1^- A)}{dt} \right] , \tag{170}$$

where R is the ratio of the longitudinal to transverse cross sections for a_1 (or $\rho\pi$) scattering. This parametrization corresponds to the approximation (84) to rel. (80) when $Q^2 << m_a^2$; on the other hand, for high Q^2-values, the second term in (80) rapidly dominates over the first term (and the interference), whence the parametrization (170). For (167) and (170), the cross sections can be approximated as in (127). It should be noted that the first term in (170) acquires an additional Q^2-dependence in the domain $2\nu / Q^2 < R_A$, where Adler's relation is violated (see [Kopeliovich 1989]).

As in the ρ meson case, two values are tested for R :

(i) $R = 0$: (171)

(ii) $R = \xi^2 Q^2 / m_a^2 = 0.4\, Q^2 / m_a^2$; $R \leq 1$. (172)

(Note that this uncertainty on R probably dominates the approximation from (80) to (170)).

For computing the elastic "a_1" - nucleus cross section, one takes -in the absence of a direct measurement- $\sigma^T (a_1 N) = 25$ mb for the total transverse cross section, but a value of the order of 50 mb could be more appropriate for $(\rho\pi)$ systems.

In the case of coherent scattering of real π mesons on nuclei, a_1 production corresponds to some 10 % of (3π) production. In the present case, however, it is not possible to isolate a_1 meson production, and one takes for the first term in (170) the total cross section corresponding to coherently produced (3π) systems (see [Marage 1991a]) :

$$\left.\frac{d\sigma\ (\ \pi N \rightarrow 3\pi N\ )}{dt}\right|_{t=0} = 2.8 \text{ mb GeV}^{-2} \ . \qquad (173)$$

On basis of this model, and taking into account the experimental conditions, the WA59 collaboration performed a Monte Carlo simulation, whose predictions are compared to the data.

5.2. Coherent signal.

The experimental study of coherent 3π systems is still more difficult than for ρ production, because two low statistics channels have to be considered, one of which requires in addition the observation of two π^0's. On the other hand, the | t |-distribution is broader, because of the large mass of the 3π systems and of the large Q^2 mean value; the background becomes larger.

The collaboration WA59 [Marage 1991a] studied three final states :

$\mu^+ \pi^- \pi^0 \pi^0$ (174)

$\mu^+ \pi^- \pi^0 \gamma$ (175)

$\mu^+ \pi^- \pi^+ \pi^-$, (176)

the final state (175) corresponding to the two π^0's channel, with one of the gammas lost. The | t |-distribution provides, for | t | < 0.10 GeV^2, a signal of (28.5 ± 6.6) events, the background estimated from the events with protons being of (8.5 ± 3) events. The signal is, for the channels (174)-(176) respectively of (6.1 ± 3.2), (5.5 ± 3.2) and (16.9 ± 4.8) events. (Taking into account the correction for events containing a track of unknown sign, the total number of events is 34.2 ± 7.9).

The experiment E180 [Ammosov 1988] reported the observation of 5 events (of which one is attributed to background) in the channel (176) with t_{min} < 0.06 GeV^2, t' < 0.10 GeV^2 and 1.0 < m($\pi^-\pi^+\pi^-$) < 1.2 GeV.

Let us also mention the unpublished result of [Bouchakour 1980], in the Gargamelle bubble chamber at the SPS, with (13 ± 9) events in the channel (176).

For the WA59 events without proton and with | t | < 0.10 GeV^2, Fig. 34 presents the (3π) invariant mass distribution (calling "pion" the isolated γ of channel (175)). Fig. 35 presents the mass distribution for all pion pairs with different charges (thus containing pairs coming from the ρ meson decay as well as "wrong" pairs). Fig. 36 presents the distribution of Fig. 35, of which was subtracted the mass distribution for the like-sign pairs : the resulting distribution should thus correspond to the ρ meson mass. The background, estimated from the events with protons, is subtracted from these distributions. For comparison, in the lower part of the figures are shown the corresponding distributions for all events with | t | > 0.10 GeV^2, and for the events with | t | < 0.10 GeV^2 containing protons (hatched).

On these distributions were superimposed the model predictions for m_a = 1.260 GeV (solid curves), m_a = 1.050 GeV (dashed), and for the mass distribution from the ARGUS spectral function (dots) (these curves are the result of the complete simulation, including the kinematic effects of the model). The mass distributions of pion pairs (Figs. 35-36) are in rather good agreement with all predictions, supporting the attribution of the signal to ($\rho\pi$) production (either resonant or not). The (3π) mass distribution (Fig. 34) favours low masses, as m_a = 1.050 GeV or the spectral function.

The mass distributions thus suggest that the coherent signal is due to the production of a_1 mesons, decaying into $\rho\pi$, or of non-resonant ($\rho\pi$) systems, and favour an effective mass lower than the a_1 mass.

5.3. Total and differential cross sections.

The distributions for the usual kinematical variables are presented in Figs. 37-38; the average values are given in Table 8. The model predictions for m_a = 1.260 GeV and B_L = 60 GeV^{-2}, and for m_a = 1.050 GeV and B_L = 30 GeV^{-2} are also given on the figures and in the Table ; the latter also gives the mean values in the case where the masses are distributed according to the spectral function. It should be underlined that a B_L-value as low as 30 GeV^{-2}, used by the WA59 Collaboration, has no real justification. Indeed, B_L is calculated reliably as soon as $\sigma(3\pi - N)$ is fixed (see sec. 1.2 and Table 2).

		Data	Model					
		B_L (GeV^2)	60	30	60	30	60	30
		m_a (GeV)	1.260		1.050		Spectral function	
E_ν	(GeV)	37.5 ± 4.9	50.6	44.6	44.8	42.1	43.7	41.1
p_μ	(GeV/c)	21.9 ± 4.3	26.4	23.2	23.3	22.7	23.2	22.7
ν	(GeV)	15.6 ± 3.1	24.3	21.4	21.5	19.4	20.5	18.4
Q^2	(GeV^2)	1.94 ± 0.52	2.65	3.07	2.27	2.58	2.27	2.59
W	(GeV/c^2)	4.90 ± 0.39	6.24	5.83	5.90	5.54	5.74	5.39
x		0.069 ± 0.012	0.062	0.080	0.060	0.077	0.062	0.080
y		0.420 ± 0.048	0.484	0.495	0.492	0.472	0.481	0.459
$\|t\|$	(GeV^2)	0.054 ± 0.005	0.043	0.047	0.040	0.045	0.039	0.043
t_{min}	(GeV^2)	0.027 ± 0.005	0.015	0.022	0.013	0.020	0.013	0.019
t'	(GeV^2)	0.027 ± 0.004	0.029	0.026	0.027	0.025	0.027	0.025

Table 8 : Average values of several kinematical quantities for the $(3\pi)^-$ coherent events with $|t| < 0.1$ GeV^2 produced by antineutrino-neon charged current interactions (WA59 Collaboration); the predictions of the model based on eq. (167), (170), (171), (127), including the effects of the experimental resolution, are given for two values of the slope B_L and for the axial mass taken as the a_1 mass, as an effective mass of 1.050 GeV/c^2, or according to the mass distribution obtained from the ARGUS spectral function.

Qualitatively, and in particular if one compares to the distributions for π and ρ coherent production, one observes the expected effects in these data : the energy related variables have higher average values, and the Q^2-distribution decreases for $Q^2 \rightarrow 0$.

However, for m_a = 1.260 GeV and B_L = 60 GeV^{-2}, the predicted | t |-, t_{min}- and x-distributions are more peaked towards small values than observed, and the predicted E-, ν-, y- and W-distributions are harder. Let us remind that, for ρ production, there were indications that the number of events at high energy might be lower than predicted by the model. In the present case, it seems unlikely that an experimental bias might explain the energy effect.

The t'-distribution being close to that predicted by the model, the disagreement for the | t | -distribution comes mainly from t_{min}. The choice of the test value B_L = 30 GeV^{-2} instead of 60 GeV^{-2} provides a better agreement in Fig. 37, but even in this case, only 5.5 events are predicted with 0.04 < t_{min} < 0.10 GeV^2, whereas 11 events are observed (less than 2 events are predicted for B_L = 60 GeV^{-2}). A lower B_L-value also provides a better agreement for the energy related variables, due to the correlation between t_{min} and ν - see Table 8.

On the other hand, if the mass m_a = 1.050 GeV is chosen instead of the a_1 mass, or if the mass is distributed along the spectral function, lower average values of E, ν, y and W are predicted (but very small effect is observed on | t |, t_{min}, t' and x).

For m_a = 1.050 GeV (or for the spectral function) and B_L = 30 GeV^{-2}, the agreement between the model predictions and the kinematical variables thus becomes acceptable. A lower value for B_L being related to a larger cross section, these two features might provide an indication of ($\rho\pi$) dominance (with a cross section larger than for only one meson), rather than a_1 dominance.

Let us finally note that the influence of the longitudinal cross section on the kinematical distributions is weak. The expected contribution of the first term in (170), which does not vanish for $Q^2 \rightarrow 0$, is only 3 % of the total cross section; for $Q^2 < 0.4$ GeV^2, one expects 50 % of its contribution, and only 10 % of the total cross section; 5 events on a total of 32 have $Q^2 < 0.4$ GeV^2.

The total cross section is (99 ± 24).10^{-40} cm^2 / neon nucleus, averaged over the CERN SPS energy spectrum with $E_{\bar{\nu}}$ > 15 GeV, after corrections. It is presented on Fig. 39, with the model predictions. The latter are increased if m_a decreases or if B_L decreases; they are multiplied by 2.5 if the total cross section of the diffracted system is 50 mb instead of 25 mb (all the other parameters being unchanged). The longitudinal cross section (for m_a = 1.260 GeV and R = 0.4 Q^2 / m_a^2) is 26 % of the total cross section.

The observed cross section being higher than predicted for $m_a = m_{a_1}$ and B_L = 60 GeV^{-2}, this again seems to favour a low m_a mass, a low B_L slope and a high cross

section for the diffracted system. However, given the uncertainties on the model, it is hard to draw more definite conclusions on the (a_1 N) or ($\rho\pi$ N) cross sections.

In conclusion, coherent 3 pion production appears to be due to the coherent production of $\rho\pi$ systems, either due to a_1 decay or produced along the Deck mechanism. Except for Q^2, the differential distributions are hardly compatible with the model predictions for $m_a = 1.260$ GeV and $B_L = 60$ GeV^{-2}. The $|t|$-, t_{min}- and x-distributions favour a low value of B_L (possibly due to a large cross section for the scattered system); this would also provide a better agreement for the energy related variables, which are systematically lower than predicted. These variable distributions, as well as the (3π) mass distribution, also favour a lower axial mass, e.g. $m_a = 1.050$ GeV. Finally, the total cross section is also in better agreement with the predictions for a lower mass, a lower B_L value, and perhaps a larger cross section for the diffracted system. In spite of the low statistical precision of the data and the uncertainties on the model, all these features suggest the dominance of non-resonant $\rho\pi$ systems rather than of a_1 mesons.

6. Conclusions.

In selecting a very special kinematical domain, the coherent interactions on nuclei provide at the same time a filter and an amplifying device which allows to isolate, with a significant cross section, some mechanisms which usually remain hidden in the background. For very small Q^2-values, the scattering of the longitudinal axial current can be studied in coherent π production; for $Q^2 \leq 2$ GeV^2, the coherent production of ρ mesons and of 3π systems allows to study separately the vector and axial currents.

For $Q^2 = 0$, the single pion coherent production is completely due to the longitudinal component of the axial current. Thanks to Adler's theorem, it provides a test of the PCAC hypothesis at high energy, and the hadron dominance model allows to extend the domain of this study for $Q^2 \leq 1$ GeV^2. The PCAC hypothesis is thus confirmed by an array of experimental data on coherent cross section, in neutral and charged current neutrino and antineutrino interactions, from 2 to 200 GeV : the intensity of the process is fixed, as expected, by the coupling constant of the pion to the weak current, f_π, and the cross section shows the energy dependence predicted by Adler's theorem. In charged current interactions, the kinematical distributions confirm this agreement with the model. The Q^2-distribution, in

particular, confirms that the axial current is dominated by the a_1 meson, the chiral partner of the ρ, or by non-resonant $\rho\pi$ systems with an effective mass of the same order.

The coherent ρ meson production is due to the scattering of the vector current, dominated by the ρ. The total cross section and the differential distributions are in good agreement with the hadron dominance model, up to ~ 2 GeV^2; in particular, in agreement with the CVC hypothesis, the cross section is compatible with vanishing for $Q^2 = 0$. However, a lack of high energy events can be suspected. Finally, the angular distributions indicate a significant contribution of the longitudinal cross section.

The three pion coherent production is due to the scattering of the axial current. The general characteristics of these interactions are roughly in agreement with the model predictions, the axial current being supposedly dominated by $\rho\pi$ systems, either resonant (from a_1 decay) or not. However, the invariant mass distributions (for 2π and 3π), the energy distributions (E, ν, y, W), the x-, | t |- and t_{min}-distributions, as well as the total cross section are hardly compatible with the dominance of the a_1 meson alone, and tend to favour a contribution to the axial current of non-resonant $\rho\pi$ systems, with an effective mass lower than a_1 mass, a low B_L parameter for the t_{min}-distribution and perhaps a cross section higher than expected for a single meson.

The general picture emerging from the study of these three reactions is thus of a general agreement with the PCAC hypothesis, the CVC hypothesis and the hadron dominance (probably non-resonant $\rho\pi$ dominance of the axial current). However, the available statistics are rather low, especially for the ρ and the a_1 / $\rho\pi$ channels (of the order of 30 events), and several uncertainties affect the details of the model (calculation of nuclear effects and hadron-nucleon cross sections).

Let us finally note, from a practical point of view, that coherent interactions with nuclei give a sizeable contribution to the low Q^2 neutrino and antineutrino cross sections, which has to be taken into account in some detailed studies (a.o. the measurement of Weinberg's angle in the study of elastic neutrino-electron scattering; see also [Pumplin *1990*]).

VI. CONCLUSIONS.

This review has shown that existing experimental data on low Q^2 and high ν neutrino and antineutrino interactions have provided a series of significant new tests of predictions derived from the PCAC hypothesis and the hadron dominance model.

The PCAC hypothesis has been successfully tested in the following processes :

1. The total cross sections for charged current neutrino and antineutrino interactions on protons, with $Q^2 < 0.1$ GeV^2 and $\nu > 2$ GeV, were measured in the bubble chamber BEBC filled with hydrogen, at CERN (WA21 Collaboration). These cross sections are non-vanishing for $Q^2 = 0$, and are well described by the predictions of Adler's theorem and of the PCAC hypothesis; the longitudinal component of the axial current gives the dominating contribution to the total cross sections in this domain.

2. The total cross sections for charged current neutrino and antineutrino interactions on neon and deuterium nuclei, measured in the bubble chamber BEBC used in similar conditions, were compared by the WA25 and WA59 Collaborations. An attenuation of the cross section per nucleon, corresponding to 4 standard deviations, is observed on neon for $x < 0.2$ and $Q^2 < 1$ GeV^2. The appearance of this shadowing effect for the smallest ν-values as well as its absolute size are in agreement with Adler's theorem and the PCAC hypothesis, in the framework of the Glauber-Gribov approach.

3. The coherent production of π mesons, by charged and neutral current interactions of neutrinos and antineutrinos, was studied by numerous experiments using bubble chambers or counters, on nuclei with atomic numbers from 20 to 30, in an energy range of 2 to 200 GeV. The total cross sections as well as the differential cross sections are in agreement with predictions based on the PCAC hypothesis for diffractive scattering of the longitudinal component of the axial current, the strength of the process being fixed by the coupling constant of the pion to the weak current.

4. Finally, it should be reminded -although this is beyond the scope of the present review- that for small ν-values ($\nu \leq 0.7$ GeV), the production of Δ (1232) resonances by charged current neutrino and antineutrino interactions on nucleons also provides a good test of the PCAC hypothesis for $Q^2 < 0.2$ GeV2.

For Q^2-values up to 1-2 GeV^2, experimental results for several reactions were compared to the predictions of a hadron dominance model where the vector current is

dominated by the ρ meson, and the axial current is dominated by the a_1 meson and / or by a non-resonant ρπ cut.

1. The total cross sections for charged current neutrino and antineutrino interactions on protons (WA21 Collaboration) are reasonably well described by this model for the region $Q^2 < 0.6$ GeV^2 and $\nu > 2$ GeV; for $Q^2 > 0.2$ GeV^2, the contributions of the vector current and of the transverse component of the axial current dominate over the longitudinal axial contribution.

2. The Q^2-dependence of the shadowing effects, studied by the WA25 and WA59 Collaborations, is in agreement with predictions based on the hadron dominance model.

3. The Q^2-dependence of coherent pion production, studied mainly by the WA59 Collaboration, is well described by a propagator containing a mass of the order of the a_1 mass, in agreement with the a_1 / ρπ dominance hypothesis.

4. The coherent ρ meson production on nuclei, studied by the Collaborations WA59 at CERN and E546 at FNAL, is also in agreement with the predictions of the hadron dominance model for the vector current behaviour, thus providing a test of the CVC hypothesis in weak interactions.

5. The coherent production of 3π systems has been studied mainly by the WA59 Collaboration. It seems to be due to the production of ρπ systems, either resonant or not. In spite of the model uncertainties and of the large experimental errors, the study of the differential and total cross sections favours the production of non-resonant ρπ systems, with an effective mass lower than the a_1 mass, and a cross section higher than expected for a single meson.

6. Finally, a few results were published on the diffractive production on nucleons of π, ρ and a_1 / ρπ systems. However, in the present stage, they do not provide useful tests of the model.

Most results quoted in this review were obtained using the large bubble chambers at CERN and FNAL, which were recently dismantled in view of their high working costs. On the other hand, significant progress in this domain would require very large statistics, in view of the low cross section of the studied processes. New results in a close future can thus only be expected from the on-going analyses of data collected by two experiments :

1. In the framework of the WA21 Collaboration, the study of charged current neutrino and antineutrino interactions on protons should provide useful results on the diffractive production of pions, ρ mesons and a_1 / ρπ systems; the latter would be particularly useful.

2. At the highest available energies, in the Tevatron neutrino beam, the E632 Collaboration should present results on the coherent production of ρ, π and a_1 / $\rho\pi$ systems. The observation of the diffractive or coherent production of D_s and D_s^* mesons would also be of the highest interest, since it would extend the hadron dominance picture to the second quark family.

In summary, a considerable number of results have been obtained, in the last few years, from several neutrino reactions with small four-momentum transfer Q^2 and high energy transfer ν. A rich and consistent picture has emerged, providing in particular several significant tests of the PCAC hypothesis, at high energy.

ACKNOWLEDGEMENTS.

It is a pleasure to thank all our colleagues who contributed to the collect and the analysis of the data presented here. In particular, we want to express our gratitude to our colleagues of the WA59 Collaboration for their constant interest and support.

REFERENCES

[Aderholz 1989] M. Aderholz et al., E632 Coll., Phys. Rev. Lett. 63 (1989) 2349

[Adler 1964] S.L. Adler, Phys. Rev. 135 (1964) B963

[Albrecht 1986] H. Albrecht et al., ARGUS Coll., Z. Phys. C33 (1986) 7

[Allasia 1983] D. Allasia et al., WA25 Coll., Z. Phys. C20 (1983) 95

[Allasia 1990] D. Allasia et al., WA25 Coll., Nucl. Phys. B343 (1990) 285

[Allen 1986] P. Allen et al., WA21 Coll., Nucl. Phys. B264 (1986) 221

[Allport 1989] P.P. Allport et al., WA59 Coll., Phys. Lett. 232B (1989) 417

[Alvensleben 1970] H. Alvensleben et al., Nucl. Phys. 18B (1970) 333

[Ammosov 1985] V.V. Ammosov et al., E180 Coll., Sov. J. Nucl. Phys. 42 (1985) 236

[Ammosov 1987a] V.V. Ammosov et al., E180 Coll., Sov. J. Nucl. Phys. 45 (1987) 1029

[Ammosov 1987b] V.V. Ammosov et al., SKAT Coll., Paper subm. to the 1987 Int. Symp. on Lepton and Photon Interactions at High Energy (Hambourg 1987)

[Ammosov 1988] V.V. Ammosov et al., E180 Coll., Paper subm. to the 13th Neutrino Conf., Boston 1988

[Arneodo 1988] M. Arneodo et al., EMC Coll., Phys. Lett. 211B (1988) 493

[Arnold 1984] R.G. Arnold et al., Phys. Rev. Lett. 52 (1984) 727

[Ashman 1988] J. Ashman et al., EMC Coll., Phys. Lett. 202B (1988) 603

[Aubert 1983] J.J. Aubert et al., EMC Coll., Phys. Lett. 123B (1983) 275

[Aubert 1985] J.J. Aubert et al., EMC Coll., Phys. Lett. 161B (1985) 203

[Ballagh 1988] H.C. Ballagh et al., E546 Coll., Phys. Rev. D37 (1988) 1744

[Ballam 1972] J. Ballam et al., Phys. Rev. D5 (1972) 545

[Ballam 1974] J. Ballam et al., Phys. Rev. D10 (1974) 765

[Baltay 1986] C. Baltay et al., Phys. Rev. Lett. 57 (1986) 2629

[Bari 1985] G. Bari et al., BCDMS Coll., Phys. Lett. B163 (1985) 282

[Bartl 1977] A. Bartl, H. Fraas, W. Majerotto, Phys. Rev. D16 (1977) 2124

[Bartl 1979] A. Bartl, H. Fraas, W. Majerotto, Phys. Rev. D19 (1979) 3222

[Bauer 1978] T.H.Bauer, R.D. Spital, D.R. Yennie, F.M. Pipkin, Rev. Mod. Phys. 50 (1978) 261

[Belkov 1987] A.A. Belkov, B.Z. Kopeliovich, Sov. J. Nucl. Phys. 46 (1987) 499

[Bell 1964] J.S. Bell, Phys. Rev. Lett. 13 (1964) 57

[Bell 1970] J.S. Bell, C.H. Llewellyn Smith, Nucl. Phys. B24 (1970) 285

[Bell 1971] J.S. Bell, Pseudoscalar Meson Dominance in Neutrino-Nucleus Interactions, in [Cunning 1971]

[Bell 1978] J. Bell et al., Phys. Rev. Lett. 40 (1978) 1226

[Benvenuti 1987] A.C. Benvenuti et al., BCDMS Coll., Phys. Lett. 189B (1987) 483

[Bergsma 1985] F. Bergsma et al., CHARM Coll., Phys. Lett. 157B (1985) 469
[Bilchak 1988] C.L. Bilchak, D. Schildknecht, J.D. Stroughair, Phys. Lett. 214B (1988) 441
[Bilchak 1989] C.L. Bilchak, D. Schildknecht, J.D. Stroughair, Phys. Lett.233B (1989) 461
[Bjorken 1973] J.D. Bjorken, J. Kogut, Phys. Rev. D8 (1973) 1341
[Bodek 1983a] A. Bodek et al., Phys. Rev. Lett. 50 (1983) 1431
[Bodek 1983b] A. Bodek et al., Phys. Rev. Lett. 51 (1983) 534
[Borer 1969] K. Borer et al., Phys. Lett. 30B (1969) 572
[Bonetti 1969] S.V. Bonetti et al., Lett. Nuovo Cimento II (1969) 877
[Bouchakour 1980] A. Bouchakour, Ph.D. Thesis, Strasbourg University (1980), unpubl.
[Bramón 1972] A. Bramón, E. Etim, M. Greco, Phys. Lett. 41B (1972) 609
[Brodsky 1969] S.J. Brodsky, J. Pumplin, Phys. Rev. 182 (1969) 1794
[Brodsky 1972] S.J. Brodsky, F.E. Close, J.F. Gunion, Phys. Rev. D6 (1972) 177
[Brodsky 1990] S.J. Brodsky, H.J. Lu, Phys. Rev. Lett. 64 (1990) 1342
[Caldwell 1979] D.O. Caldwell et al., Phys. Rev. Lett. 42 (1979) 553
[Cassel 1981] D.G. Cassel, Phys. Rev. D24 (1981) 2787
[Chen 1977] M.S. Chen, F.S. Henyey, G.L. Kane, Nucl. Phys. B118 (1977) 345
[Cohen 1982] I. Cohen et al., Phys. Rev. D25 (1982) 634
[Cooper 1984] A.M. Cooper et al., WA59 Coll., Phys. Lett. 141B (1984) 133
[Dankowych 1981] J.A. Dankowych et al., Phys. Rev. Lett. 46 (1981) 580
[Daum 1981] C. Daum et al., Nucl. Phys. B182 (1981) 269
[Deck 1964] R.T. Deck, Phys. Rev. Lett. 13 (1964) 169
[del Papa 1979] C. del Papa et al., Phys. Rev. D19 (1979) 1303
[Devenish 1976] R. Devenish, D. Schildknecht, Phys. Rev. D14 (1976) 93
[De Vries 1987] H. De Vries, C. De Vries, N. De Jaeger, Atomic Data and Nuclear Data Tables 36 (1987) 495
[Ditsas 1975] P. Ditsas, B.J. Read, G. Shaw, Nucl. Phys. B99 (1975) 85
[Ditsas 1976] P. Ditsas, G. Shaw, Nucl. Phys. B113 (1976) 246
[Dombey 1969] N. Dombey, Rev. Mod. Phys. 41 (1969) 236
[Donnachie 1978a] A. Donnachie, G. Shaw, ed., Electromagnetic Interactions of Hadrons, Plenum, New-York (1978)
[Donnachie 1978b] A. Donnachie, G. Shaw, Generalized Vector Dominance, in [Donnachie 1978a], vol. 2
[Faissner 1983] H. Faissner et al., Phys. Lett. 125B (1983) 230
[Feynman 1958] R.P. Feynman, M. Gell-Mann, Phys. Rev. 103 (1958) 193
[Fraas 1969] H. Fraas, D. Schildknecht, Nucl. Phys. B14 (1969) 543
[Fraas 1975a] H. Fraas, B.J. Read, D. Schildknecht, Nucl. Phys. B86 (1975) 346

[Fraas 1975b] H. Fraas, B.J. Read, D. Schildknecht, Nucl. Phys. B88 (1975) 301
[Frankfurt 1989] L.L. Frankfurt, M.I. Strikman, Nucl. Phys. B136 (1989) 340
[Franz 1981] J. Franz et al., Z. Phys. C10 (1981) 105
[Gaillard 1976] M.K. Gaillard, S.A. Jackson, D.V. Nanopoulos, Nucl. Phys. B102 (1976) 326; B112 (1976) 545
[Gaillard 1977] M.K. Gaillard, C.A. Piketty, Phys. Lett. 68B (1977) 267
[Gershtein 1955] S.S. Gershtein, Ya.B. Zeldovich, ZhETF 29 (1955) 698
[Glauber 1955] R.J. Glauber, Phys. Rev. 100 (1955) 242
[Goodman 1981] M.S. Goodman et al., Phys. Rev. Lett 47 (1981) 293
[Grabosch 1986] H.J. Grabosch et al., SKAT Coll., Z. Phys. C31 (1986) 203
[Grabosch 1989] H.J. Grabosch et al., SKAT Coll., Z. Phys. C41 (1989) 527
[Grammer 1978] G. Grammer, J.D. Sullivan, Nuclear Shadowing and Electromagnetic Processes, in : [Donnachie 1978a], vol. 2
[Gribov 1969a] V.N. Gribov, ZhETF. 56 (1969) 892; Sov. Phys. JETP 29 (1969) 483
[Gribov 1969b] V.N. Gribov, ZhETF. 57 (1969) 1306; Sov. Phys. JETP 30 (1970) 709
[Gsopner 1979] A. Gsopner et al., Phys. Rev. Lett. 42 (1979) 9
[Guy 1987] J. Guy et al., WA59 Coll., Z. Phys. C36 (1987) 337
[Hand 1963] L.N. Hand, Phys. Rev. 129 (1963) 1834
[Holder 1977] M. Holder et al., Phys. Lett. 69B (1977) 377
[Holder 1970] M. Holder, Lett. N. Cim. III (1970) 445
[Hung 1981] P.Q. Hung, J.J. Sakuraï, Ann. Rev. Nucl. Part. Sci. 31 (1981) 375
[Isiksal 1984] E. Isiksal, D. Rein, J.G. Morfin, Phys. Rev. Lett. 52 (1984) 1096
[Jones 1987] G.T. Jones et al., WA21 Coll., Z. Phys. C37 (1987) 25
[Jones 1989] G.T. Jones et al., WA21 Coll., Z. Phys. C43 (1989) 527
[Joos 1976] P. Joos et al., Nucl. Phys. B113 (1976) 53
[Kancheli 1973] O.V. Kancheli, JETP Lett. 18 (1973) 274
[Kazarinov 1976] Yu. M. Kazarinov et al., JETP 70 (1976) 1152
[Kölbig 1968] K.S. Kölbig, B. Margolis, Nucl. Phys. B6 (1968) 85
[Kopeliovich 1989] B.Z. Kopeliovich, Phys. Lett. 227B (1989) 461
[Kwiecinski 1988] J. Kwiecinski, B. Badelek, Phys. Lett. 208B (1988) 508
[Kwiecinski 1989] J. Kwiecinski, B. Badelek, Z. Phys. C43 (1989) 251
[Leith 1978] D.W.G.S. Leith, High-Energy Photoproduction : Diffractive Processes, in [Donnachie 1978a], vol. 1
[Marage 1984] P. Marage et al., WA59 Coll., Phys. Lett. 140B (1984) 137
[Marage 1986] P. Marage et al., WA59 Coll., Z. Phys. C31 (1986) 191
[Marage 1987] P. Marage et al., WA59 Coll., Z. Phys. C35 (1987) 275
[Marage 1989] P. Marage et al., WA59 Coll., Z. Phys. C43 (1989) 523
[Marage 1991a] P. Marage et al., WA59 Coll., Z. Phys. C49 (1991) 385

[Marage 1991b] P. Marage, Thèse d'Agrégation de l'Enseignement supérieur, Brussels University (1991), unpubl.
[Masnou 1972] J.L. Masnou, J. Six, Nuovo Cimento 10A (1972) 87
[McClellan 1971] G. McClellan et al., Phys. Rev. D4 (1971) 2683
[Miller 1981] M. Miller et al., Phys. Rev. D24 (1981) 1
[Mishra 1989] S.R. Mishra, F. Sciulli, Annu. Rev. Nucl. Part. Sci. 39 (1989) 259
[Mishra 1990] S.R. Mishra, F. Sciulli, Phys. Lett 244B (1990) 341
[Morrison 1978] D.R.O.Morrison, Proc. of the 1978 Int. Meeting on Frontier of Physics, K.K. Phua. C.K. Chew, Y.K. Lim ed., Singapore 1978
[Murthy 1975] P.V.R. Murthy et al., Nucl. Phys. B92 (1975) 269
[Nikolaev 1975] N.N. Nikolaev, V.I. Zakharov, Phys. Lett. 55B (1975) 397
[Nikolaev 1990] N.N. Nikolaev, B.G. Zakharov, Z. Phys. C49 (1991) 607
[PDG 1990] J.J. Hernández et al., Particle Data Group, Phys. Lett. 239B (1990) 1
[Picard 1979] D. Picard, Production cohérente des Mésons Vecteurs dans l'Expérience Wide-Band du PS, LAL-79/38, unpubl.
[Piketty 1970] C.A. Piketty, L. Stodolsky, Nucl. Phys. B15 (1970) 571
[Pumplin 1968] J. Pumplin, M. Ross, Phys. Rev. Lett. 21 (1968) 1778
[Pumplin 1990] J. Pumplin, Phys. Rev. Lett. 64 (1990) 2751
[Qiu 1987] J. Qiu, Nucl. Phys. B291 (1987) 746
[Rein 1981] D. Rein, L.M. Sehgal, Ann. Phys. 133 (1981) 79
[Rein 1983] D. Rein, L.M. Sehgal, Nucl. Phys. B223 (1983) 29
[Rein 1986] D. Rein, Nucl. Phys. B278 (1986) 61
[Rein 1987] D. Rein, Z. Phys. C35 (1987) 43
[Sakuraï 1969] J.J. Sakuraï, Phys. Rev. Lett. 22 (1969) 981
[Sakuraï 1972] J.J. Sakuraï, D. Schildknecht, Phys. Lett. 40B (1972) 121
[Schildknecht 1973] D. Schildknecht, Nucl. Phys. B66 (1973) 378
[Schilling 1973] K. Schilling, G. Wolf, Nucl. Phys. B61 (1973) 381
[Shambroom 1982] W.D. Shambroom et al., Phys. Rev. D26 (1982) 1
[Shaw 1989] G. Shaw, Phys. Lett. 228B (1989) 125
[Stein 1975] S. Stein et al., Phys. Rev. D12 (1975) 1884
[Stodolsky 1964] L. Stodolsky, Phys. Rev. 134 (1964) 1099B
[Stodolsky 1967] L. Stodolsky, Phys. Rev. Lett. 18 (1967) 135
[Stodolsky 1970] L. Stodolsky, Coherence in High Energy Reactions, in : Methods in Subnuclear Physics, M. Nikolic ed., vol IV, part 1, Gordon & Breach, New-York (1970) 259
[Whitlow 1990] L.W. Whitlow et al., Phys. Lett. 250B (1990) 193
[Zakharov 1975] V.I. Zakharov, N.N. Nikolaev, Sov. J. Nucl. Phys. 21 (1975) 227

FIGURE CAPTIONS.

Fig. 1. The (Q^2,ν) plane in neutrino interactions.

Fig. 2. Kinematics of neutrino scattering.

Fig. 3. Q^2-distribution for charged current neutrino-nucleon interactions at the CERN PS. Curve (a) presents PCAC derived predictions; for curve (b), the axial transverse and the vector current contributions are included in addition; effects of shadowing are included [Masnou 1972].

Fig. 4. Q^2-distributions for charged current neutrino- and antineutrino-proton interactions with $\nu > 2$ GeV (WA21 Collaboration). The curves represent (1) the longitudinal axial contribution, along PCAC hypothesis; (2) the transverse axial and the vector contribution; (3) the upper limit for the interference between the vector and axial currents. The solid curve is the sum of contributions (1) and (2), the hatched region correspond to the uncertainty on this prediction [Jones 1987].

Fig. 5. ν-distribution for charged current neutrino- and antineutrino-proton interactions with $Q^2 < 0.1$ GeV^2 (WA21 Collaboration); the curves have the same meaning as in Fig. 4 [Jones 1987].

Fig. 6. E-distribution for charged current neutrino- and antineutrino-proton interactions with $Q^2 < 0.1$ GeV^2 and $\nu > 2$ GeV (WA21 Collaboration); the curves have the same meaning as in Fig. 4 [Jones 1987].

Fig. 7. Distribution of (a) the invariant mass $(p\pi^+)$ for $\mu^-p\pi^+$ events; (b) the invariant mass $(p\pi^-)$ for $\mu^+p\pi^-$ events (WA21 Collaboration). The curves represent the prediction of the model for resonance production of Rein and Sehgal [Allen 1986].

Fig. 8. Q^2-distributions of the $\mu^-p\pi^+$ and $\mu^+p\pi^-$ events with $W < 1.4$ GeV and $p_p^L > 0.2$ GeV/c (WA21 Collaboration). The solid curves represent the predictions of the PCAC - based model for Δ resonance production; the dashed curves represent the prediction of a model with conserved axial current [Jones 1989].

Fig. 9. W^2-distribution for the combined $\mu^-p\pi^+$ and $\mu^+p\pi^-$ events (WA21 Collaboration). The curve represents the predictions of the model for pion diffractive production with a slope $b = 7$ GeV^{-2} and an axial mass $m_a = 1.1$ GeV [Rein 1986].

Fig. 10. Energy dependence of the ratio A_{eff} / A for the total cross sections of real photons on C, Al, Cu, Pb; the curves represent the predictions of vector meson dominance models [Bauer 1978, Fig. 35].

Fig. 11. Energy dependence of the ratio A_{eff} / A for the total cross sections of real photons on C, Cu and Pb, at high energy [Cadwell 1979].

Fig. 12. x-dependence of the total cross section per nucleon of virtual photons on several nuclei, divided by the total cross section per nucleon on deuterium, with $0.3 \leq Q^2 \leq 3.2\ GeV^2$ (EMC Collaboration) [Ameodo 1988].

Fig. 13. x-dependence of the total cross section per nucleon of virtual photons on copper nuclei, divided by the total cross section per nucleon on deuterium, with $5 \leq Q^2 \leq 35\ GeV^2$ (EMC Collaboration) [Ashman 1988].

Fig. 14. Ratio of neutrino cross sections per nucleon on several nuclei, at the CERN PS (a) for $\theta_{\mu\nu} \leq 29°$, with $< Q^2 > \leq 35\ GeV^2$; (b) as a function of $\theta_{\mu\nu}$ [Borer 1969].

Fig. 15. Q^2-dependence of the ratio of cross sections per nucleon on neon and on deuterium nuclei, with $x < 0.3$ (a) for neutrinos; (b) for antineutrinos; (c) for the combined statistics (WA25 and WA59 Collaborations). The normalization assumes the equality of the total cross sections per nucleon, integrated over the complete samples. The curve represents the predictions for shadowing of Bell's optical model, based on the PCAC hypothesis [Allport 1989].

Fig. 16. x-dependence of the ratio of the cross sections per nucleon on neon and on deuterium nuclei (neutrinos and antineutrinos combined), for several Q^2-intervals (WA25 and WA59 Collaborations). Normalization and curve are defined as in Fig. 15.

Fig. 17. (a) ν-dependence; (b) W-dependence of the ratio of the cross sections per nucleon on neon and on deuterium nuclei (neutrinos and antineutrinos combined), for $x < 0.2$ and $Q^2 < 0.2\ GeV^2$ (WA25 and WA59 Collaborations). Normalization and curve are defined as in Fig. 15.

Fig. 18. Elastic scattering of the axial current on a nucleus (a) one-step process; (b) first inelastic correction in the two-step process.

Fig. 19. Kinematics of neutrino coherent scattering on a nucleus A.

Fig. 20. | t |-distribution of (a) two-prong events ($\mu^+\pi^-$ and possible γ's); (b) three-prong events from antineutrino-neon scattering (WA59 Collaboration). The solid histograms correspond to interactions without protons or nuclear fragments; the dashed histograms correspond to interactions with protons with momentum below 320 MeV/c or with nuclear fragments; the latter are normalized to the former for $|t| > 0.1$ GeV^2 [Marage 1984].

Fig. 21. Distributions of the angle $\theta_{\pi 0}$ between the directions of the π^0 meson and of the incident (anti)neutrino, for the production of an isolated π^0 (solid histograms) or of a π^0 accompanied by the presence of a proton (dashed histograms) (Aachen-Padova experiment).The curves represent the predictions of a resonance production model [Faissner 1983].

Fig. 22. Mechanisms for coherent pion production on a nucleus A.

Fig. 23. Energy dependence of pion coherent production by neutrinos and antineutrinos on atomic nuclei; the experimental results have been normalized to correspond to charged current interactions on neon nuclei. The curves correspond to the prediction of the model (135), (127), (147)-(149), including the effects of the experimental resolution, for two values of the axial mass.

Fig. 24. Distributions of E, ν, Q^2, w, x, y for the $\mu^+\pi^-$ coherent events with $x < 0.3$, $Q^2 < 4$ GeV^2 and $|t| < 0.05$ GeV^2 (WA59 Collaboration). The incoherent background, estimated from the events with protons of momentum < 320 MeV/c, is shown hatched. The curves, normalized to the signal, represent the predictions of the model (135), (127), (146)-(149), including the effects of the experimental resolution. The dashed histograms correspond to the full charged current statistics, divided by a factor 100 [Marage 1986].

Fig. 25. Distributions of | t | and t', as in Fig. 24 [Marage 1986].

Fig. 26. Mechanism for ρ meson coherent production on a nucleus A.

Fig. 27. Distribution of the invariant mass of the $(\pi^-\pi^0)$ system in the $\mu^+\pi^-\pi^0$ events with $|t| < 0.1$ GeV^2 (WA59 Collaboration); the 4 events containing protons are shown hatched. The full curve represents the prediction of the model (156), (127), including the effects of the experimental resolution; the dashed curve is obtained by including the skewing factor $(m_\rho / m_{\pi\pi})^3$ [Marage 1987].

Fig. 28. Energy dependence of the cross section for coherent ρ^- production by charged current antineutrino interactions on neon nuclei (WA59 Collaboration). The curves represent the predictions of the model (156), (127), for R = 0 (eq. (160), full curve) and for $R = 0.4\ Q^2 / m_\rho^2$, $R \leq 1$ (eq. (161), dashed curve) [Marage 1987]

Fig. 29. Distributions of E, ν, Q^2, W, x, y for the $\mu^+\pi^-\pi^0$ coherent events with $|t| < 0.1$ GeV^2 (WA59 Collaboration). The incoherent background, estimated from the events with protons, is shown hatched. The curves, normalized to the signal, represent the predictions of the model (156), (127), (147)-(149), with R = 0 (160), including the effects of the experimental distribution; the predictions for $R = 0.4\ Q^2 / m_\rho^2$, $R \leq 1$ (161) are very close to the curves shown [Marage 1987].

Fig. 30. Distributions of ν, Q^2, x, y for the $\mu^+\pi^-\pi^0$ (shaded histograms) and the $\mu^+\pi^-$ (solid histograms) coherent events (WA59 Collaboration); the distributions are normalized to each other [Marage 1987].

Fig. 31. Distributions of $|t|$ and t', as in Fig.29 [Marage 1987].

Fig. 32. Distributions of $\cos\theta$, θ being the angle between the nucleus and the π^- directions in the ρ center of mass system, for the $\mu^+\pi^-\pi^0$ events with $|t| < 0.1$ GeV^2 (WA59 Collaboration). The incoherent background, estimated from the events with protons, is shown hatched [Marage 1987].

Fig. 33. (a) Coherent scattering of an a_1 meson on a nucleus A; (b) coherent Deck mechanism.

Fig. 34. Distribution of the mass m(3π) for the ($\pi^-\pi^0\pi^0$, $\pi^-\pi^0\gamma$, $\pi^-\pi^+\pi^-$) systems for the channels (174)-(176) (WA59 Collaboration) : (a) coherent signal for $|t| < 0.1$ GeV^2, after subtraction of the incoherent background estimated from the events with protons; the curves represent the predictions of the model (167), (170), (171), (127), including the effects of the experimental resolution, for m_a = 1.260 GeV (full lines), for m_a = 1.050 GeV (dashed lines) and for the mass distribution obtained from the ARGUS spectral function (dots); (b) events with protons and with $|t| < 0.1$ GeV^2 (hatched, arbitrary scale), and events with or without protons, with $|t| > 0.1$ GeV^2 (full histogram, distribution normalized to that of Fig. 34 (a)) [Marage 1991a, b].

Fig. 35. Distribution of the masses m ($\pi\pi$) for pairs of different charges ($\pi^-\pi^0$, $\pi^-\gamma$, $\pi^-\pi^+$); (a) and (b) and curves as in Fig. 34 [Marage 1991a, b].

Fig. 36. Distribution of the masses m ($\pi\pi$) for pairs of differents charges ($\pi^-\pi^0$, $\pi^-\gamma$, $\pi^-\pi^+$), after subtraction of like-sign pairs ($\pi^0\pi^0$, $\pi^0\gamma$, $\pi^-\pi^-$); (a) and (b) and curves as in Fig. 34 [Marage 1991a].

Fig. 37. Distributions of $|t|$, t_{min} and t' for the ($\mu^+\pi^-\pi^0\pi^0$, $\mu^+\pi^-\pi^0\gamma$, $\mu^+\pi^-\pi^+\pi^-$) coherent events with $|t| < 0.1$ GeV^2 (WA59 Collaboration), after subtraction of the incoherent background estimated from the events with protons. The curves, normalized to the coherent signal, represent the predictions of the model (167), (170), (171), (127), including the effects of the experimental resolution, for m_a = 1.260 GeV^2 and B_L = 60 GeV^{-2} (full lines) and for m_a = 1.050 GeV and B_L = 30 GeV^{-2} (dashed lines) [Marage 1991a].

Fig. 38. Distributions of E_ν, ν, Q^2, W, x, y, as for Fig. 37 [Marage 1991a].

Fig. 39. Energy dependence of the cross section for coherent production of 3π system, by charged current antineutrino interactions on neon nuclei (WA59 Collaboration). The curves represent the predictions of the model (167), (170), (171), (127), with m_a = 1.260 GeV and B_L = 60 GeV^{-2} (full lines) and for m_a = 1.050 GeV and B_L = 30 GeV^{-2} (dashed lines) [Marage 1991a].

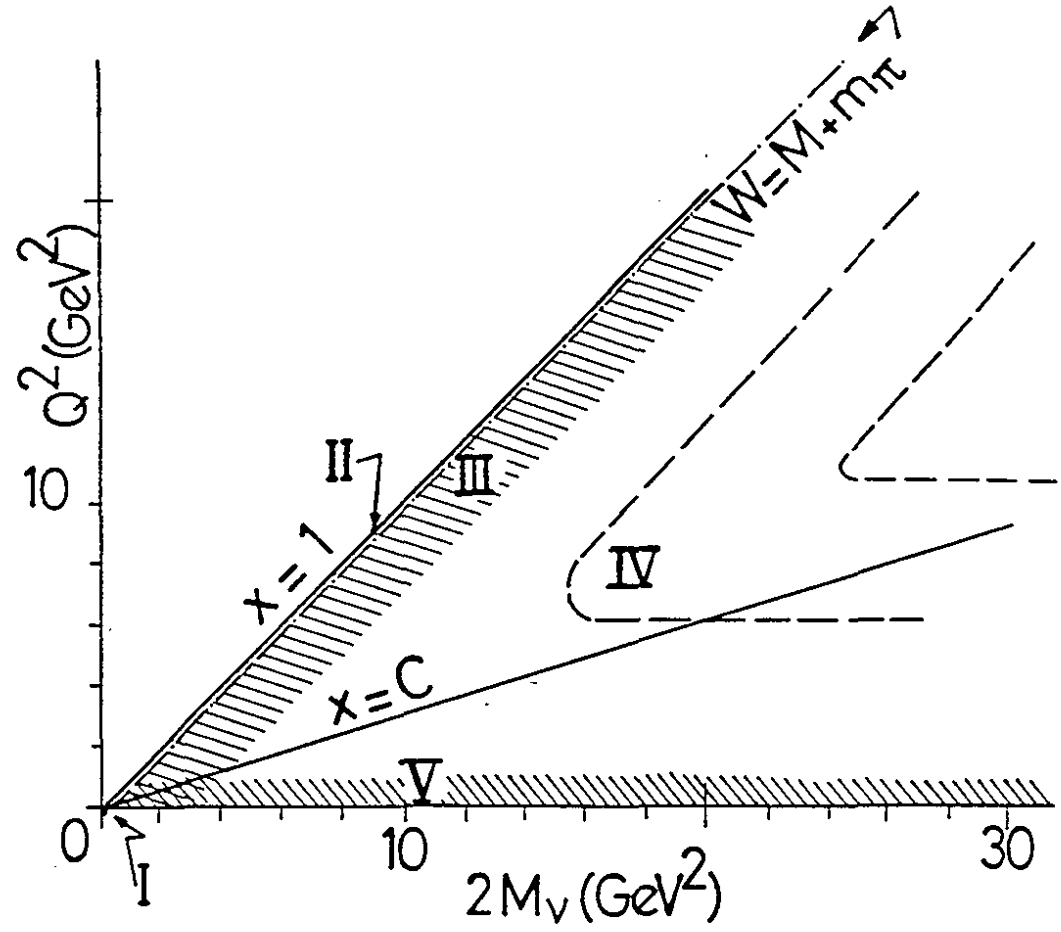
$Q^2(GeV^2)$
10
0
10
30
$2M_V(GeV^2)$
$W=M+m_\pi$
x=1
x=C
I
II
III
IV
V

fig. 1

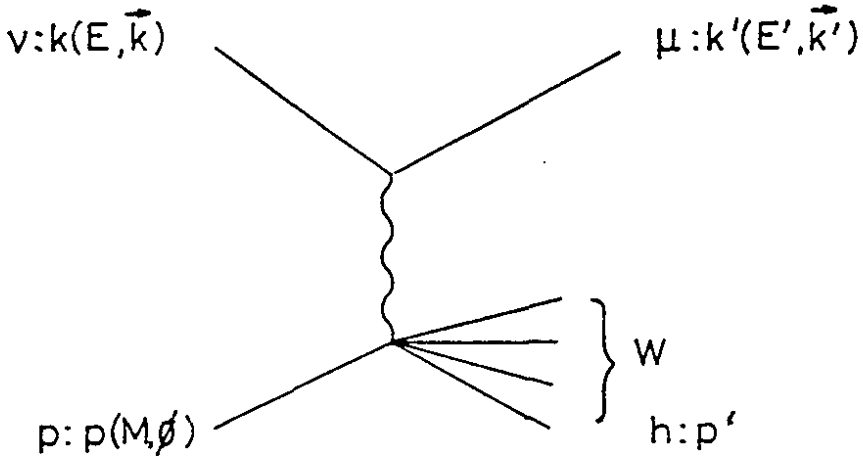
ν:k(E,k)
μ:k'(E',k')
p:p(M,ø)
W
h:p'

fig. 2

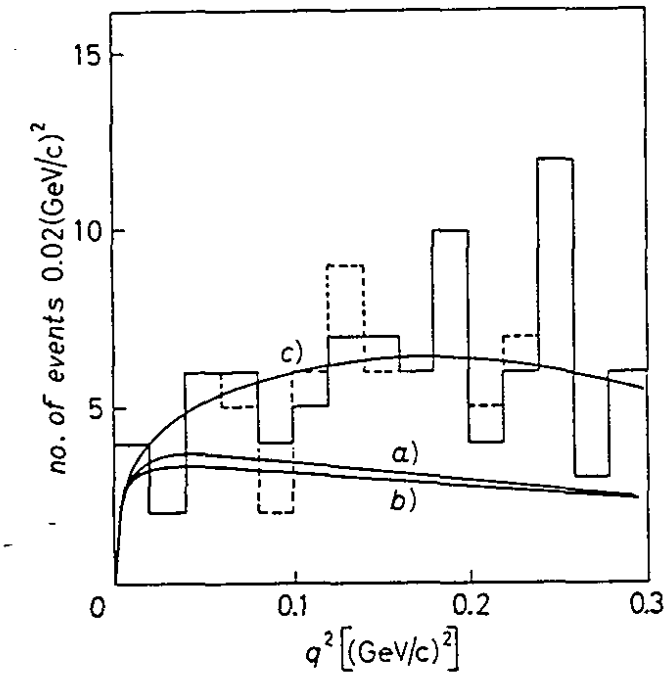
15
10
5
0
0.1
0.2
0.3
no. of events 0.02(GeV/c)²
q² [(GeV/c)²]
c)
a)
b)

fig. 3

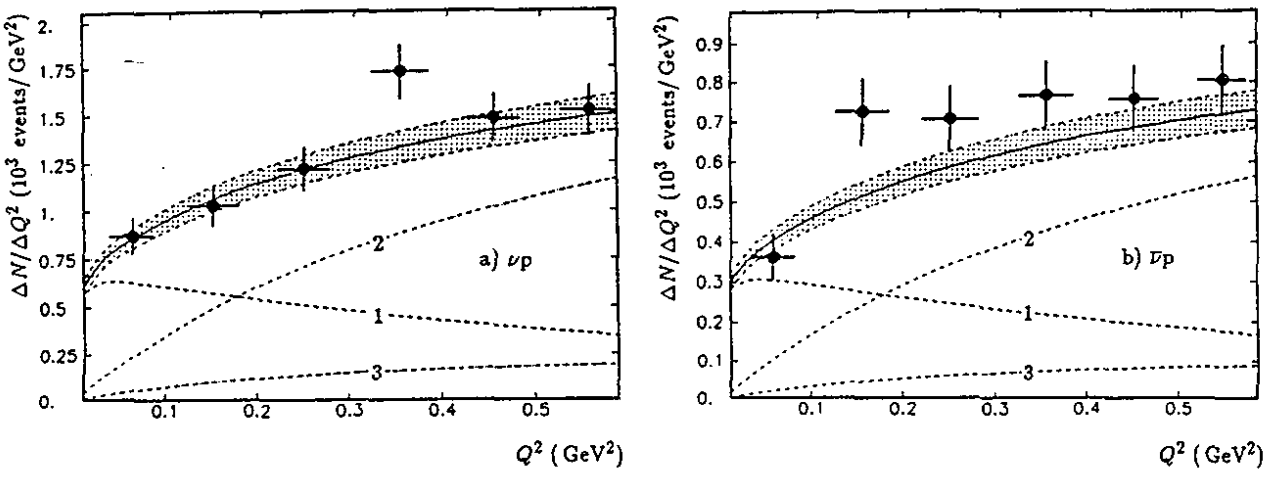
ΔN/ΔQ² (10³ events/GeV²)
Q² (GeV²)
a) νp
b) ν̄p
1
2
3

fig. 4

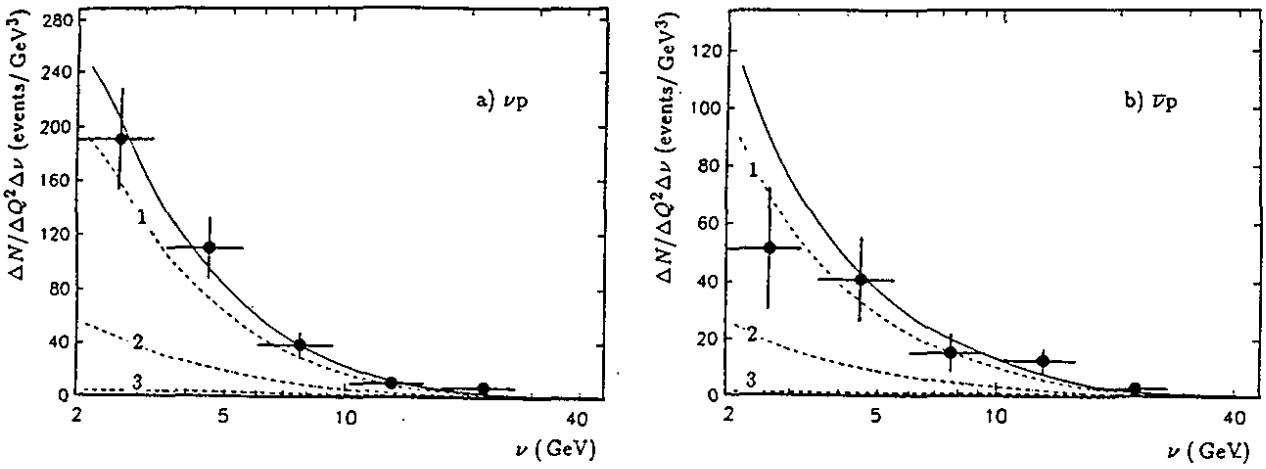
a) νp
b) ν̄p
ΔN/ΔQ²Δν (events/GeV³)
ν (GeV)
1
2
3

fig. 5

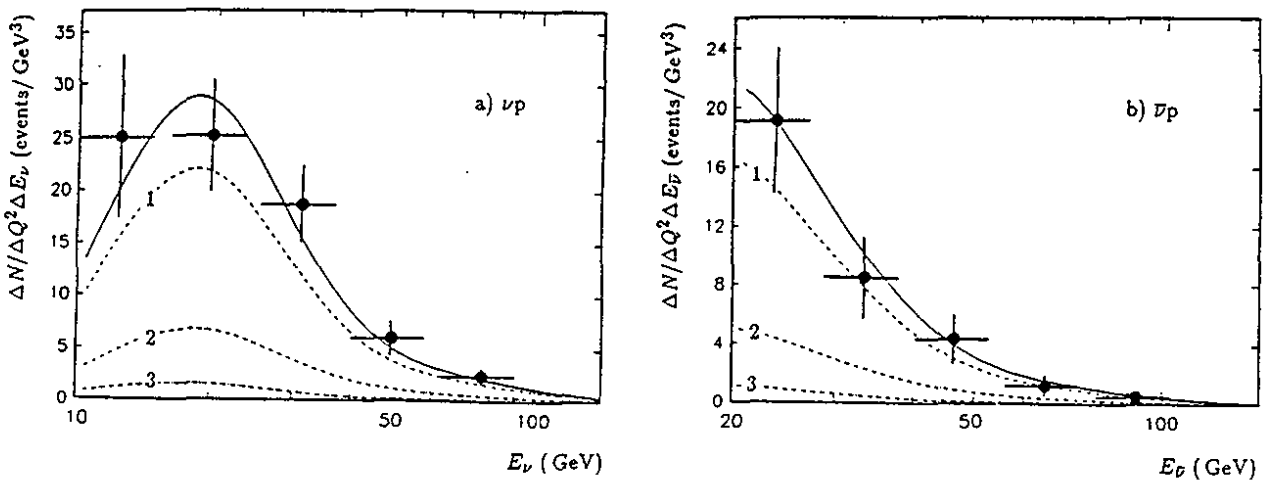
a) νp
b) ν̄p
ΔN/ΔQ²ΔE_ν (events/GeV³)
ΔN/ΔQ²ΔE_ν̄ (events/GeV³)
E_ν (GeV)
E_ν̄ (GeV)
1
2
3

fig. 6

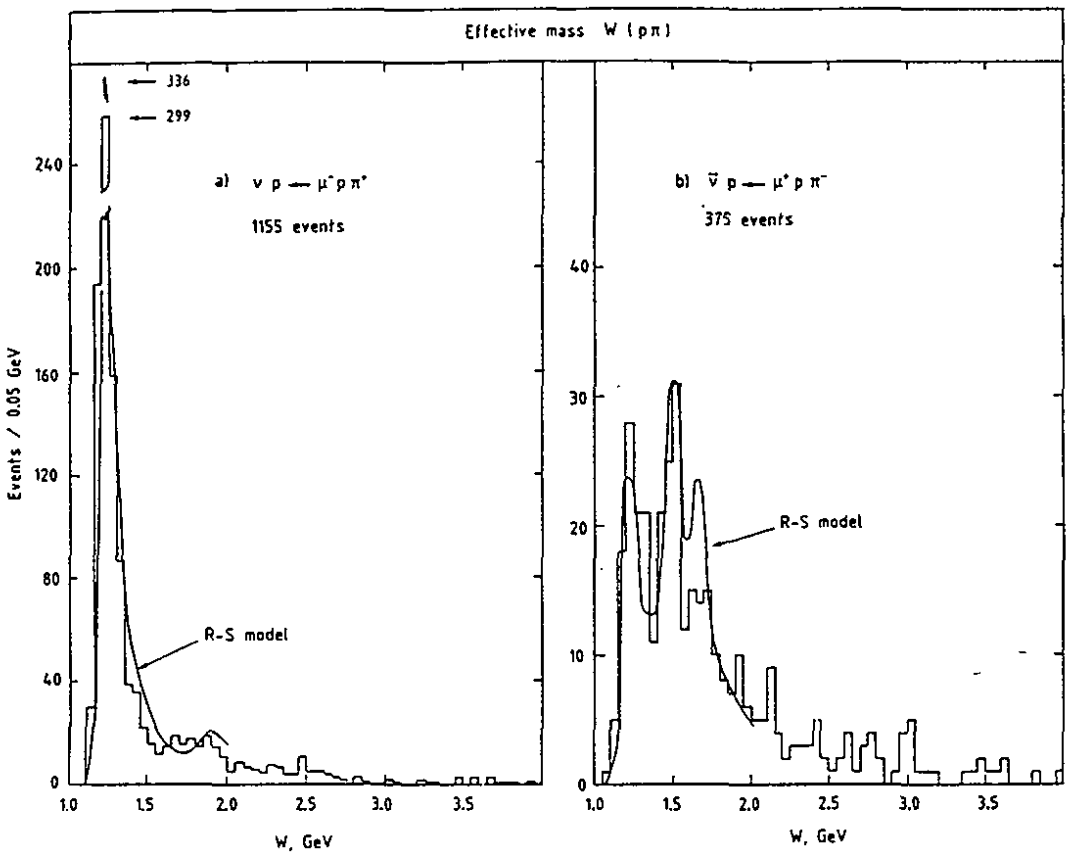
Effective mass W (pπ)
336
299
a) ν p → μ⁻ p π⁺
1155 events
b) ν̄ p → μ⁺ p π⁻
375 events
R-S model
R-S model
Events / 0.05 GeV
W, GeV
W, GeV

fig. 7

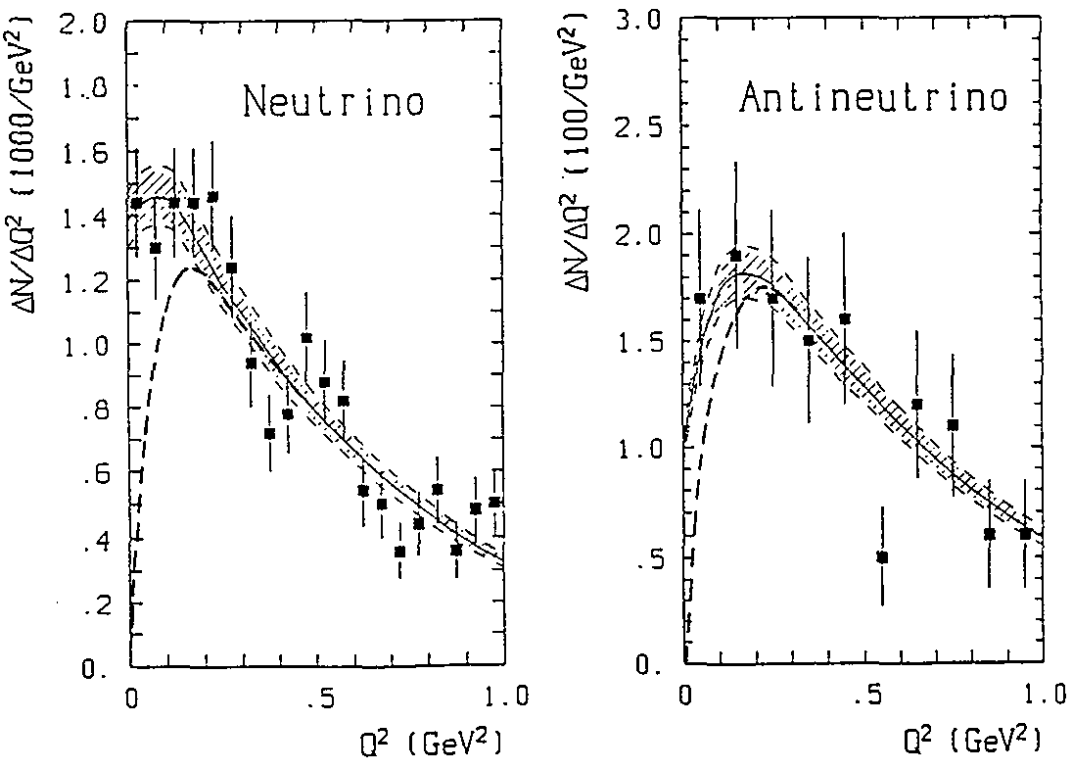
Neutrino
Antineutrino
ΔN/ΔQ² (1000/GeV²)
ΔN/ΔQ² (100/GeV²)
Q² (GeV²)
Q² (GeV²)

fig. 8

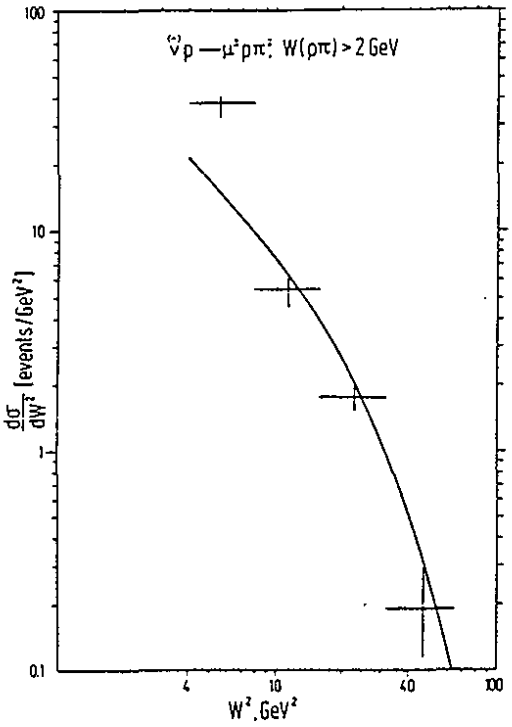

fig. 9

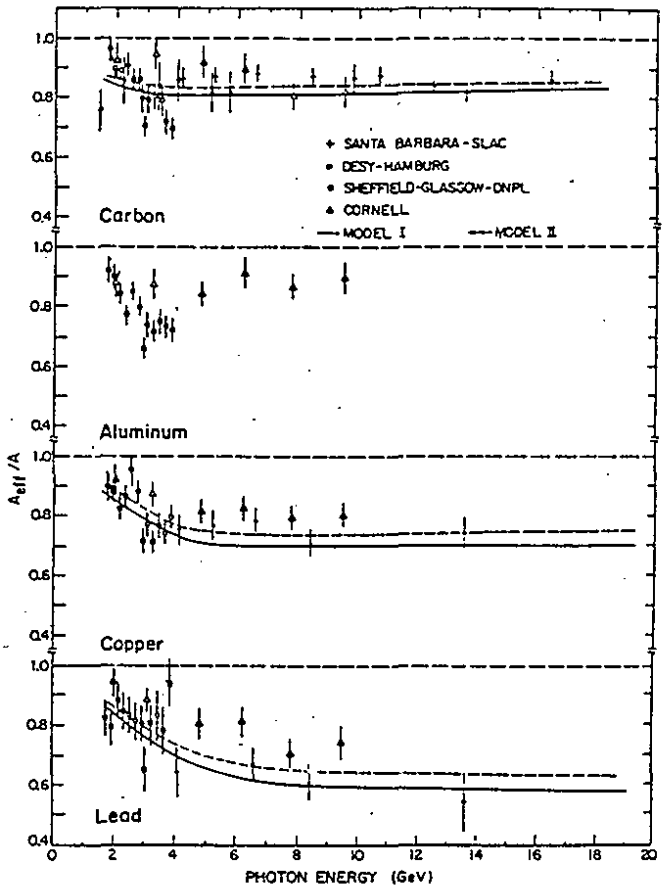

fig. 10

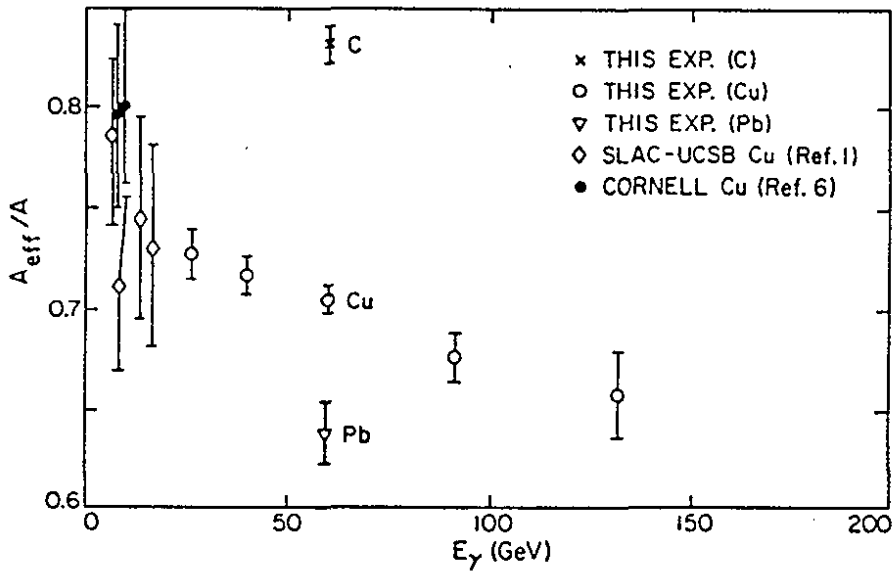

fig. 11

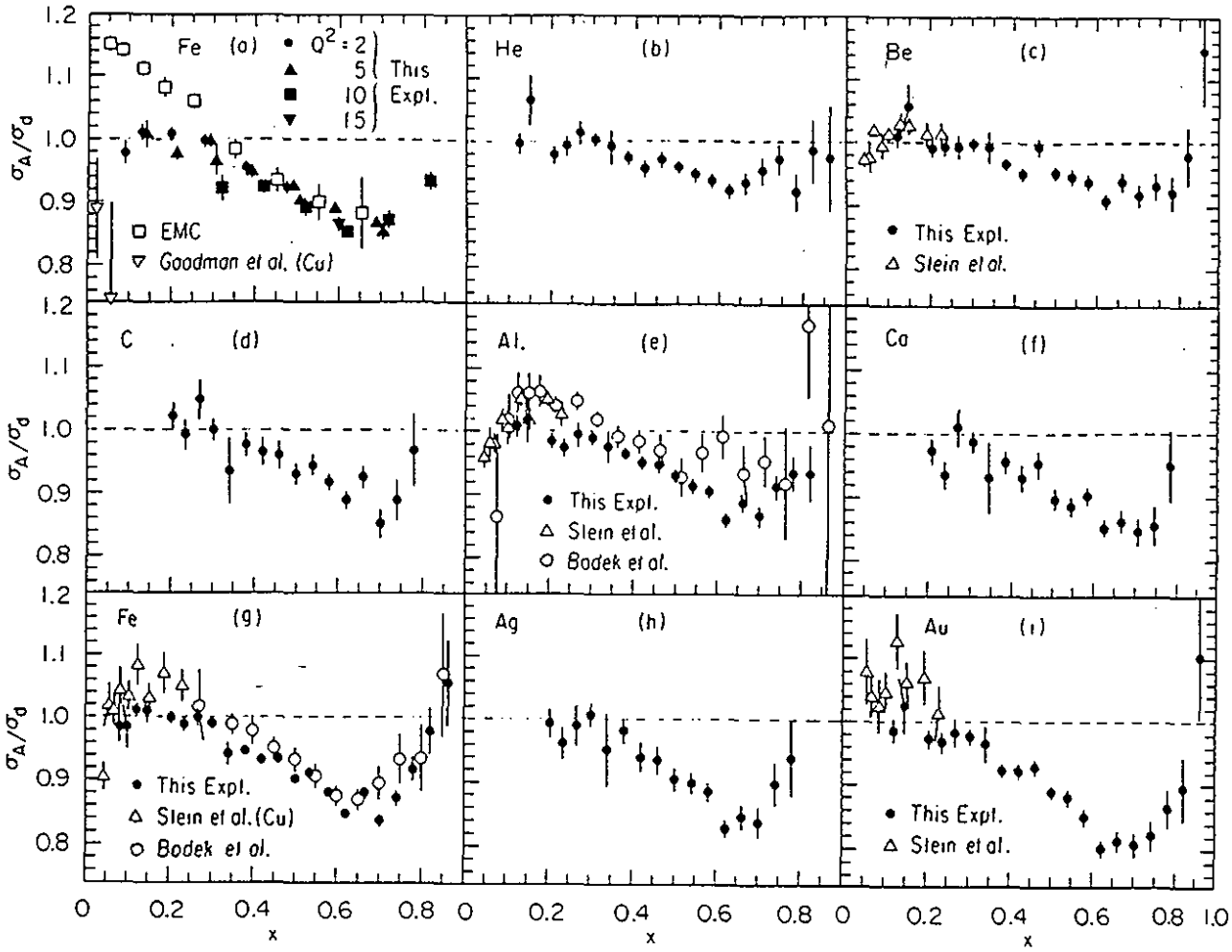
Fe (a)
Q^2 = 2
5
10
15
This Expt.
EMC
Goodman et al. (Cu)
He (b)
Be (c)
This Expt.
Stein et al.
C (d)
Al (e)
This Expt.
Stein et al.
Bodek et al.
Ca (f)
Fe (g)
This Expt.
Stein et al. (Cu)
Bodek et al.
Ag (h)
Au (i)
This Expt.
Stein et al.
σ_A/σ_d
x

fig. 12

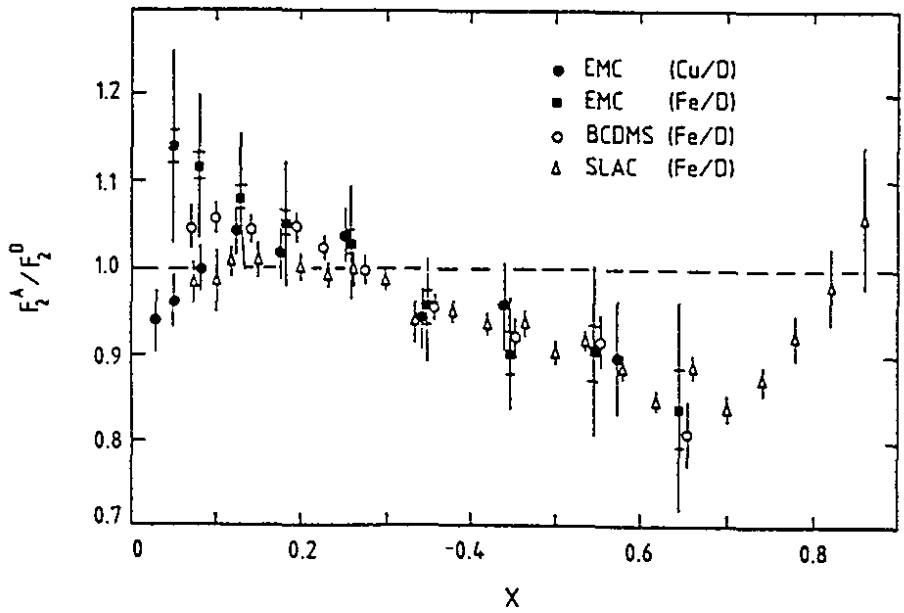
EMC (Cu/D)
EMC (Fe/D)
BCDMS (Fe/D)
SLAC (Fe/D)
F_2^A/F_2^D
X

fig. 13

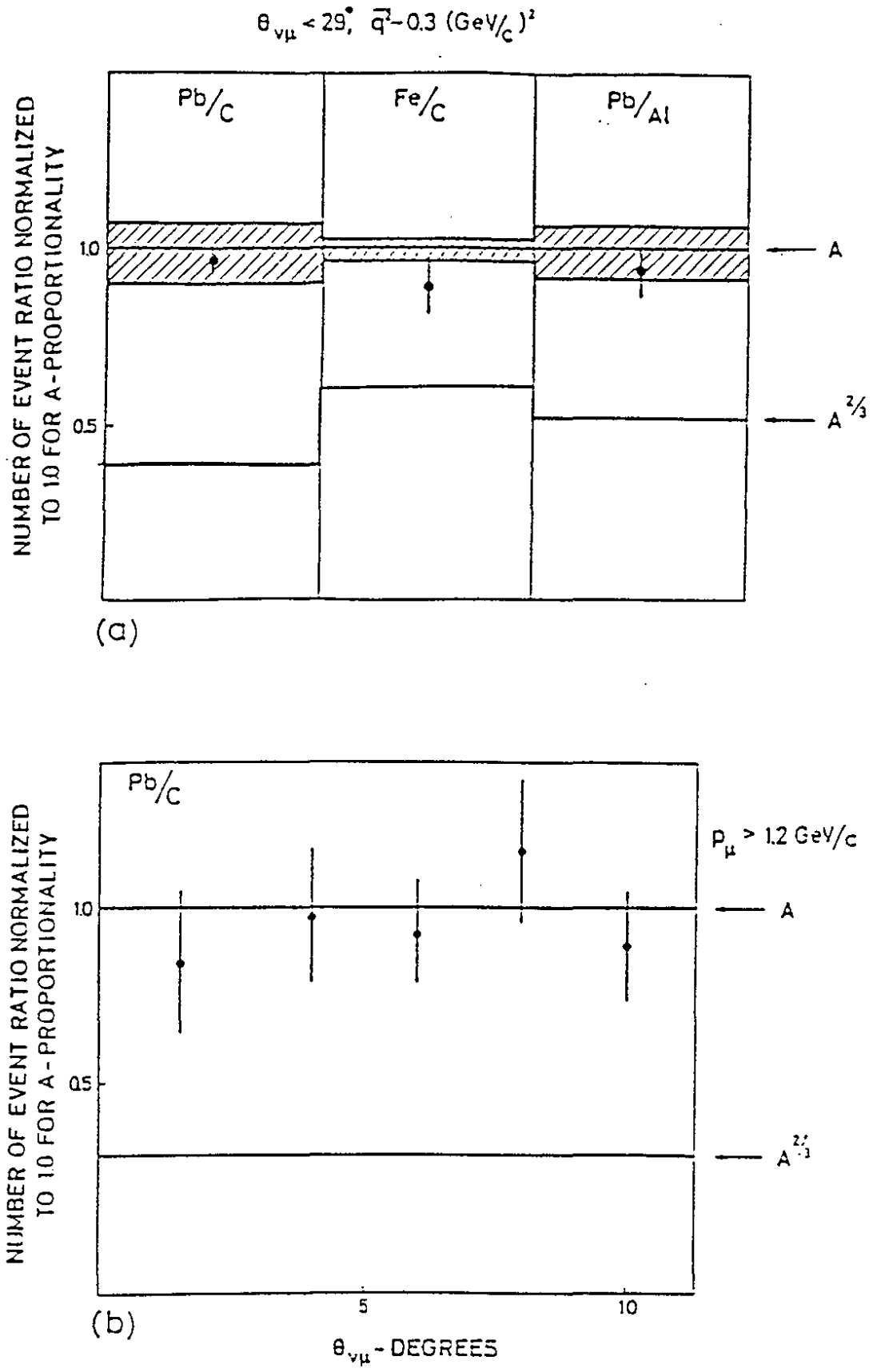
θνμ < 29°, q² ~ 0.3 (GeV/c)²
Pb/C
Fe/C
Pb/Al
NUMBER OF EVENT RATIO NORMALIZED TO 1.0 FOR A-PROPORTIONALITY
1.0
0.5
A
A^2/3
(a)
Pb/C
Pμ > 1.2 GeV/c
A
A^2/3
5
10
θνμ - DEGREES
(b)

fig. 14

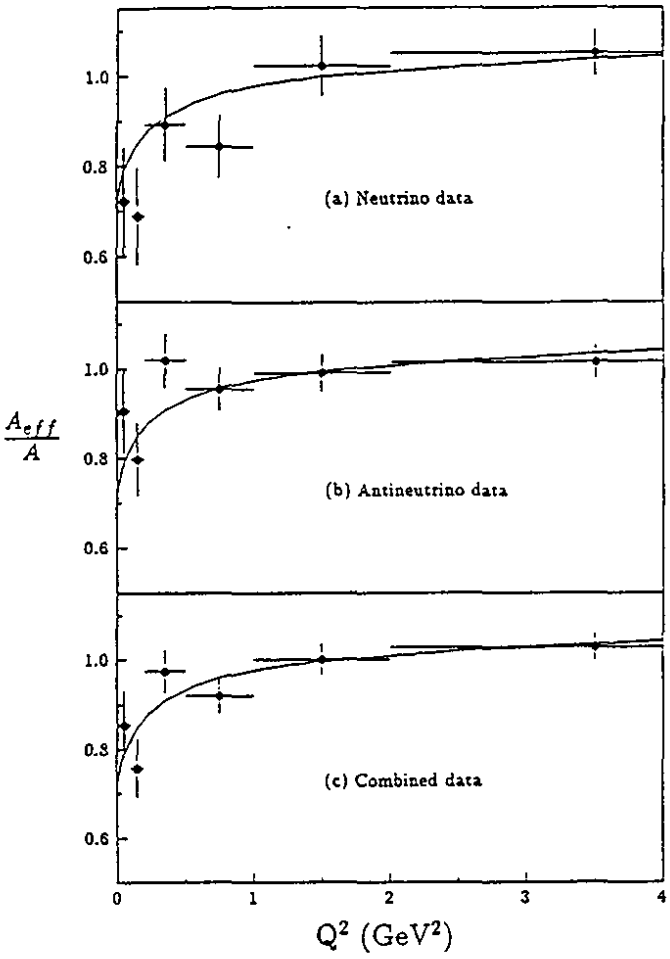

fig. 15

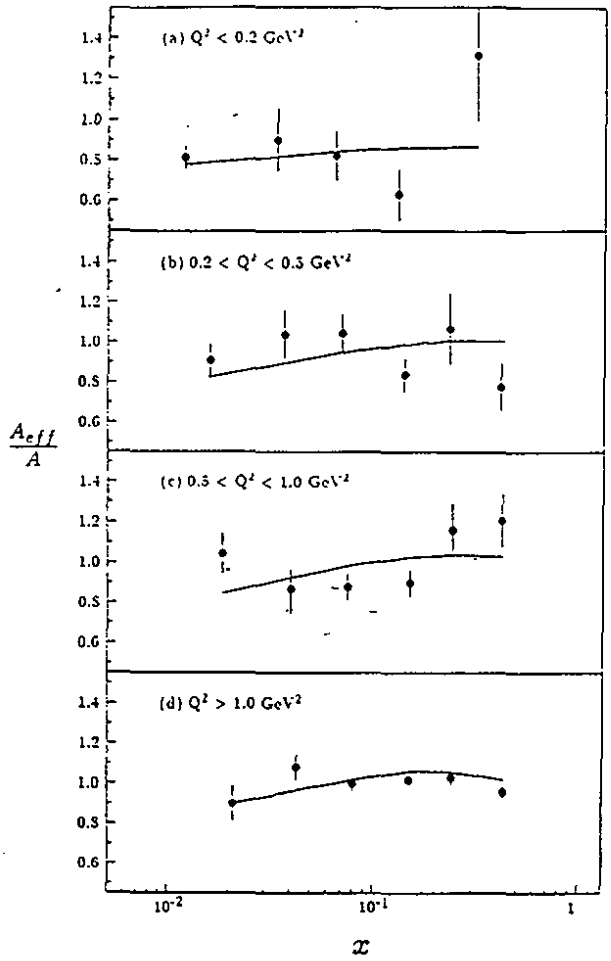

fig. 16

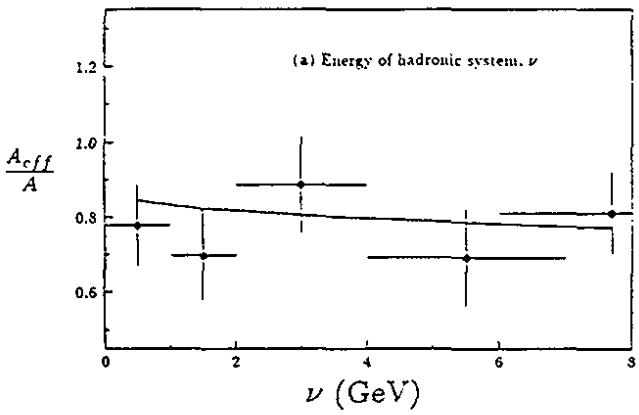

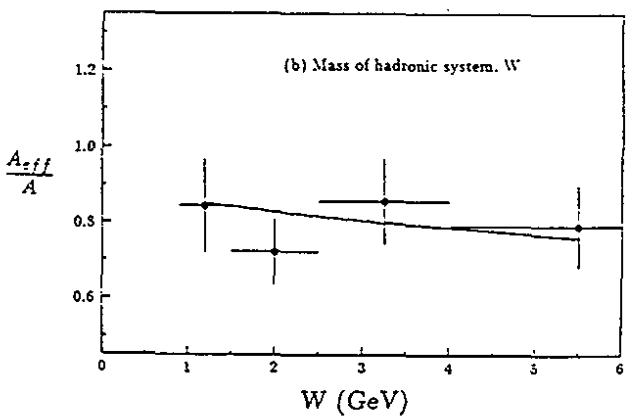

fig. 17

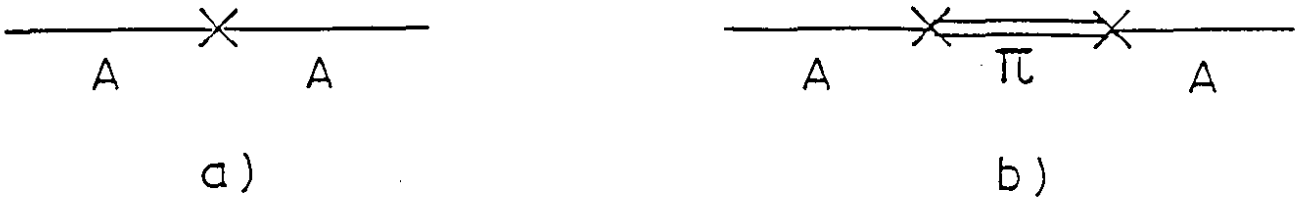

fig. 18

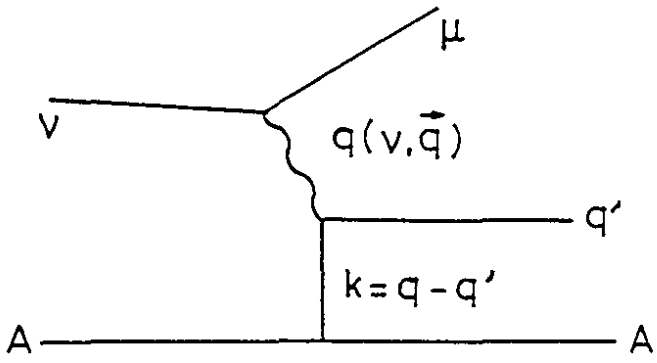

fig. 19

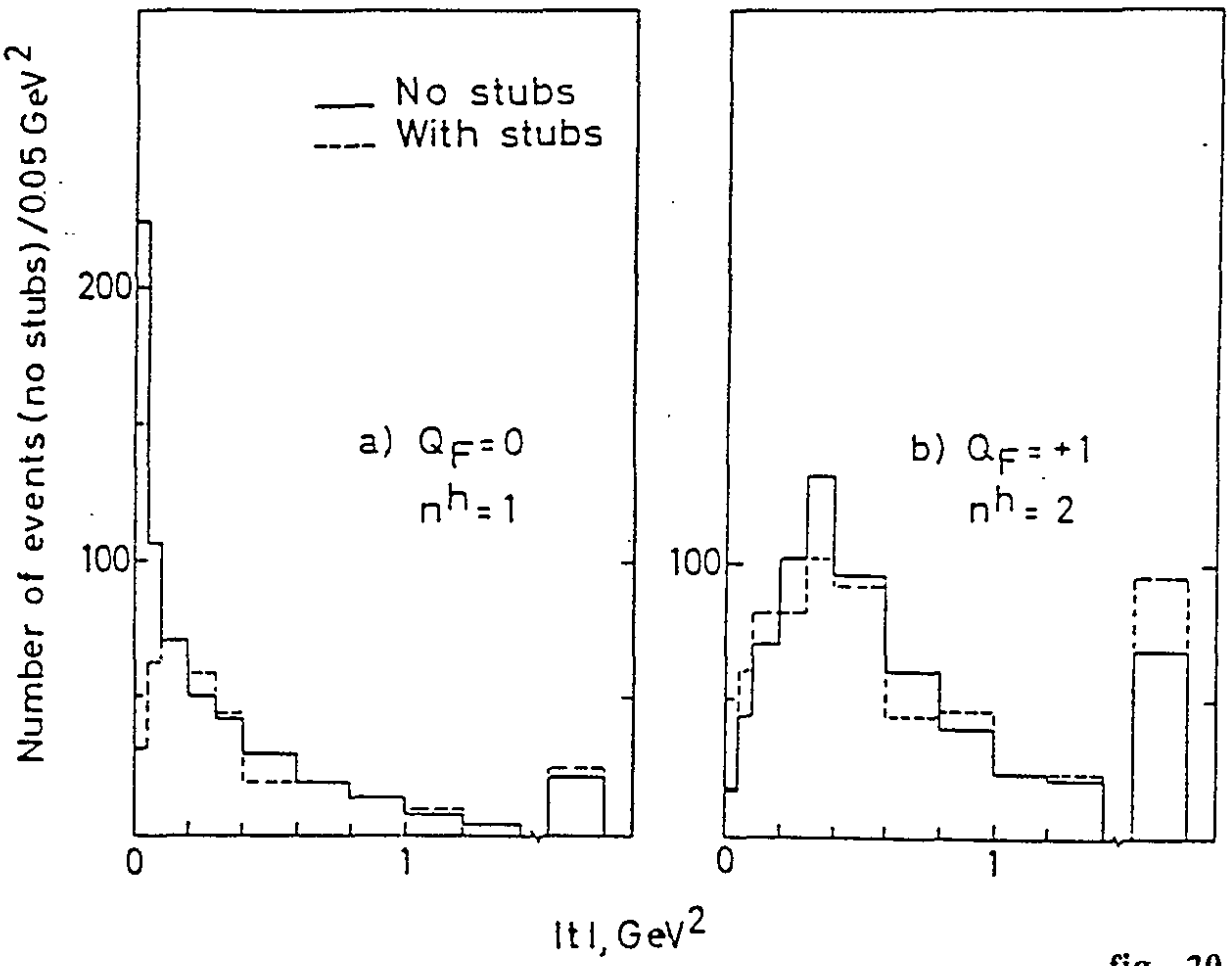

fig. 20

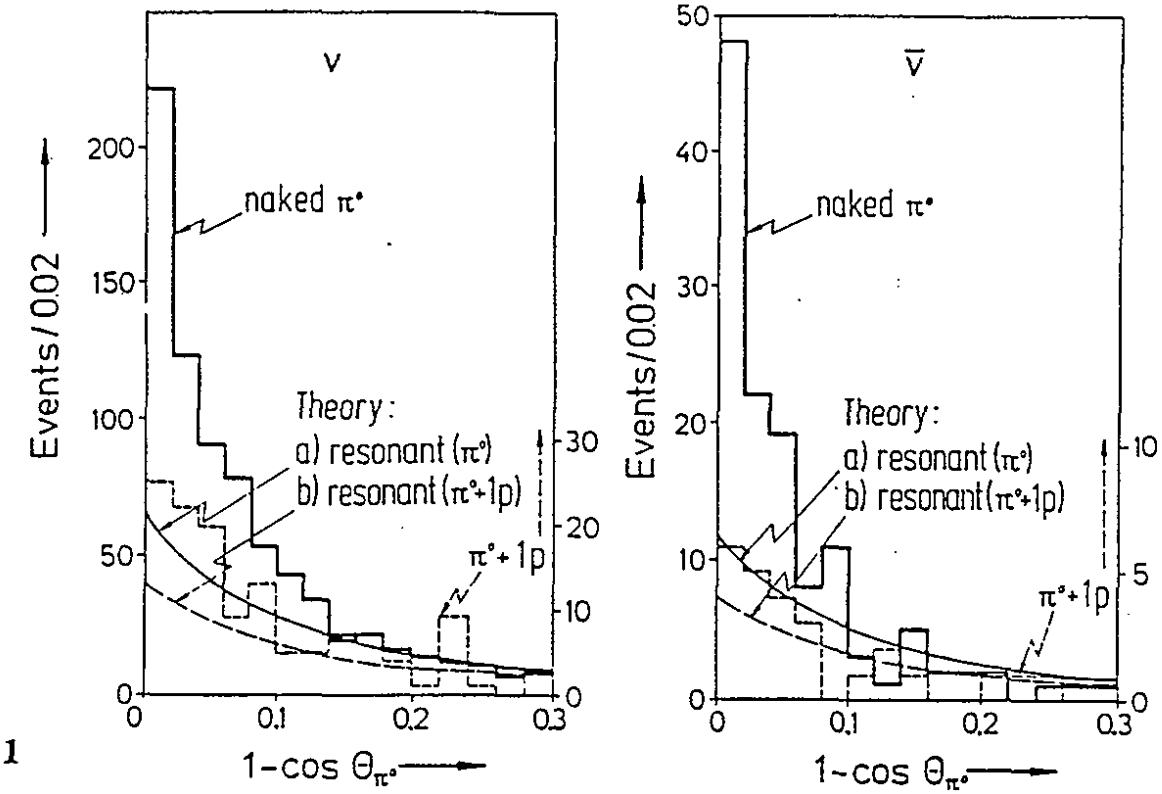

fig. 21

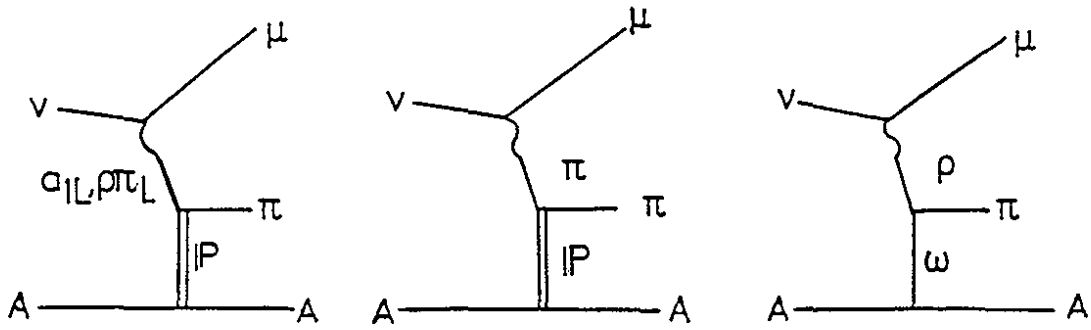

fig. 22

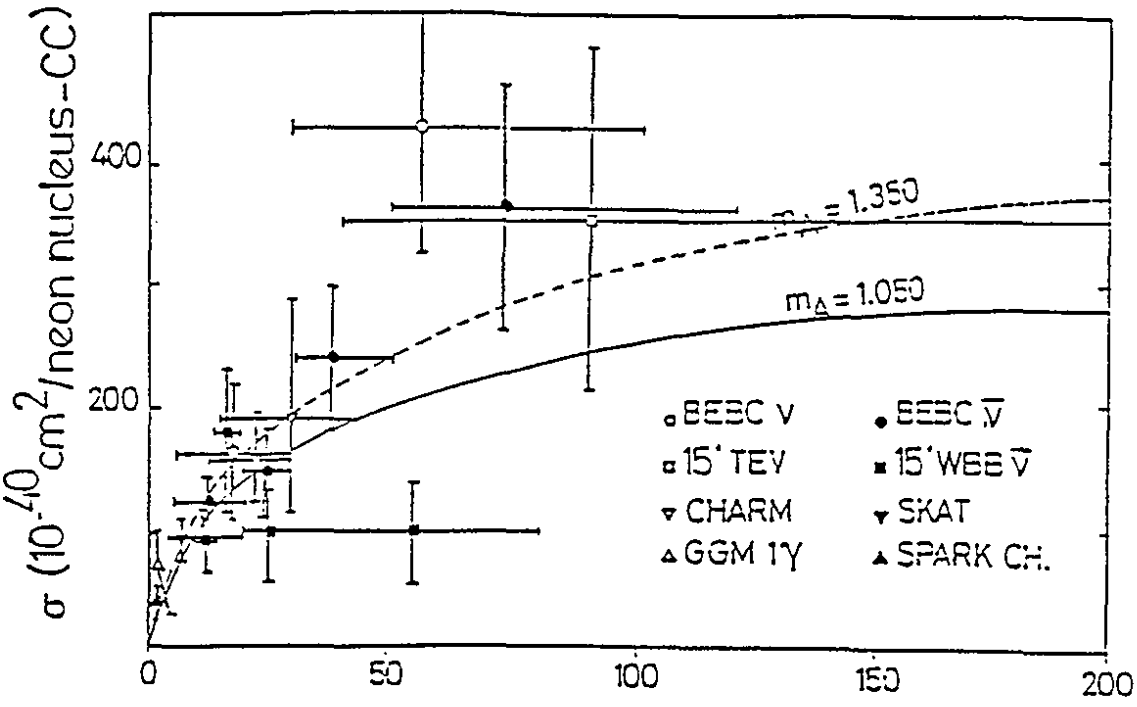

fig. 23

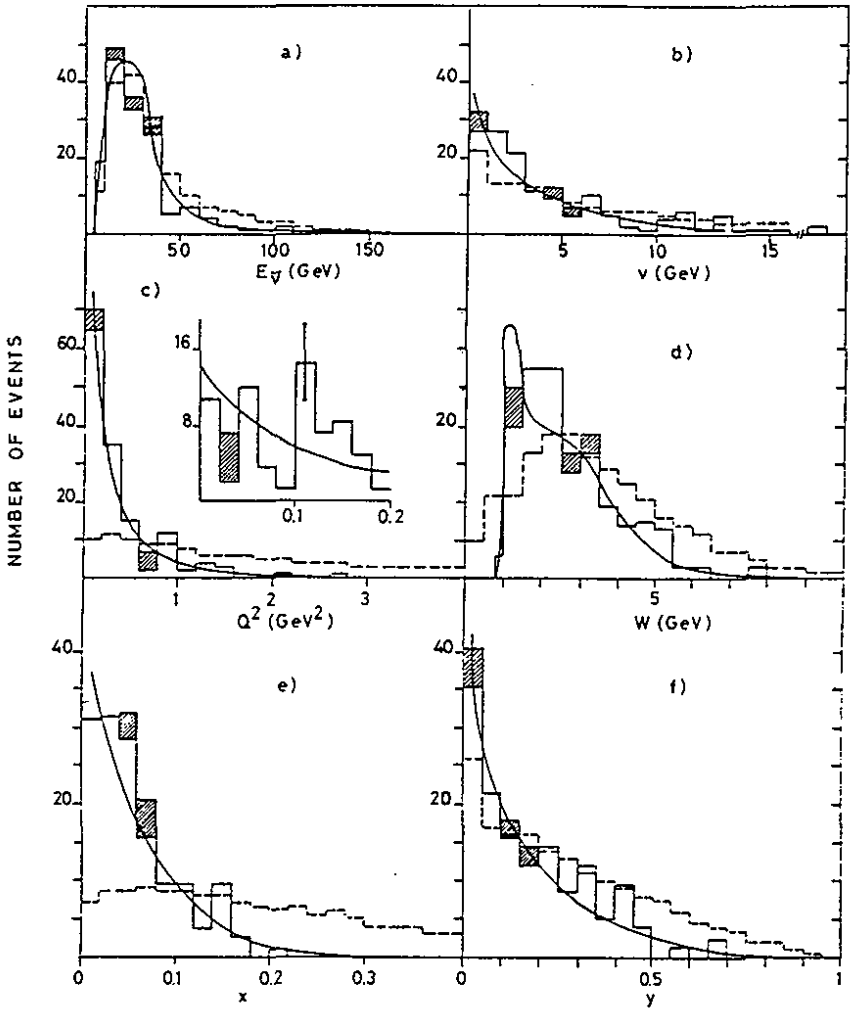

fig. 24

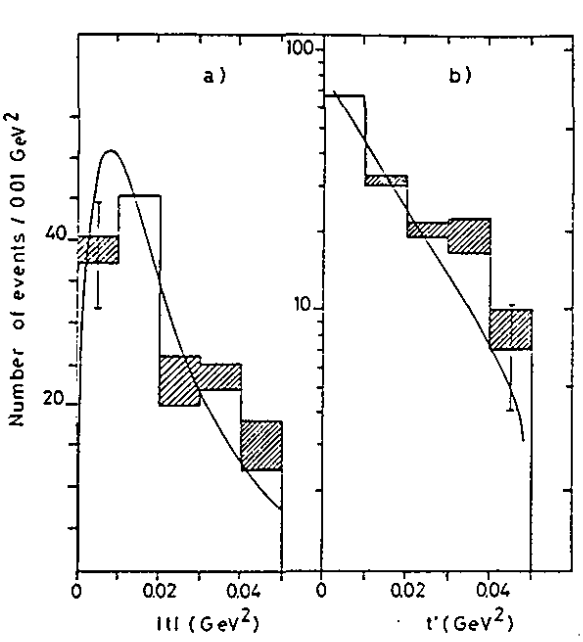

fig. 25

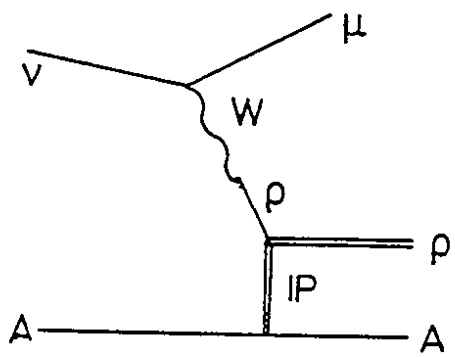

fig. 26

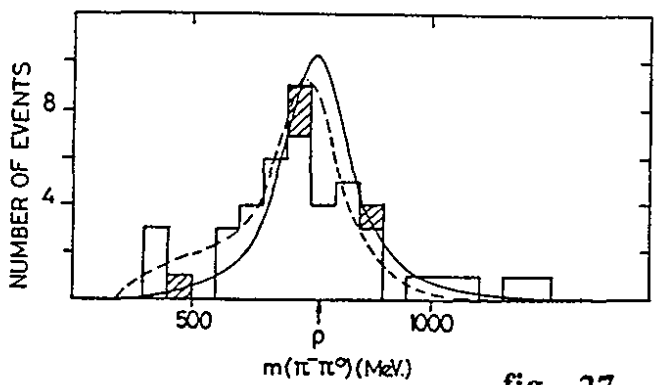

fig. 27

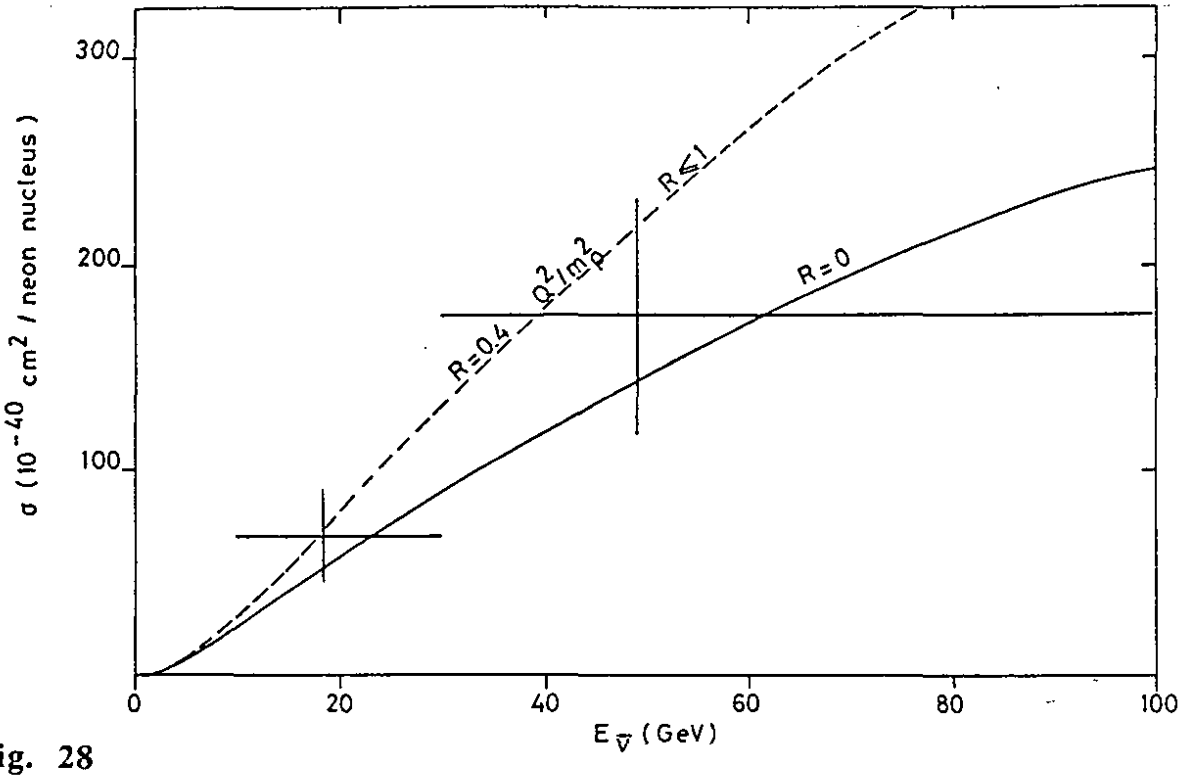
σ (10⁻⁴⁰ cm² / neon nucleus)
E ν̄ (GeV)
R≤1
R=0
R=0.4
Q²≥m²A

fig. 28

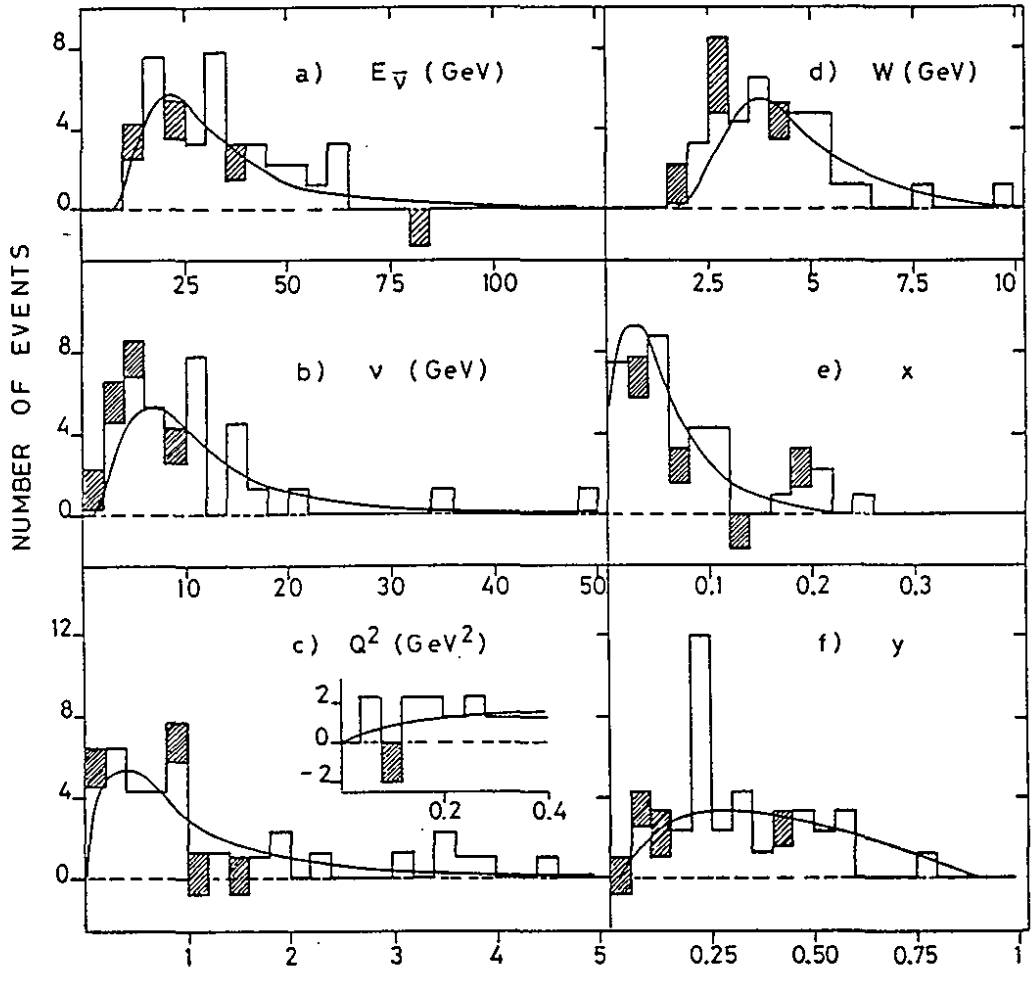
NUMBER OF EVENTS
a) E ν̄ (GeV)
b) ν (GeV)
c) Q² (GeV²)
d) W (GeV)
e) x
f) y

fig. 29

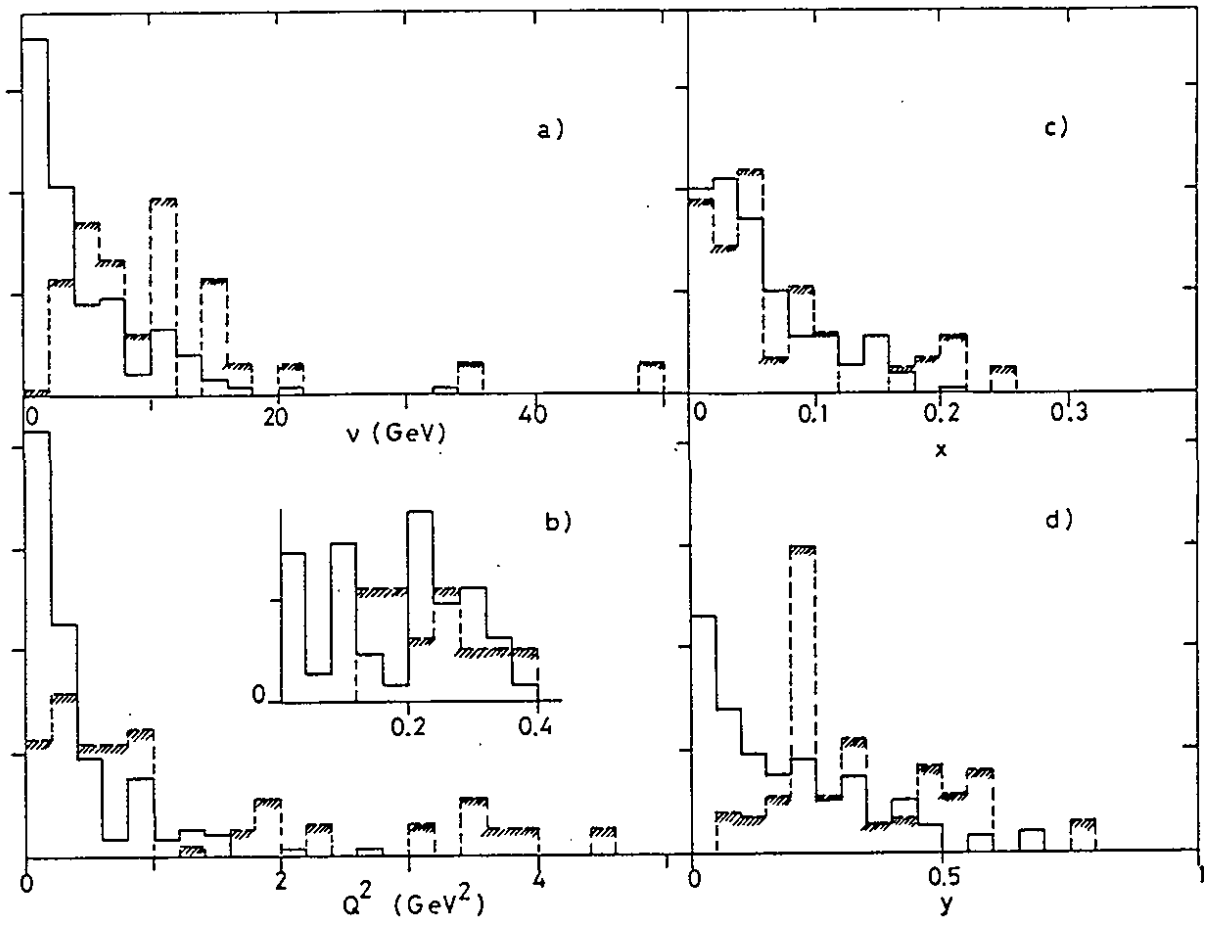

fig. 30

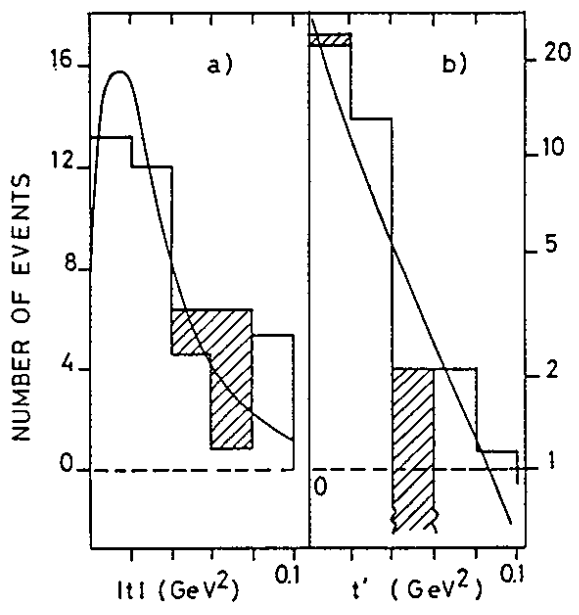

fig. 31

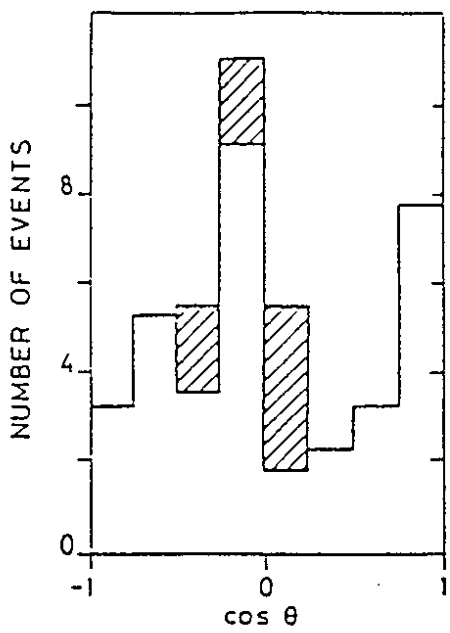

fig. 32

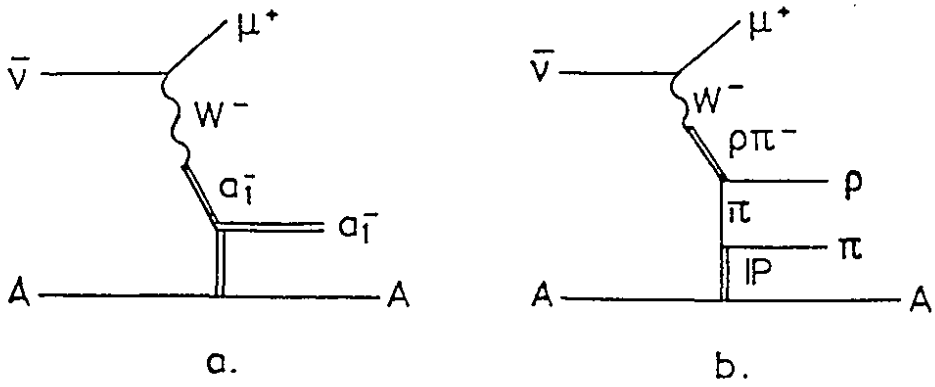

fig. 33

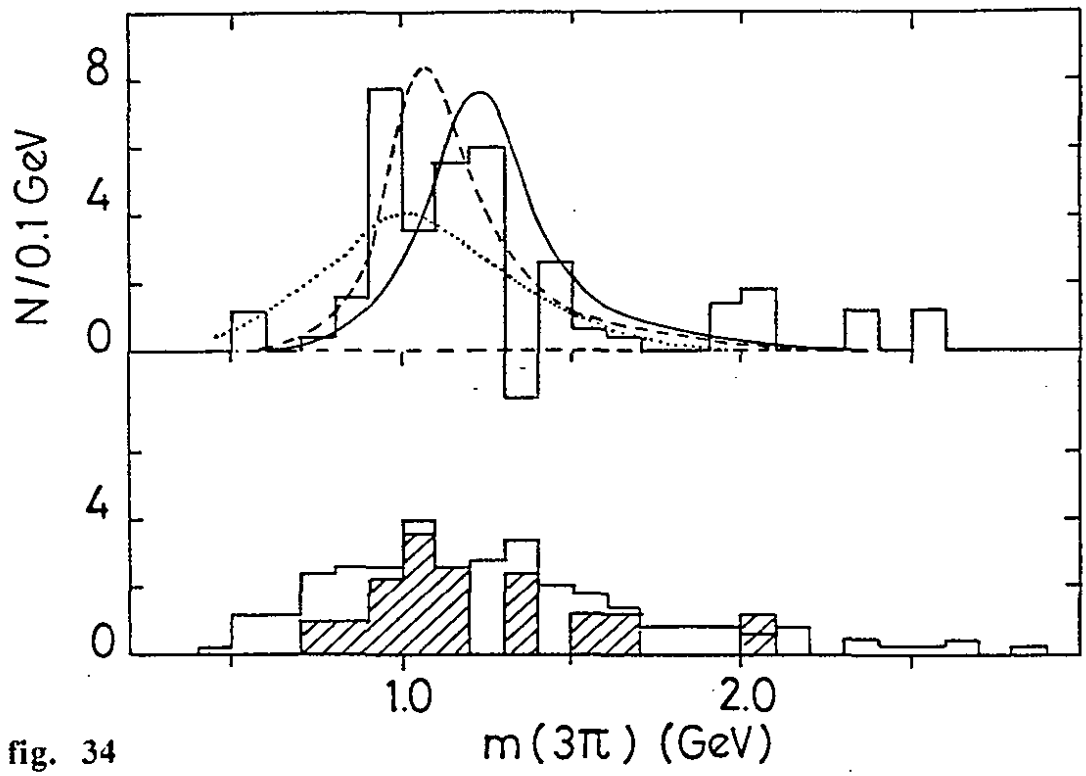

fig. 34

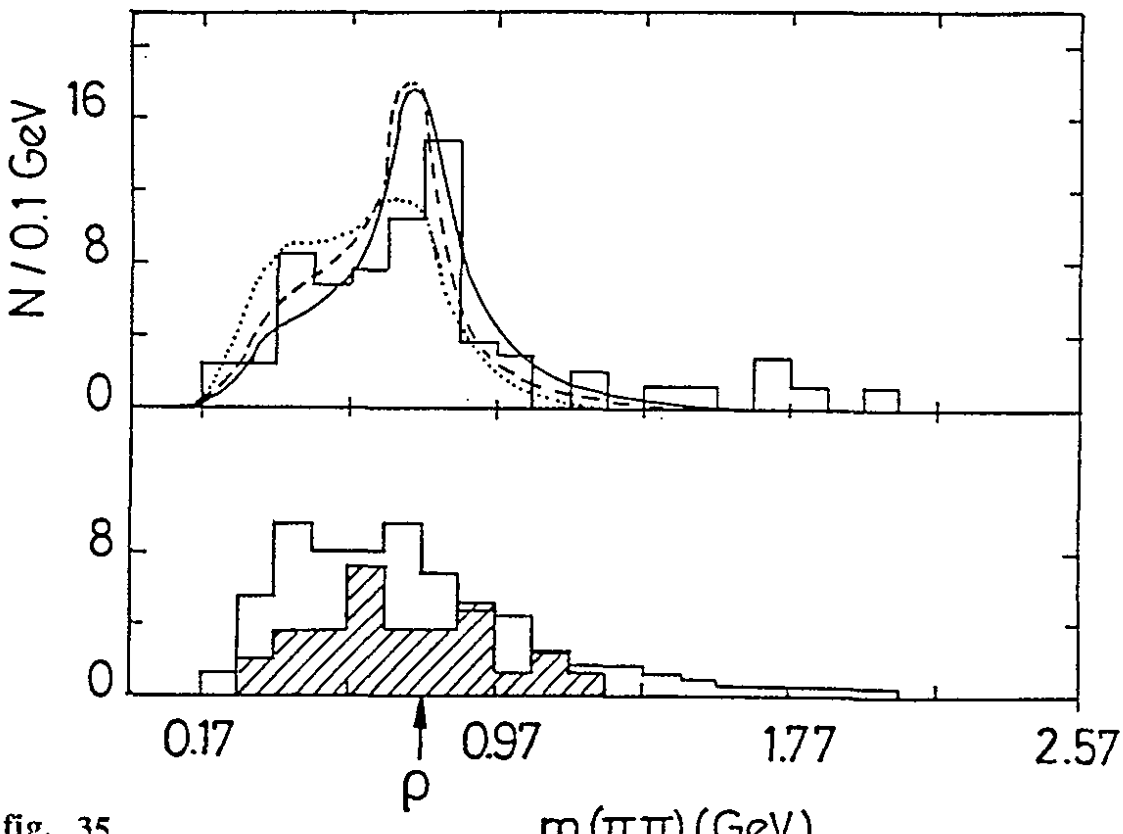

fig. 35

fig. 36

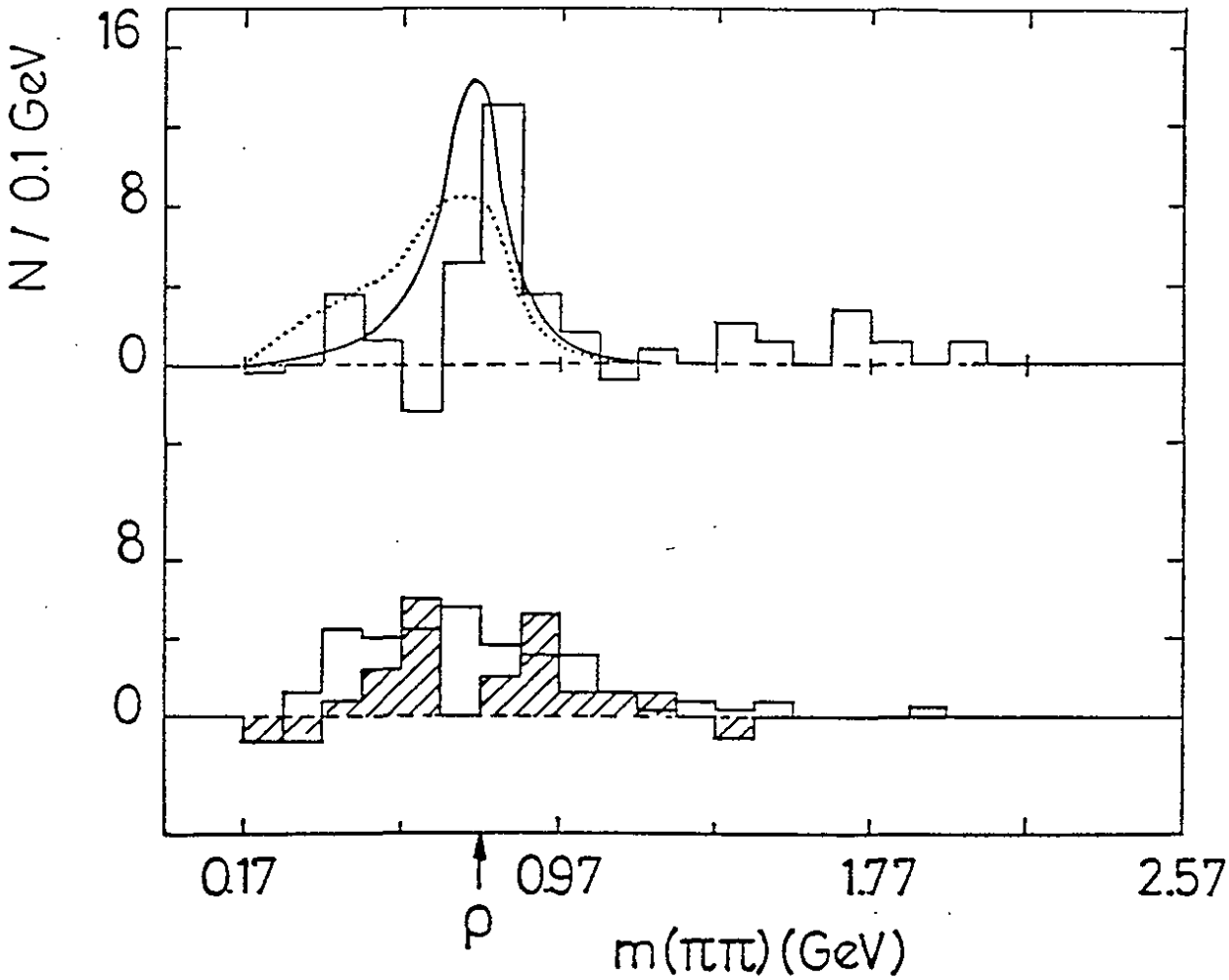
N / 0.1 GeV
16
8
0
8
0
0.17
ρ
0.97
1.77
2.57
m(ππ) (GeV)

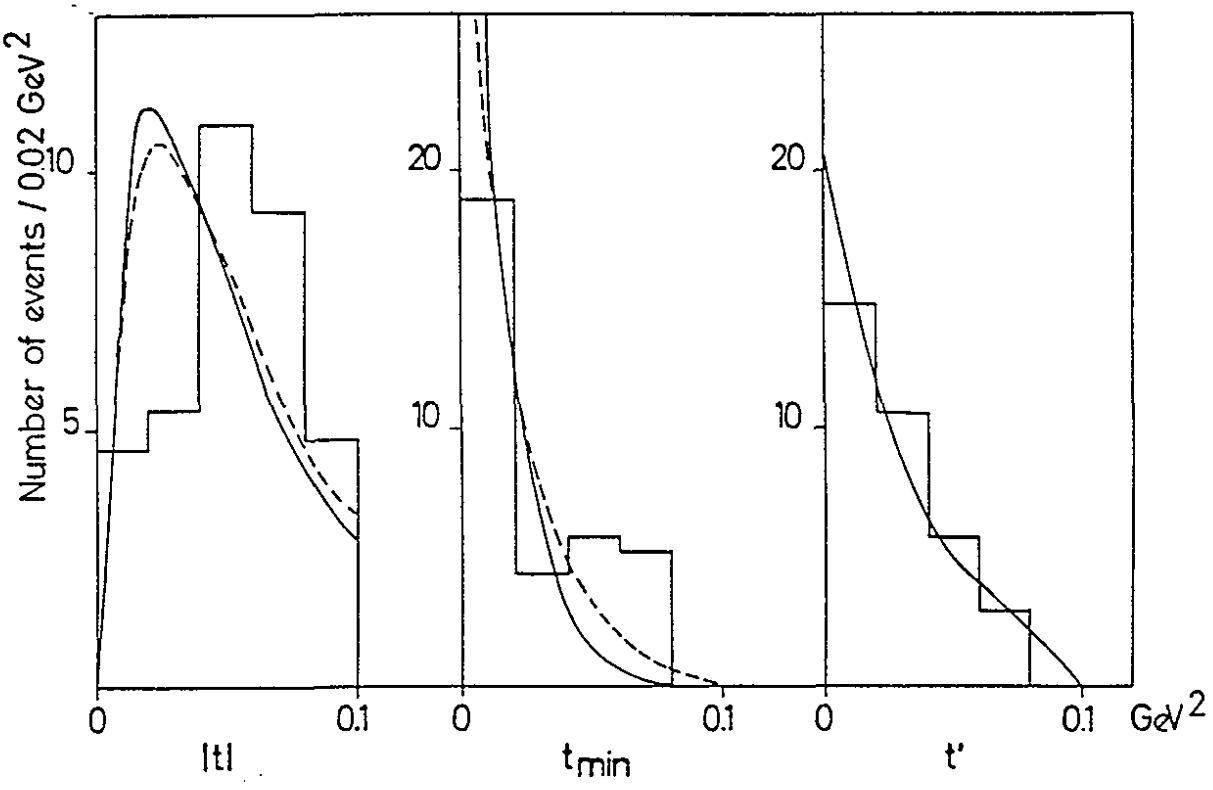
Number of events / 0.02 GeV²
10
5
20
10
20
10
0
0.1
|t|
0
0.1
t_min
0
0.1
t'
GeV²

fig. 37

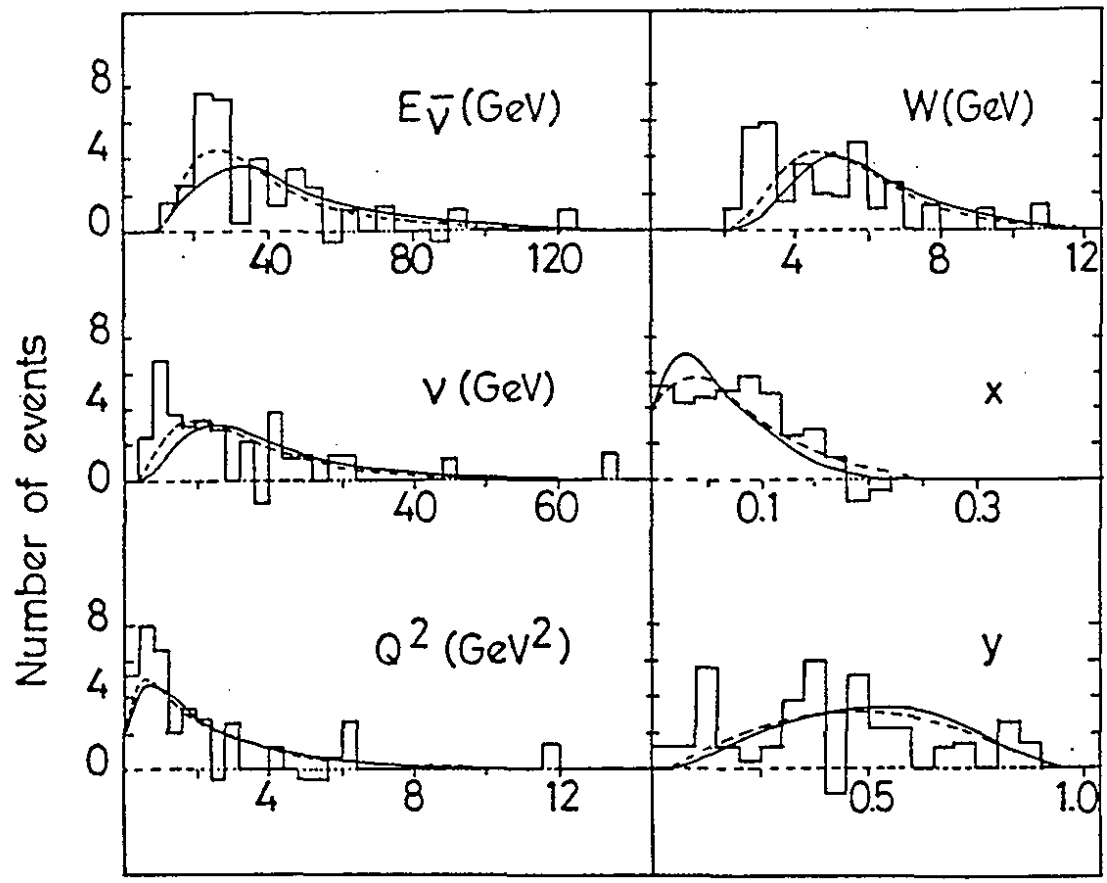
Number of events
$E_{\bar{\nu}}$ (GeV)
W(GeV)
ν (GeV)
x
Q^2 (GeV^2)
y
8
4
0
40
80
120
4
8
12
60
0.1
0.3
0.5
1.0

fig. 38

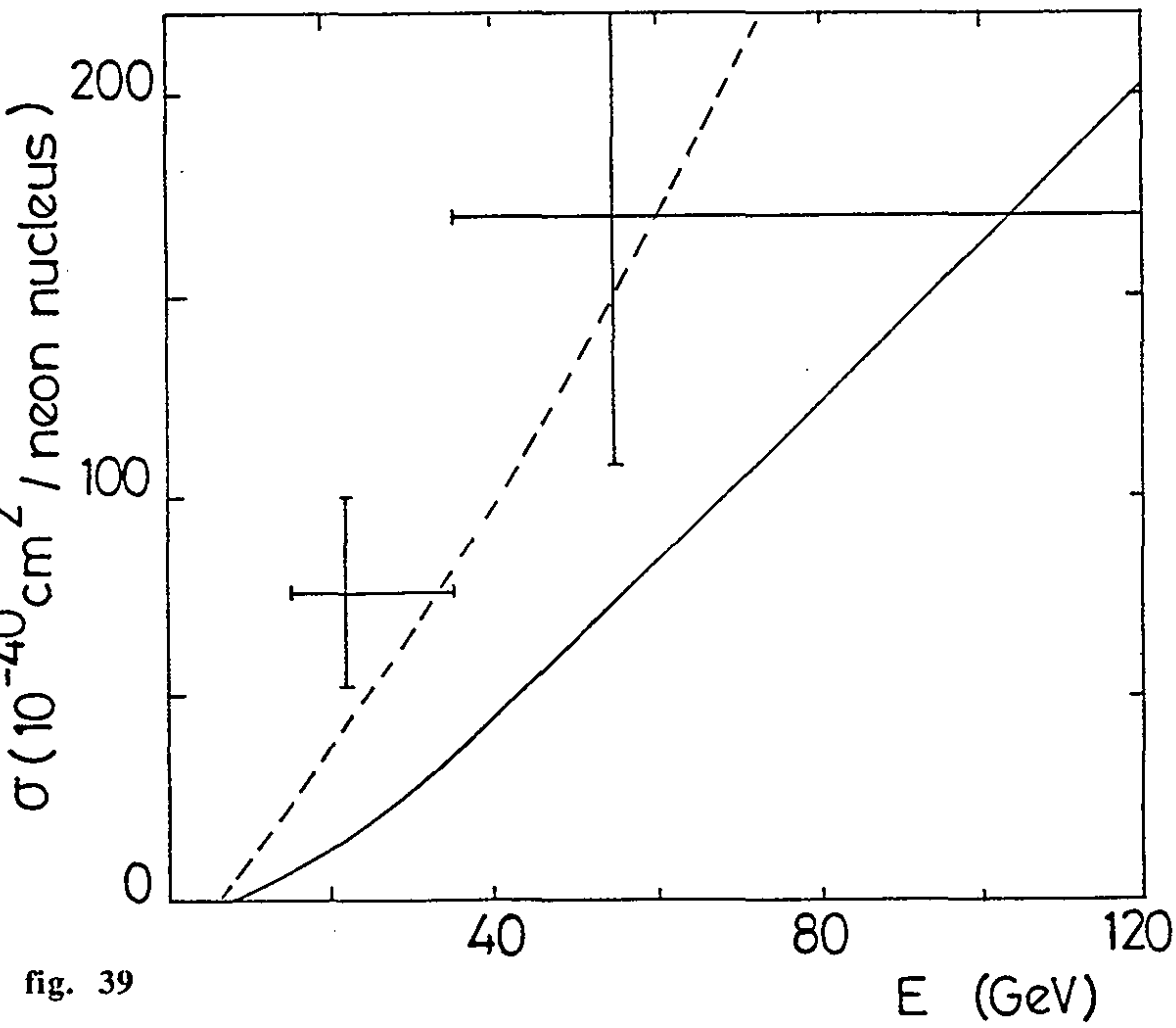
σ (10^{-40} cm^2 / neon nucleus)
E (GeV)
200
100
0
40
80
120

fig. 39

APPENDIX

A. The Glauber-Gribov theory of hadron-nucleus diffractive interactions

A.1 Elastic scattering. Eikonal approximation.

In this appendix, we summarize the main ideas and present the major results of the Glauber-Gribov multiple scattering theory. A detailed derivation, which will not be given here, can be found for instance in ([Glauber 1959], [Gribov 1969a], [Cziz 1970], [Glauber 1970]). This approach relies on the basic assumption that the nucleus can be treated as a frozen gas of weakly bound nucleons, whose properties do not differ from those of free nucleons; possible improvements to this approximation will be considered below.

The hadron-nucleus scattering amplitude can be represented as the sum of all contributing diagrams of Figs. 1a,b. In the impact parameter representation, the partial amplitude for the hadron-nucleus elastic scattering has the form,

$$f_{el}^{hA}(b) = i\{1 - [\,1 - \frac{1}{2A}\,\sigma_{tot}^{hN}(1 - i\,\alpha_{hN})\,T(b)\,]^A\} \ . \qquad (A1)$$

Here, α_{hN} is the ratio of the real to imaginary parts of the forward hadron-nucleon elastic scattering amplitude, which is much smaller than one at high energies. The nucleus profile function,

$$T(b) = \frac{1}{2\pi B}\int d^2b'\ T_0(b')\ e^{-\frac{(b-b')^2}{2B}} \qquad (A2)$$

is obtained by convoluting the hadron-nucleon elastic scattering amplitude

$$f_{el}^{hN}(b) = \sigma_{tot}^{hN}(1 - i\alpha_{hN})\ \frac{1}{2\pi B}\ e^{-\frac{b^2}{2B}} \qquad (A3)$$

with the nuclear optical thickness,

$$T_0(b) = \int_{-\infty}^{\infty} dz\, \rho_A(b,z). \qquad (A4)$$

B is the slope parameter of the hadron-nucleon elastic scattering differential cross section. $\rho_A(r)$ is the nuclear density function, normalized as

$$\int d^3r\, \rho_A(r) = A \quad , \qquad (A5)$$

of which a realistic form is given by the Woods-Saxon parametrization.

The meaning of expression (A1) is straightforward. The scattering amplitude for hadron-nucleus interactions equals one minus the product of amplitudes for the hadrons not to interact with any of the target nucleons. If one neglects the contribution of the real part ($\alpha_{hN} = 0$), and goes to the limit of high A in expression (A1), one gets

$$\sigma_{tot}^{hA} \approx 2 \int d^2b \left\{ 1 - e^{-\frac{1}{2}\sigma_{tot}^{hN} T(b)} \right\} \quad , \qquad (A6)$$

the amplitudes being normalized by the unitarity relation

$$\sigma_{tot} = 2 \int d^2b\, \mathrm{Im}\, f_{el}(b) \quad . \qquad (A7)$$

The expression (A6) is known as the optical approximation. Hereafter, we use this approximation everywhere for the sake of simplicity, although all numerical calculations can be done with the exact expression (A1).

Note that the forward hadron-nucleon elastic scattering amplitude is nearly imaginary at high energy; from the point of view of unitarity, this means that the interaction is mainly absorptive. Therefore, the stronger the absorption (i.e. σ_{tot}^{hN}), the more "black" the nucleus (Im $f_{el}(b)$ is closer to one), and the higher the total cross section σ_{tot}^{hA}. This emphasizes the absorptive character of the high energy elastic scattering. It should be noted that the expression used by Rein and Sehgal [Rein 1983] contains the opposite relation : as the absorption increases, so does the absorption factor F_{abs}, and the hadron-nucleus elastic scattering cross section vanishes.

The differential cross section for elastic hadron-nucleus scattering is related to the Fourier transform of the amplitude (A1) :

$$\frac{d^2\sigma_{el}^{hA}}{d^2k_T} = |F_{el}^{hA}(k_T)|^2 \quad , \qquad (A8)$$

where

$$F_{el}^{hA}(k_T) = \frac{1}{2\pi} \int d^2b\, f_{el}^{hA}(b)\; e^{-ik_T b} \quad . \tag{A9}$$

The exponential factor in the elastic hadron-nucleus cross section (A9) originates from the condition of coherence of waves with different impact parameters. If no such condition was imposed, for instance if the nucleus was broken, one would have to sum the probabilities of elastic scattering on different nucleons of the nucleus.

In the impact parameter representation, the total elastic scattering cross section has a simple form:

$$\sigma_{el}^{hA} = \int d^2b\, |F_{el}^{hA}(b)|^2 = \int d^2b \left\{ 1 - e^{-\frac{1}{2}\sigma_{tot}^{hN} T(b)} \right\}^2 , \tag{A10}$$

whereas the total inelastic cross section is given by

$$\sigma_{in}^{hA} = \int d^2b \left\{ 1 - e^{-\sigma_{tot}^{hN} T(b)} \right\} \quad . \tag{A11}$$

Experimentalists usually measure an "absorption cross section", defined as

$$\sigma_{abs}^{hA} = \sigma_{tot}^{hA} - \sigma_{el}^{hA} - \sigma_{Qel}^{hA} \quad . \tag{A12}$$

The eikonal expression for σ_{abs}^{hA} differs from (A11) only by the replacement of σ_{tot}^{hN} by σ_{in}^{hN}. The last term in (A12) is the quasielastic scattering cross section i.e. elastic scattering on individual nucleons. The inclusive cross section for the quasielastic scattering has the form :

$$\frac{d^2\sigma_{Qel}^{hA}}{d^2k_T} = \frac{d^2\sigma_{el}^{hN}}{d^2k_T} \int d^2b\, T(b)\; e^{-\sigma_{in}^{hN} T(b)} \quad . \tag{A13}$$

The slope parameter in quasielastic scattering on a nucleus is the same as on a nucleon target, which is much smaller than in the elastic hadron-nucleus scattering. This fact helps to separate the elastic scattering from the quasielastic background.

A.2 Inelastic shadowing.

Let us now consider the Gribov inelastic corrections to the Glauber eikonal approximation presented above. It is known that hadrons are not eigenstates of the interaction hamiltonian, and that they can be excited into new states as a result of the interaction. These off- diagonal transitions are called diffraction dissociation. They should be taken into account in the diagram of Fig. 1a, for example as it is depicted in Fig.1b. The computation of all these corrections faces a serious problem due to the lack of experimental information on the possible elastic and inelastic diffractive amplitudes for the interaction of the excited hadronic states with nucleons. Nevertheless, some approximations can be made here. One such approximation, suggested by Karmanov and Kondratyuk [Karmanov 1973], assumes that the off-diagonal diffractive amplitudes are small in comparison with the diagonal ones (which is confirmed in the rare cases where data exist); in this case, one can restrict oneself to only one intermediate diffractive excitation. As a result, the correction to the total cross section has the form

$$\Delta_{in}\,\sigma_{tot}^{hA} = -4\pi \int d^2b \int dM^2 \left.\frac{d\sigma_{DD}}{dk^2 dM^2}\right|_{k^2=0} |\,F(k_L, b)\,|^2\; e^{-\frac{1}{2}\sigma_{tot}^{hN} T(b)}, \quad (A14)$$

where the negative sign comes from the double scattering term (see also the discussion below). We have no information on the attenuation of the inelastic intermediate state in nuclear matter; therefore, we assume that it is the same as that for the incoming hadron. The integration is performed over all possible masses M of the intermediate states. The difference between the masses of the incoming hadron and M gives rise to a phase shift due to the longitudinal momentum transfer, k_L, at the diffractive dissociation vertex :

$$k_L = \frac{M^2 - m_h^2}{2E}\,, \quad (A15)$$

where E is the incident energy in the laboratory frame. This phase shift is taken into account by a longitudinal form factor $F(k_L, b)$ of the nucleus :

$$F(k_L, b) = \int_{-\infty}^{\infty} dz\, \rho_A(b, z)\; e^{ik_L z} \quad (A16)$$

At high energies, if $k_L R_A \ll 1$, $F(k_L, b) = T(b)$. At low energies, when $1 / k_L$ is smaller than the mean internucleon distance, the inelastic corrections disappear and the Glauber approximation becomes exact.

Although the above approximation to $\Delta_{in}\,\sigma_{tot}^{hA}$ seems to be quite crude, it provides a good description of the data on high energy total cross sections for neutron-nuclei [Murthy 1975] and kaon-nuclei [Gsponer 1979] interactions. This success is due to the fact that the inelastic correction applies to the exponential term in (A6), which itself is small with respect to one : the value of $\Delta_{in}\,\sigma_{tot}^{hA} / \sigma_{tot}^{hA}$ usually does not exceed a few percent. However, the inelastic corrections can be large in some cases (see below), and can even exceed the eikonal contribution.

The effective way to sum over all types of inelastic corrections is to use the eigenstate method [Kopeliovich 1978]. Let us go from the basis of physical states $|\,h>$ to a set of eigenstates of the interaction Hamiltonian $|\,\alpha>$. In the old-fashioned parton model with short correlations in the rapidity scale, these were states with a definite number of wee partons. In QCD motivated models, they are hadronic fluctuations with definite transverse size ([Zamolodchikov 1981], [Bertch 1981]).

Any physical state $|\,h>$ can be expanded in this new basis :

$$|\,h> = \sum_{\alpha} C_{\alpha}^{h}\,|\,\alpha> \quad , \tag{A17}$$

where the coefficients C_{α}^{h} obey the conditions

$$\sum_{\alpha} C_{\alpha}^{h}\,(C_{\alpha}^{g})^{*} = \delta_{hg} \; ; \qquad \sum_{h} C_{\alpha}^{h}\,(C_{\beta}^{h})^{*} = \delta_{\alpha\beta} \tag{A18}$$

The diagonal and off-diagonal hadronic scattering amplitudes can be represented as

$$<h|\,\hat{f}\,|h> = \sum_{\alpha} |\,C_{\alpha}^{h}\,|^{2}\,f_{\alpha} \tag{A19}$$

$$<g|\,\hat{f}\,|h> = \sum_{\alpha} C_{\alpha}^{h}\,(C_{\alpha}^{g})^{*}\,f_{\alpha} \quad , \tag{A20}$$

where f_{α} are the eigenvalues of the scattering amplitude :

$$\hat{f}\,|\,\alpha> = f_{\alpha}\,|\,\alpha> \quad . \tag{A21}$$

Note that it follows from (A20) that inelastic diffraction is possible only thanks to the variation of f_α with α : otherwise, the states $| h >$ are eigenstates themselves. The crucial point is that the eikonal approach of Glauber is exact for the interaction of an eigenstate with a nucleus, because no inelastic correction exists. As for the hadron-nucleus elastic scattering amplitude given by (A19), it is equal to an average value of the eigenamplitudes, weighted by the factors $| C_\alpha^h |^2$:

$$f_{el}^{hA}(b) = i \left\{ 1 - < e^{-\frac{1}{2}\sigma_\alpha T(b)} >_\alpha \right\} \quad , \tag{A22}$$

where $\sigma_\alpha = 2 \, \mathrm{Im} \, F_\alpha$ is the total cross section for the interaction between the state $| \alpha >$ and a nucleon, $< \sigma_\alpha >_\alpha = \sigma_{tot}^{hN}$.

An essential assumption used in (A22) was that the different states $| \alpha >$ do not mix during the propagation through the nucleus, in spite of the fact that these states are not eigenstates of the vacuum hamiltonian. This is possible only if the incident energy E is high enough :

$$\frac{2E}{\Delta m_h^2} >> R_A \quad . \tag{A23}$$

The mass parameter Δm_h^2, which determines the fluctuation time of the states $| \alpha >$, is the difference between the squares of the masses of the hadron h and its nearest excited state h* [Kopeliovich 1981].

The expression (A22) differs from (A1) or (A6) by the averaging procedure : in (A22), the whole exponential is averaged, whereas in the eikonal approximation, only the exponential index undergoes averaging. The difference between the two expressions is just the sum of all the inelastic corrections. For example, for the total cross section,

$$\Delta_{in} \sigma_{tot}^{hA} = - \int d^2b \left\{ < e^{-\frac{1}{2}\sigma_\alpha T(b)} >_\alpha - e^{-\frac{1}{2}<\sigma_\alpha>_\alpha T(b)} \right\}$$

$$\approx - \frac{1}{4} \int d^2b \, T^2(b) \left\{ < \sigma_\alpha^2 >_\alpha - <\sigma_\alpha>_\alpha^2 \right\} \quad . \tag{A24}$$

The upper expression is exact, whereas the second one neglects all the terms of order higher than σ_α^2 . However, the latter approximation coincides with (A14) [Nikolaev 1981] in the limit (A23), when the mixing of the states $| \alpha >$ during the interaction can be neglected. Indeed, using the expressions (A19) - (A20) for the diffractive amplitudes and the condition

(A18), one can check that $< \sigma_\alpha^2 >_\alpha$ is equal to the sum of the cross sections for all the diffractive channels, including the elastic one. So the difference in the braces in (A24) is the total diffractive dissociation cross section, multiplied by a factor 4π.

It is worth emphasizing that the negative sign of the inelastic correction (A24) is related to the fact that the average of a square is always larger than the square of the average. The physical meaning of this sign is that the inelastic shadowing makes nuclear matter more transparent for a given hadron h. This can be understood as due to the possibility of returning to the initial state $| h >$ after inelastic diffractive scattering, as is shown in Fig. 1b.

In a QCD motivated approach, as mentioned above, the role of the index α is played by the transverse dimension of the hadronic fluctuations, because the interaction cross section of colourless objects is determined by their colour dipole moments [Gunion 1977] : the smaller the transverse size of a hadronic fluctuation, the more transparent the nuclear matter. Therefore, one has to average over different fluctuations, and the nucleus becomes more transparent than would be expected in the eikonal approximation. For example, the scattering amplitude for a hadron h travelling through a nucleus at impact parameter b without interaction can be written as

$$A(b) = \int d^2\rho \, | \psi(\rho) |^2 \, e^{-\frac{1}{2} \sigma(\rho) T(b)} . \qquad \text{(A25)}$$

Let us consider the limit of a large profile function $T(b) \to \infty$. In this limit, only the region of small ρ contributes, where $\sigma(\rho) = \sigma_0 \rho^2$. Then (A25) can be evaluated as :

$$A(b) \approx \pi \, | \psi(0) |^2 \frac{2}{\sigma_0 T(b)} . \qquad \text{(A26)}$$

Due to the contribution of short interquark distances in the incoming hadron wave function, the nucleus becomes more transparent than in the eikonal approximation, where an exponential attenuation of hadrons in nuclear matter is expected. This phenomenon is an essential consequence of QCD, frequently called colour transparency of nuclei. A much more pronounced effect is expected in hard processes on nuclei ([Müller 1982], [Brodsky 1982]), for instance in quasielastic scattering on bound nucleons with high momentum transfer. No attenuation is expected at high energy. This is also the result of inelastic shadowing.

A.3 Diffraction dissociation on nuclei.

Let us start with the eikonal approximation. If a hadron h of mass m and energy E produces, after diffractive interaction with a nucleus, a final hadronic state g of mass M, and if the nucleus remains intact, the partial amplitude for this reaction has the form

$$f_{coh}^{hA} = F_{DD}^{hN}(k_T^2=0) \int_{-\infty}^{\infty} dz\, \rho_A(b, z')\, e^{ik_L z} \times$$

$$e^{-\frac{1}{2}\sigma_{tot}^{hN} \int_{-\infty}^{z} dz' \rho_A(b, z')} \; e^{-\frac{1}{2}\sigma_{tot}^{gN} \int_{z}^{\infty} dz'' \rho_A(b, z'')}, \quad \text{(A27)}$$

where $F_{DD}^{hN}(k_T^2=0)$ is the amplitude for the diffractive dissociation $hN \rightarrow gN$ in the forward direction. The first exponential factor in (A27) takes into account the coherence condition. It contains the relative phase shift between waves coming from different longitudinal coordinates. The two other exponentials take into account the attenuation of the incoming and outgoing particles in nuclear matter. At high energy, the longitudinal momentum transfer $k_L = (M^2 - m^2) / 2E$ can be neglected, and the expression (A27) is considerably simplified :

$$f_{coh}^{hA}(b) = \frac{2F_{DD}^{hN}(k_T^2=0)}{\sigma_{tot}^{gN} - \sigma_{tot}^{hN}} \left(e^{-\frac{1}{2}\sigma_{tot}^{hN} T(b)} - e^{-\frac{1}{2}\sigma_{tot}^{gN} T(b)} \right) \quad \text{(A28)}$$

The coherence condition for waves with different impact parameters gives rise to an amplitude in the k-representation :

$$f_{coh}^{hA}(k_T) = \frac{1}{2\pi} \int d^2b\, f_{coh}^{hA}(b)\; e^{-ik_T b} \quad \text{(A29)}$$

The analysis of experimental data on coherent diffraction dissociation on nuclei using formulae (A27) - (A29), proposed in [Kölbig 1968], was widely used, with the goal of measuring the interaction cross section σ_{tot}^{gN} of the produced unstable hadrons. The results were rather confusing : the attenuation of several pion systems was found to be the same or even smaller than for a single pion (see e.g. [Bellini 1982]). Moreover, the diffractive dissociation cross section on a nucleon target, used in these analyses as a free parameter too, was found considerably smaller than the one following from direct measurements [Dakhno 1983]. This puzzle can be explained by the fact that the inelastic shadowing was neglected.

In the eigenstate approach, the incident hadron is a definite superposition of the interaction eigenstates. When traversing a nucleus, this superposition is distorted because of the different attenuations of the different states. As a result, the final state can be projected onto states differing from the initial one, i.e. diffraction dissociation becomes possible. The wave function of the final state hadron $| g >$ is really formed far behind the nucleus, and it is meaningless to treat the attenuation in the nucleus as the result of the absorption of g. In fact, as was demonstrated above, the true attenuation is weaker than in the eikonal approximation, especially in the off-diagonal transitions. Therefore, the cross section for diffractive production increases, and this simulates a decrease of the cross section σ_{tot}^{gN} in expression (A28). This is confirmed by a direct "theoretical experiment" [Kopeliovich 1990] : after the total cross section for diffraction dissociation on a nucleus has been computed using the eigenstate method with no free parameter, one can fit the result using the eikonal formulae. The result of this fit leads to an effective absorption of the final state which is abnormally small.

B. Spectral function of axial current

Unlike the spectral function for the vector current, which can be measured directly in e^+e^- annihilation, only limited or model-dependent information can be obtained for the axial current. The most straightforward determination of the latter comes from τ-lepton decay, namely $\tau \rightarrow \nu_\tau\, 3\pi$. The partial width of this decay is [Okun 1982]

$$\frac{d\Gamma\,(\tau \rightarrow \nu_\tau\, 3\pi)}{ds} = \frac{G^2\cos^2\theta}{16\pi m_\tau^3}\,(m_\tau^2 + 2s)\,(m_\tau^2 - s)^2\,\rho_T(s)\ , \qquad \text{(B1)}$$

where s is the 3π effective mass squared. Only the transverse part of the spectral function $\rho_T(s)$ is considered, since the longitudinal contribution disappears in the chiral limit. The spectral density $\rho_T(s)$ has been measured by the ARGUS Collaboration [Albrecht 1986]. These data exist of course in the limited range of $s < m_\tau^2$ and represent only a 3π cut contribution to $\rho_T(s)$. However, these conditions are well suited to the study of 3π diffractive neutrinoproduction.

The first important thing which can be tested using these data, is the second Weinberg sum rule [Weinberg 1967], used for calculating a_1 (or 3π) neutrinoproduction :

$$\int ds\ s\ \rho_V(s) = \int ds\ s\ \rho_T(s) \qquad \text{(B2)}$$

Assuming ρ meson dominance of the vector current spectral function, one finds for the left-hand side of this relation

$$\int ds\, s\, \rho_V(s) = 2\, m_\rho^4 / \gamma_\rho^2 \quad , \tag{B3}$$

where γ_ρ is the γ-ρ coupling, $\gamma_\rho^2 / 4\pi = 2.4$.

In order to integrate the right-hand side of (B2), it is convenient to fit the data of Fig. 2 with an analytical expression of the type :

$$\rho(s) = \left(\frac{s}{s_0} - 1\right)^\alpha \sum_{i=1,2} \frac{n_i}{(s - m_i^2)^2 + m_i^2 \Gamma_i^2} \tag{B4}$$

The results are shown in Fig. 2 and in Table B1.

Solutions	s_0	α	n_1 (GeV^4)	m_1 (GeV)	Γ_1 (GeV)	n_2 (GeV^4)	m_2 (GeV)	Γ_2 (GeV)
I	0.106	12.4	0.0042	1.21	0.313	0.002	1.02	0.226
II	0.123	10.7	0.0025	1.25	0.302	0.0037	1.06	0.282

Table 1 : Results of the fit of the ARGUS spectral function for $\tau \rightarrow \nu_\tau\, 3\pi$ to the form (B4).

Two solutions (I and II) are found, with about the same χ^2 ; the corresponding curves are shown in Fig. It is worth emphasizing that in both cases the larger mass corresponds well to the known value of m_a [PDG 1990]. The left-hand maximum can be interpreted as due to non-resonant background.

The integration on the right-hand side of (B2) can now be performed; one obtains $\int ds\, s\, \rho_T(s) \approx 0.027$ GeV^4, in good agreement with (B3). The second Weinberg sum rule is thus experimentally verified, and could be used to fix f_a, the a_1 coupling constant, if one believed in the a_1 dominance of the axial current. However, one has just seen that the latter contradicts the results of a fit of the axial spectral function. Thus, it seems better to use the spectral function directly to describe diffractive 3π neutrinoproduction. For this purpose one should change f_a^2 into $\rho_T(M^2)\, M^4$.

REFERENCES OF THE APPENDIX

[Albrecht 1986] H. Albrecht et al., ARGUS Collaboration, Z. Phys. C 33 (1986) 7

[Bellini 1982] G. Bellini et al., Nucl.Phys. B199 (1982) 1

[Bertch 1981] J. Bertch et al., Phys. Rev. Lett. 47 (1981) 267

[Brodsky 1982] S.J. Brodsky, in : Proc. XIII Int. Symp. on Multiparticle Dynamics, W. Kittel, W. Metsger, A. Steroid eds., World Scientific, Singapore 1982, p. 963

[Cziz 1970] W. Cziz, L. Lesniak, H. Wolek, Nucl. Phys. B19 (1970) 125

[Dakhno 1983] L.G. Dakhno, Yad. Fiz. 37 (1983) 993

[Glauber 1959] R.G. Glauber, in : Lectures in Theoretical Physics., W.E. Brittin, L.G. Dunham eds., Interscience Publishers, New-York 1959, V.I, p. 315

[Glauber 1970] R.G. Glauber, G. Matthiae, Nucl. Phys. B21 (1970) 135

[Gunion 1977] J.F. Gunion, D.E. Soper, Phys. Rev. D15 (1977) 2617

[Karmanov 1973] V.A. Karmanov, L.A. Kondratyuk, JETP Lett. 18 (1973) 451

[Kölbig 1968] K.S. Kölbig, B. Margolis, Nucl. Phys. 6 (1968) 68

[Kopeliovich 1978] B.Z. Kopeliovich, L.I. Lapidus, JETP Lett. 28 (1978) 614

[Kopeliovich 1981] B.Z. Kopeliovich, L.I. Lapidus, JETP Lett. 33 (1981) 309

[Kopeliovich 1990] B.Z. Kopeliovich, Physics of Elementary Particles and Atomic Nuclei 21 (1990) 117

[Müller 1982] A. Müller, in : Proc. of XVII Rencontres de Moriond, J. Tran Thanh Van ed., Editions Frontières, Gif-sur-Yvette 1982, p. 13

[Nikolaev 1981] N.N. Nikolaev, Sov. Phys. JETP 81 (1981) 814

[Okun 1982] L.B. Okun, Leptons and Quarks, North Holland, Amsterdam 1982

[Weinberg 1967] S. Weinberg, Phys. Rev. Lett. 18 (1967) 507

[Zamolodchikov 1981] Al.B. Zamolodchikov, B.Z. Kopeliovich , L.I. Lapidus, JETP Lett. 33 (1981) 595

FIGURE CAPTIONS OF THE APPENDIX

Fig. 1 : Diagrams for elastic scattering : a) Glauber's term; b) inelastic contribution.

Fig. 2 : Distribution of the axial vector spectral density $\rho_T(s)$ for the decay $\tau \rightarrow \nu_\tau (3\pi)$, as measured by the ARGUS Collaboration [Albrecht 1986]. The curves correspond to the solutions of eq. (B4), with the parameters given in Table B1.

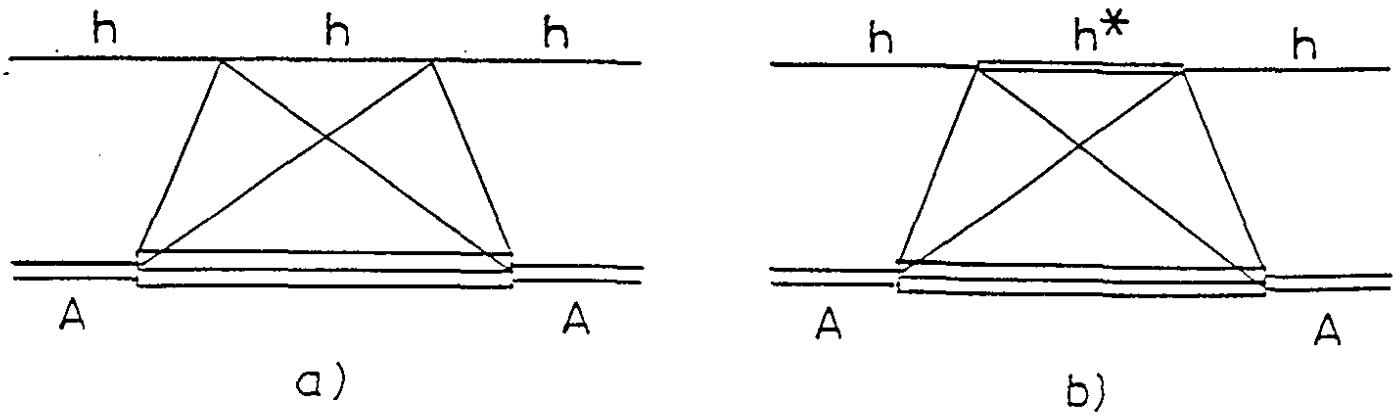

fig. 1

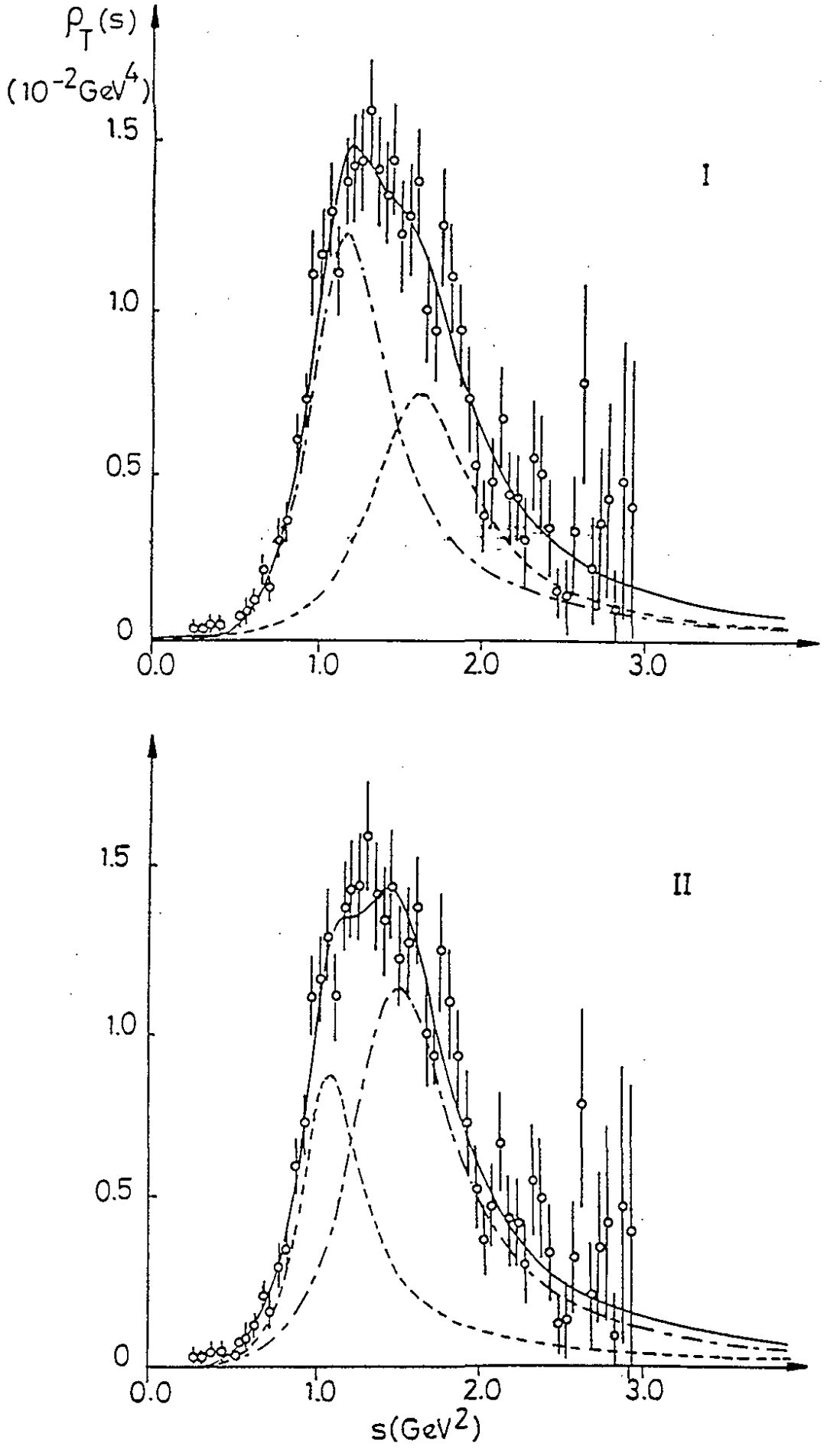

fig. 2